Simulation of bainitic transformation with the phase field method

zur Erlangung des akademischen Grades eines
Doktors der Ingenieurwissenschaften (Dr.-Ing.)
der Fakultät für Maschinenbau
der Universität Paderborn

genehmigte
Dissertation

von
Martin Düsing, M.Sc.
aus Paderborn

Tag des Kolloquiums: 12. Oktober 2018
Referent: Prof. Dr.-Ing. Rolf Mahnken
Korreferenten: Prof. Dr.-Ing. Ralf Müller
Univ.-Prof. Dr. mont. Thomas Antretter

Abstract

Bainite is a steel microstructure with useful properties for the industry. It combines a high toughness with a hardness value between that of pearlitic and martensitic steels. It occurs as upper and lower bainite which can be distinguished by the size and place of carbides precipitating from austenite or bainitic ferrite, respectively. While the phase transformation from austenite to bainitic ferrite is considered to be displacive, the subsequent carbon diffusion is crucial to the precipitation of carbides and in turn crucial to the formation of the two different morphologies, upper and lower bainite. In this work a phase field model is presented describing the complex transformation from austenite to upper and lower bainite, considering the displacive phase transition from austenite to bainitic ferrite, different diffusion mechanisms, the precipitation of carbides and anisotropic growth due to eigenstrains. The model uses a thermodynamic framework which is derived in this work. The framework is based on generalized stresses and forces providing a strict distinction between universal laws, such as the first and second law of thermodynamics, and constitutive equations which are chosen for the actual transformation process. Prototype models are proposed and numerically solved using the finite element method. The results show the capability of the derived thermodynamic framework and the expected behaviour of bainite.

Zusammenfassung

Bainit ist ein Gefüge mit hervorragenden Eigenschaften, das durch gezieltes Abkühlen von Stahl entsteht. Durch dessen hohe Zähigkeit und gleichzeitig hohe Härte ist es für unterschiedliche Einsatzzwecke in der Industrie sehr gut geeignet. Bainit tritt als oberer und unterer Bainit auf. Die beiden Morphologien unterscheiden sich durch Größe und Ort von Karbidausscheidungen. Während die Phasenumwandlung von Austenit zu bainitischem Ferrit unabhängig von der Kohlenstoffdiffusion abläuft, ist die anschließend einsetzende Diffusion für die Ausscheidung der Carbide von entscheidender Bedeutung. In dieser Arbeit wird ein Modell präsentiert, das die Umwandlung von Austenit zu oberen und unteren Bainit mit der Phasenfeldmethode beschreibt. Dabei werden die Phasenumwandlung von Austenit zu bainitischen Ferrit, die anschließenden Diffusionsprozesse, das Ausscheiden von Carbiden und das anisotrope Wachstum durch Eigendehnungen simuliert. Das Model nutzt ein thermodynamisches Rahmenmodell, welches in dieser Arbeit hergeleitet wird und auf der Theorie der generalisierten Spannungen basiert. Diese Formulierung bietet eine Unterscheidung zwischen universellen physikalischen Gesetzen und konstitutiven Gleichungen, die speziell für den abzubildenden Transformationsprozess gewählt werden. Das mathematische Model wird numerisch mit der Methode der finiten Elemente gelöst. Die Ergebnisse zeigen das Potenzial des Rahmenmodells und den beschriebenen Transformationsprozess des Bainits.

Vorwort

Diese Arbeit ist während meiner Zeit als wissenschaftlicher Mitarbeiter an der Universität Paderborn, Lehrstuhl für Technische Mechanik entstanden. Ich danke Herrn Professor Dr. Rolf Mahnken für die Betreuung, die vielen Diskussionen und kritischen Fragen. Für die Begutachtung der Arbeit gilt mein Dank auch den beiden Korreferenten Herrn Professor Dr.-Ing. Ralf Müller von der Technischen Universität Kaiserslautern und Herrn Universitätsprofessor Dr. mont. Dipl.-Ing. Thomas Antretter von der Montanuniversität Leoben, Österreich. Bei Professor Dr. Antretter möchte ich mich insbesondere für den motivierenden Austausch und das entgegengebrachte Interesse an meiner Arbeit bedanken. Mein Dank gilt auch Professor Dr.-Ing. Volker Schöppner für die Übernahme des Vorsitzes der Promotionskommission und Professor Dr. Schaper als weiteres Mitglied der Kommission.

Am Erfolg dieser Arbeit haben auch meine Kollegen Alex Dridger, Xiaozhe Ju, Dr. Ismail Caylak, Eduard Penner, Thorben Leismann, Nicole Nörenberg, Chun Cheng, Peter Lenz, Kai-Uwe Widany, Ulrich Ehlenbröker und Christian Dammann einen Anteil, die mir, ebenso wie meine Verlobte Jenny Van, immer scharfsinnige Sparringspartner waren. Am Lehrstuhl für Technische Mechanik habe ich während dieser Zeit mit viel Freude gelehrt und wünsche meinen neuen Kollegen Vahab Narouie, Felix Flachmann und Hendrik Westermann eine ebenso erfüllende Zeit und viel Erfolg. An der Universität Paderborn bedanke ich mich außerdem bei Elena Schlegel, Manfred Fortmeier, Heinrich Dirkmorfeld, Cornelia Wessel, Cornelia Meinders-Pongratz und Sonja Mantzouridis für viele kleine Dinge. Meinen Eltern Mechthild und Winfried, meinen beiden Schwestern Karin und Maria, meinem Bruder Christoph und Jenny danke ich für alles.

Paderborn, Oktober 2018 Martin Düsing

List of Pre-Publications

Parts of this thesis are already published in the following pre-publications:

- M. Düsing and R. Mahnken. A coupled phase-field – Cahn-Hilliard model for lower bainitic transformation. *Proceedings in Applied Mathematics and Mechanics* 15 (2015), 285–286.
- M. Düsing and R. Mahnken. A phase-field approach for lower bainitic transformation coupled with carbon diffusion. *Conference Proceedings of the YIC GACM* (2015), 76–79.
- M. Düsing and R. Mahnken. A thermodynamic framework for coupled multiphase field and diffusion models for lower bainite transformation. *Proceedings in Applied Mathematics and Mechanics* 16 (2016), 321–322.
- M. Düsing and R. Mahnken. A thermodynamic framework for coupled multiphase Ginzburg-Landau/Cahn-Hilliard systems for simulation of lower bainitic transformation. *Archive of Applied Mechanics* 86.12 (2016), 1947–1964.
- M. Düsing and R. Mahnken. Simulation of lower bainitic transformation with the phase-field method considering carbide formation. *Computational Materials Science* 111 (2016), 91–100.
- R. Mahnken, C. Cheng, M. Düsing, U. Ehlenbröker, and T. Leismann. The concept of generalized stresses for computational manufacturing and beyond. *GAMM-Mitteilungen* 39.2 (2016), 229–265.
- M. Düsing and R. Mahnken. A coupled multiphase-field and carbon diffusion model for lower bainitic transformation. *Proceedings of the Coupled Problems in Science and Engineering VII* (2017), 993–998.

- M. Düsing and R. Mahnken. A coupled phase transformation and solute diffusion model for bainitic transformation. *Proceedings in Applied Mathematics and Mechanics* 17 (2017), 505–506.
- M. Düsing and R. Mahnken. A coupled phase field/diffusion model for upper and lower bainitic transformation. *International Journal of Solids and Structures* 135 (2018), 172–183.
- M. Düsing and R. Mahnken. A coupled phase field/diffusional/mechanical framework for simulation of upper and lower bainitic transformation. *submitted* (2018).
- M. Düsing and R. Mahnken. Simulation of upper and lower bainitic transformation with a coupled phase field/diffusion/deformation framework. *Proceedings in Applied Mathematics and Mechanics* 18 (2018), accepted.
- R. Mahnken and M. Düsing. Simulation of upper and lower bainitic transformation in a unified phase field model. *Proceedings of the 6th European Conference on Computational Mechanics (ECCM 6)* (2018), submitted.

Contents

1 Introduction

In recent years bainitic steels have been attracting the attention of steel-producers and engineers, because bainite provides a desirable combination of high ductility, enhanced strength and high hardness. In industrial applications bainitic workpieces have gained a growing importance, especially after hot-forming and quenching of relatively bulky parts, as the cooling rates within large pieces are too slow to produce martensite, but high enough to transform a considerable fraction into bainitic ferrite [31]. As an alternative to traditional high-strength low alloy steels, dual-phase steels (DPS) consisting of bainite and ferrite have gained increased popularity by the car and aerospace industry, because of their advantages in formability and light-weight potential [21, 25]. The Deutsche Bahn, for example, uses bainitic steel in an important part of railroad switches [24]. The so called *frog* of a railroad switch, illustrated in Figure 1.1, is a heavily loaded workpiece which has to be very hard. Bainite is the optimal material for such frogs and therefore, chosen for the 15000 most loaded railroad switches in Germany.

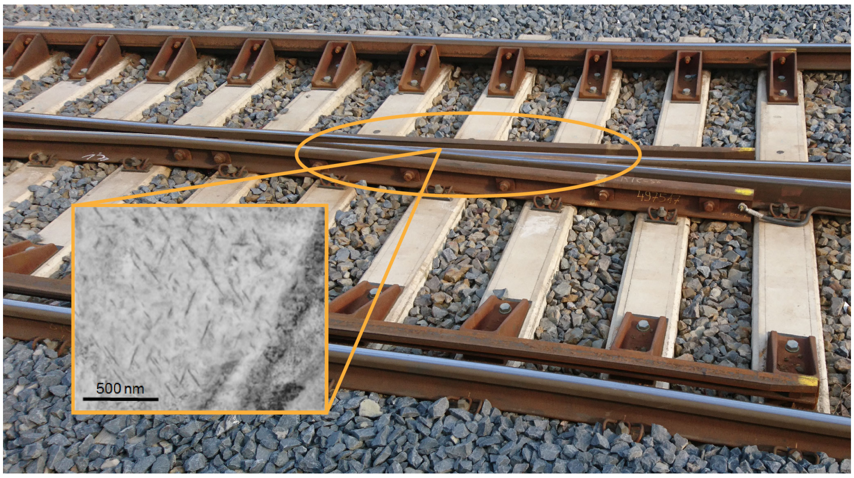

Figure 1.1: Bainitic frog of a railroad switch with a transmission electron microscopy image of the microstructure

The microstructural transformation of bainite is a complex process which is described and simulated in this scientific work. In mechanics, as a part of physics, the observation of an event, for example a movement or a phase transformation, is the starting point for any scientific work and should ideally result in the successful description of this physical event. To make such a description it is necessary to explain these observations which often leads to the development of a mathematical model. In physics and especially in mechanics the basis of the mathematical model is commonly a differential equation. In today's research in mechanics the fundamental equations, like the balances of linear and angular momentum and the first and second law of thermodynamics are determined while constitutive equations change depending on the material. The distinction between universal physical laws and constitutive equations is a fundamental reason for the great success of engineering mechanics. Simulations predicting deformations of complex structures such as cars or planes are of high accuracy and widely used in the industry.

Macroscopic material properties of most materials in modern technology strongly depend on their microstructure. Therefore, it is important to study and understand the phase transformations on a microscopic level. The modeling of phase transformations plays an important role in designing new materials with new properties. The different distributions and morphologies of a microstructure are a result of complex transformations whose evolution depends on the complex interaction between different physical phenomena, such as chemical diffusion, mechanics (elasticity and plasticity), interfacial energies and electro-magnetism.

Mechanics has many relations to materials sciences as the observations needed to develop new models or constitutive equations originate in materials science. Several groups of scientists in mechanics have found interesting problems in the field of phase transformations. Phase transformations and mechanical problems are described by partial differential equations and are solved, for example, with the finite element method. In this field it is also possible to apply the strict separation between universal physical laws and constitutive equations as successfully done in classical mechanics. This strict separation is described in detail in Section 3.2 and in Paper B. Furthermore, a coupling of these generalized stresses with mechanics can be found in Paper D.

2 The formation of bainite

2.1 Preliminaries on bainite

Bainite is a steel microstructure first observed by E. S. Davenport and Edgar Bain and clearly identified in 1930 [27]. A distinction between two morphologies called upper and lower bainite is made. The morphologies show different macroscopic mechanical behaviour and different microstructural compositions. Both morphologies form when austenite is cooled past a critical temperature. The microstructure consists of aggregates, termed sheaves, of bainitic ferrite sub-units surrounded by carbides and retained austenite.

In the time-temperature-transformation diagram in Figure 2.1 (a) the pearlite area, the bainite area at lower temperatures and the martensite start temperature underneath can be seen. Pearlite is built at high temperatures and slow cooling rates. The microstructure is two-phased and lamellar. Layers of carbide and ferrite alternate as shown in Figure 2.1 (b). The carbon separates in areas of high and low concentration where carbide and ferrite grow cooperatively. Due to the high temperature the carbon is mobile and can move fast.

The martensite transformation proceeds completely different. If a steel workpiece is cooled so fast that the pearlite and bainite areas in the time-temperature-transformation diagram are not touched and the martensite start temperature is reached, martensite grows. The transformation from austenite to martensite is very fast and diffusionless. The carbon diffusion velocity is very low due to the low temperature. Furthermore, the transformation is so fast that there is neither time for the carbon to diffuse nor to build accumulations nor even to precipitate as carbides. Instead martensite forms displacive from face-centered cubic austenite to a body-centered tetragonal form. The new martensite is highly strained and supersaturated with carbon.

While there is a general agreement in science that the pearlite growth is cooperative with the carbon diffusion and rather slowly, and that martensite forms diffusionless, very fast and in a displacive manner, the growth of bainitic ferrite is controversially discussed in materials science. The main disagreement is on whether the growth mechanism is

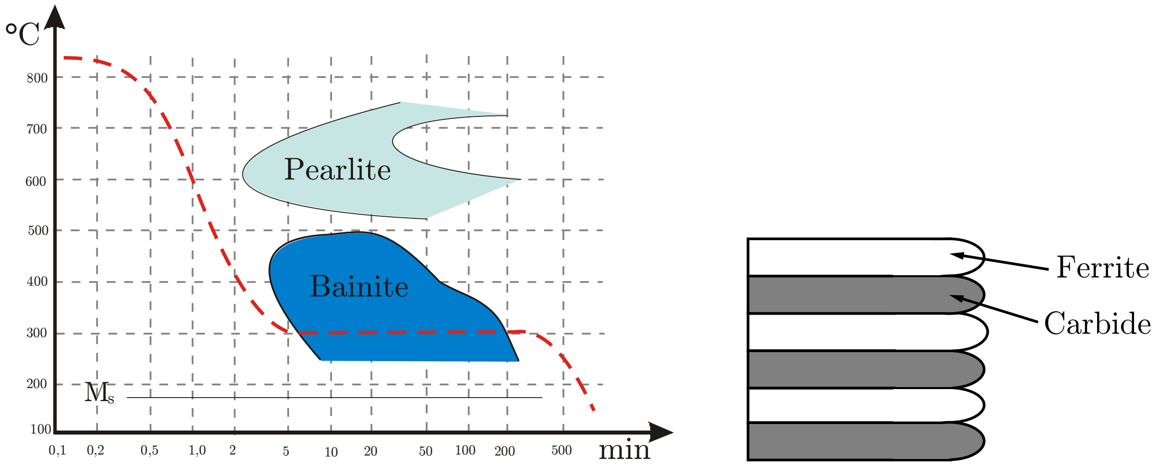

(a) Time-temperature-transformation diagram [36]

(b) Pearlite growth

Figure 2.1: **(a)** Schematic time-temperature-transformation diagram of steel and **(b)** Schematic representation of pearlite growth

controlled by the diffusion of carbon as it is for pearlite or if it is displacive and diffusionless as it is for martensite [27]. A majority of material scientists agree on the assumption that the bainitic ferrite grows displacively and that it is supersaturated with carbon shortly after the phase transformation [12]. This thesis follows this assumption.

The displacive transformation from austenite to bainitic ferrite can be regarded as a deformation of the austenite phase combined with a change of the atomic configuration. The resulting permanent strain is called transformation plasticity [12]. The transformation starts after a fast cooling below a certain temperature, by applying stress to the specimen or by a combination of both factors [12]. The habit plane and a displacement vector describe an invariant plane strain which is a deformation system for transformation plasticity. The transformation plasticity can be obtained at a much smaller yield stress than of the stable austenite phase.

2.2 Morphologies and diffusion processes

The movement of the carbon within the supersaturated bainitic ferrite is strongly dependent on the temperature as it influences the mobility and speed of the carbon atoms. This dependency leads to two different morphologies, called upper and lower bainite. At high temperatures (within the bainite nose, see Figure 2.1 (a)) the diffusion mobility is high

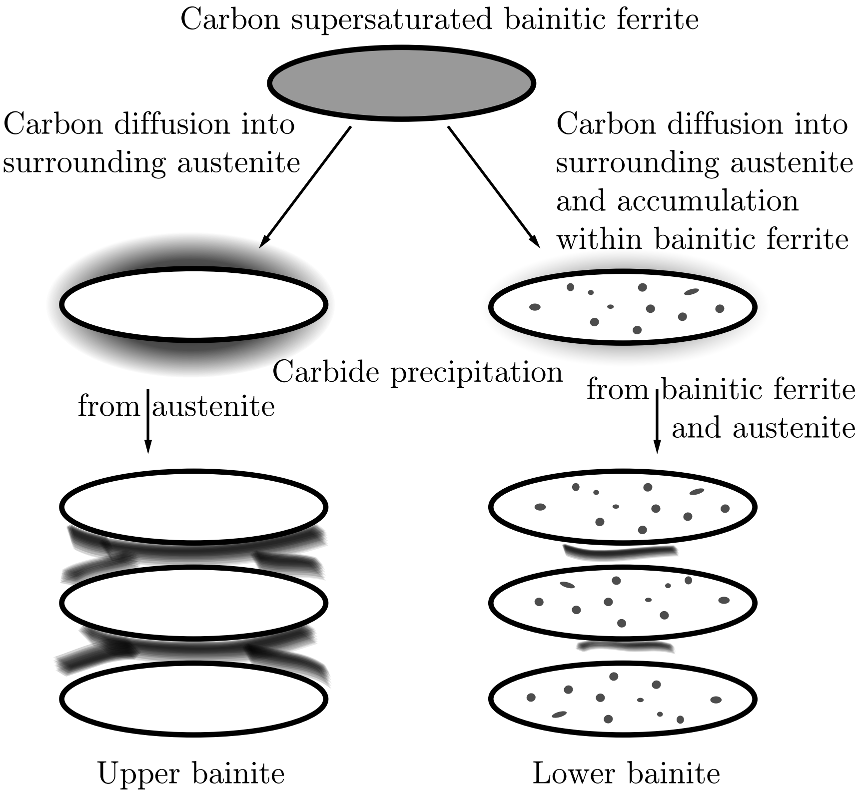

Figure 2.2: Schematic visualisation of upper and lower bainite. Recreated [12]

and the carbon atoms are able to move out of the supersaturated bainitic ferrite into the austenite phase. Within the enriched austenite phase, carbides precipitate at places where the carbon concentration is high enough. The resulting microstructure is called upper bainite.

In lower bainite the diffusion mobility is much lower, such that only a few atoms close to the interface succeed in leaving the supersaturated bainitic ferrite into the austenite while most of the carbon is trapped within the bainitic ferrite. There the remaining carbon separates to build accumulations surrounded by areas with an equilibrium concentration. At those carbon accumulations, carbides precipitate within the bainitic ferrite. This is the main difference to upper bainite, where carbides precipitate only from the austenite phase. The micrograph in Figure 3 of Paper B shows a microstructure of lower bainite with a bainitic sheaf and circular carbides within the sheaf.

Figure 2.2 illustrates the two different processes in comparison. Both start with the grey illustrated supersaturated bainitic ferrite. On the left hand side upper bainite is illustrated. Here the carbon diffuses out of the bainitic ferrite into the surrounding austenite, leaving the bainitic ferrite with its equilibrium concentration of carbon, illustrated in white. On the right hand side, the lower bainite transformation is illustrated. Opposed to the formation of upper bainite, most of the carbon stays within the bainitic ferrite and accumulates while only a small amount of carbon diffuses out of the bainitic ferrite. In both morphologies carbides precipitate at accumulations of carbon. In upper bainite this takes place only within the austenite phase while in lower bainite most of the carbides precipitate directly within the bainitic ferrite.

The diffusion mechanisms of carbon in bainite are described and illustrated in Section 2 of Paper C.

3 Generalized stresses and the phase field method

3.1 Preliminaries on the phase field method

The phase field technique can be used to simulate the evolution of a microstructure on the mesoscale. The main characteristics of the phase field method are functions which are continuous in space and time, called phase field variables or order parameters specifying the configurations, arrangements or densities of atoms [10]. The phase field variables vary in the interface between two phases while they are nearly constant in bulk microstructures. Due to the mandatory interface regions, this approach belongs to the diffusive interface models. A main advantage of the these models is that there is no need to track the interfaces during the phase transformation [17].

Phase-field models are based on partial differential equations. The most important ones are the Ginzburg-Landau and the Cahn-Hilliard equations. They can be derived from the general laws of thermodynamics and kinetic principles, for example with the microforce balance [10]. Phase-field approaches are always continuous models, which do not describe the behaviour of individual atoms, but the configurations of atoms. Hence, the models contain material specific phenomenological properties that are determined based on experimental or theoretical information [17].

Phase-field variables can be distinguished between conserved and non-conserved variables. Composition variables describe concentrations or molar fractions. They are normally conserved, since the number of atoms or moles of a component in a system is conserved. Changes in the local concentration c of a certain component can only occur by fluxes $\boldsymbol{J}$ of atoms of this component within the system. The conservation law holds for all conserved variables

$$\frac{\partial c}{\partial t} = -\nabla \cdot \boldsymbol{J}. \tag{3.1}$$

The simplest example of a conserved phase field equation is Fick's law of diffusion. A more complex one is the Cahn-Hilliard equation.

Non-conserved phase field variables are used to distinguish between different phases, microstructures or states of matter. They are often denoted by ϕ and can transform from one to the other. They cannot be conserved.

More than a century ago van der Waals [3] was one of the first to use a density function that varies continuously. In 1950, Ginzburg and Landau [1] published their theory of superconductivity using order parameters and its gradients. Some years later Cahn and Hilliard [2] presented their model for phase fields with higher order concentration gradients. The concept of order parameters used today was introduced by Landau [4] 30 years ago. More detailed historical information can be found in [17, 19].

Another important paper which has strongly inspired the present work was written by Kobayashi [7] in 1993. The paper is about the simulation of dendritic growth by coupling a Ginzburg-Landau equation with a heat equation. For the simulation of diffusion, especially of diffusion across the interface of phases the names Wheeler, Boettinger and McFadden [5, 8, 11] are to be mentioned. In the field of phase transformations there are numerous papers in which the phase field method is used, for example to simulate austenite-to-ferrite [14, 13] and austenite-to-pearlite transitions [16]. Furthermore, the formation of Widmanstätten patterns [15] and the important austenite-to-martensite transformation [18, 29] is simulated with the phase field method.

Only a few models describe parts of the bainitic transformation. Song et al. [22] simulate the transformation from austenite to upper bainite with the phase field method, though neglecting the precipitation of carbides. The work by Arif and Qin [26] describes the autocatalysis of sub-units. To the author's knowledge, the first phase field models for the lower bainitic transformation are presented in [34] and [33] simulating the separation of carbon within the bainitic ferrite and the precipitation of carbides. In addition, this model is e.g. applied in [37], extended to upper bainite considering the diffusion of carbon across the interface in [38] and improved by coupling with mechanics in [39].

In recent years the phase field method has become an even more multifunctional tool. There is already a large community working on phase field methods to predict crack nucleation and propagation e.g. [32] and fracture e.g. in [20, 23]. There are also scientists studying tumour growth [30, 40] or the deformation processes in lithium-ion batteries [35] by means of the phase field method.

3.2 The idea of generalized stresses

Gurtin and Fried [6, 9, 10] developed a framework for Ginzburg-Landau and Cahn-Hilliard equations based on a balance law for so called "microforces". Both equations describe the configurations, arrangements or densities of atoms characterized by order parameters to model phase transformations or diffusion processes. The equations can be derived straightforward using a suitable free energy function and variational derivatives, but they lack a deeper physical understanding and a separation between basic balance laws and constitutive equations [10]. Gurtin and Fried propose a new way to derive these equations by introducing microforces and microstresses comparable to those of continuum mechanics. While forces in continuum mechanics change the state of movement or the shape of a body, the new microforces change the configurations or arrangements of atoms on a much smaller scale.

The key idea is to copy the most successful concept of continuum mechanics, the separation between basic balance laws and constitutive equations, which accelerated the progress in mechanics fundamentally. Gurtin and Fried postulate that phase transformations and movements of atoms (diffusion) take place due to microforces. They introduce a phase order parameter ϕ which can be conserved (as c in equation (3.1)) or non-conserved, and a vector stress $\boldsymbol{\xi}$, a scalar internal body force π and an external body force γ. The integrals

$$\int_V -\boldsymbol{\xi} \cdot \nabla\dot{\phi}\, dV, \quad \int_V \pi\dot{\phi}\, dV, \quad \int_V \gamma\dot{\phi}\, dV \tag{3.2}$$

describe powers on the atoms of V and are used to formulate a microforce balance

$$\nabla \cdot \boldsymbol{\xi} + \pi + \gamma = 0 \quad \text{in} \quad V. \tag{3.3}$$

This is shown in detail in Papers B and D for a multiphase model coupled to diffusion and in case of Paper D, with mechanics. To achieve an evolution equation for ϕ constitutive equations have to be specified. In this example that would be $\boldsymbol{\xi}, \pi$ and γ. These constitutive equations cannot be chosen freely. They have to fulfil the first and the second law of thermodynamics. Especially with the help of the Clausius-Duhem inequality in Papers B and D, restrictions for constitutive equations are formulated which are necessary conditions for the validity of the model. The sketched derivation leads in the simplest case to the classical Ginzburg-Landau equation

$$\beta\dot{\phi} = r\Delta\phi - f'(\phi) \tag{3.4}$$

where f is a double-well potential and β and r are material parameters. The classical Cahn-Hilliard equation

$$\dot{c} = D\Delta\left(f'(c) - \rho\Delta c\right), \tag{3.5}$$

can be derived in the same manner. One main difference is that the conservation law (3.1) is used. In equation (3.5) f' is again a double-well potential, D is a constant diffusion coefficient and ρ is a constant material parameter.

The derivation within the framework of generalized stresses is very universal and can be used to derive equations for diverse problems considering physical principles, such as the microforce balance and the first and the second law of thermodynamics.

4 Objectives

The objectives of the present work are as follows:

- The first objective is to develop a thermodynamical framework based on generalized stresses as introduced by Gurtin [10] to model the lower and upper bainite transformation. To do so a combination of a multiphase Ginzburg-Landau equation and a Cahn-Hilliard diffusion equation is required which can be found in Paper B. Furthermore, the coupling with mechanics is necessary, such that a multiphase field/diffusion/mechanical framework is required which is derived in Paper D.
- The second objective is the development of prototype models based on the thermodynamic frameworks to simulate the bainitic transformation. In this step constitutive equations have be to proposed to achieve a coupled system of partial differential equations. Prototype models can be found in each paper within this thesis. A main challenge of this objective is the modelling of the carbon diffusion for upper and lower bainite. The idea and resulting model can be found in Paper C.
- The third objective is a finite element implementation and programming of the proposed system of partial differential equations. The documentations of the finite element implementations can be found in each paper.
- The fourth objective is to solve some elementary initial boundary value problems on a finite size domain. The results should show the transformation characteristics of bainite. Results of the corresponding prototype models can be found in the related papers.

Paper A

M. Düsing and R. Mahnken

Simulation of lower bainitic transformation with the phase-field method considering carbide formation

Computational Materials Science 111, 91–100, 2016

Simulation of lower bainitic transformation with the phase-field method considering carbide formation

Martin Düsing and Rolf Mahnken

Chair of Engineering Mechanics, Paderborn University,

Warburger Str. 100, 33098 Paderborn, Germany

Abstract

Lower bainite is a steel microstructure composed of austenite, ferrite and carbides within the ferrite. The transformation of austenite to lower bainite is one of the most complex transformation in steel. The carbon concentration of bainitic ferrite is of major importance for the carbide precipitation. A phase-field model to simulate the transformation of lower bainite including carbon diffusion and carbide formation is presented in this work. The model is based on a classical phase-field approach coupled with a viscous Cahn-Hilliard equation to simulate the separation of the carbon. During the isothermal simulation a sheaf of bainitic ferrite grows. The carbon starts to diffuse within the supersaturated ferrite which can only contain a fraction of the carbon which was stored in the austenite. At the accumulations of the carbon concentration carbides are precipitated. The simulations show successfully the described growth characteristics of the lower bainite transformation including carbide formation.

Keywords: Phase-field, Bainite, Phase transformation, Diffusion, Cahn-Hilliard

1 Introduction

Bainite is a microstructure of steel that can be formed by heat treating. It can be build by continuous cooling or isothermal between the temperatures of perlite and martensite (250 °C – 550 °C). In materials science a distinction between upper bainite and lower bainite is made. Upper bainite forms at higher temperatures whereas lower bainite forms at temperatures closer to the martensite start temperature. The transformation always starts from austenite. At first bainitic ferrite sheaves grow from the borders of the grain. These sheaves consists of smaller sub-units. Within the supersaturated ferritic sheaf the carbon starts to diffuse, because ferrite can contain much less carbon than austenite [1]. In upper bainite the majority of the carbon partitions into austenite and precipitates as carbides where the concentration is high enough. At lower temperatures the diffusion is slower and most of the carbon cannot partition out of the ferrite. It starts to build accumulations and precipitates as carbides within the sheaf. This movement of the carbon within bainitic ferrite can be denoted as uphill diffusion. The resulting microstructure is lower bainite.

Due to its advantageous balance of strength and ductility, bainite has applications in the automotive industry, in highly loaded parts of the railway and in other divisions of engineering. Models to describe the formation of bainite can be helpful tools to accelerate the development of new applications, because the transformation is a very time-consuming process.

In materials science the phase-field method is widely used to model diffusive/reconstructive transformations as well as displacive ones [2, 3]. It is based on a system of partial differential equations which describes the growth of phases and can be derived from the Ginzburg-Landau equation [2]. The evolution of the so called order-parameters is modeled. At the interfaces of the phases the parameters vary continuously. Therefore the solution does not show sharp interfaces, but diffuse ones which can be governed by a thickness parameter. The advantage of this approach is that it is not necessary to track the interfaces.

Especially for steel there are many approaches describing the transformations austenite-to-ferrite [4, 5], austenite-to-perlite [6], Widmanstätten formation [7], austenite-to-martensite [8, 9] and others. Phase-field models with coupled diffusion equations exist, too [10]. However there are few phase-field models for the bainitic transformation [11, 12], because it is one of the most complex transformations in steel. Song et al. [12] simulate the growth of a bainitic sheaf with the phase-field method combined with a modified Fick's diffusion equation to model the partitioning of carbon at the interface between bainitic ferrite and austenite. This model is more relevant for upper bainite and it does not include the precipitation of carbides. They show high-quality HRTEM images. Arif and Qin [11] simulate the evolution of the subunits which arise on a lower scale than bainitic sheaf growth. Therefore they do not show a partitioning of carbon within the bainitic ferrite phase but a diffusion out of the phase. Remarkable is the three dimensional autocatalysis simulation. The formation of lower bainite, the partitioning of carbon within the bainitic ferrite and the precipitation of carbides have, up to our knowledge, not been considered until now.

There are other approaches simulating the evolution of bainite different to the phase-field method in the literature. For example Sidhu et al. [13] present a model describing the kinetics for an isothermal transformation. They calculate the volume fraction of bainite depending on the transformation time and the temperature. Another work [14] also focuses on the volume fraction growth and the incubation time of the bainitic transformation. Lambert-Perlade et al. [15] report about multi-scale crystallographic and metallographic investigations with analytical micromechanical models. Mahnken et al. [16] focus on the multi-scale simulation of the transformation. On the micro level it is based on an ordinary differential equation which considers the growth of different crystallographic variants. Another publication [17] discusses a macroscopic model with transformation plasticity.

In this work we present a model to simulate the bainitic transformation considering bainitic ferrite, austenite, carbide and the diffusion of carbon within a bainitic sheaf. The displacive transformation [1] between austenite and bainitic ferrite is described by a phase-field method. To simulate the complex diffusion behavior of the carbon within the bainitic ferrite the Cahn-Hilliard equation is used. This equation is central to materials science because it describes the movement of atoms between cells [2] and has been applied to simulate carbon diffusion before [7, 11]. Fick's law cannot applied here, because it does not describe uphill diffusion within one phase. The precipitation of carbides will be simulated with the phase-field method again. We do not consider crystallographic orientation, crystalline anisotropy or any kind of stress and strain.

An outline of this work is as follows: In Section 2 the governing equations of the coupled initial boundary value problem are presented. Firstly the multi-phase-field model based on the Ginzburg-Landau equation is derived from the local free energy. In a second step this model is extended by anisotropy. In Subsection 2.3 the diffusion equation is introduced. This equation is coupled to the phase propagation. The last subsection of Section 2 is about the precipitation of carbides. Section 3 provides a detailed insight into the implementation of the model. In Section 4 three numerical examples are presented showing the lower bainitic transformation. The last section is a summary and gives an outlook for further investigations.

2 The phase-field theory

2.1 Governing equations

The phase-field model is based on the Ginzburg-Landau equation [2]. It can be derived using a functional of the local free energy F which depends on the local phase-field order-parameters ϕ_i and their spatial derivatives $\nabla\phi_i$ [18, 19, 7]

$$F(\phi_1, ..., \phi_n, \nabla\phi_1, ..., \nabla\phi_n) = \int\limits_V \sum_{i,j\ (i<j)}^{N_p} \left\{ f_{ij}^{intf}(\phi_i, \phi_j, \nabla\phi_i, \nabla\phi_j) + f_{ij}^{pot}(\phi_i, \phi_j) \right\} dV, \tag{1}$$

where N_p denotes the number of phases. The density of the local free energy functional is defined as the sum of an interfacial energy density f_{ij}^{intf} and a potential free energy density f_{ij}^{pot}. As a working solution we use the interfacial energy density [18] with the gradient energy coefficient ϵ_{ij}

$$f_{ij}^{intf} = \frac{1}{2}\epsilon_{ij}\left(\phi_i\nabla\phi_j - \phi_j\nabla\phi_i\right)^2. \tag{2}$$

For the potential energy term there are different approaches in the literature [3]. Figure 1 illustrates two commonly used potentials, the double well potential and the double obstacle potential. We use the standard double well potential such that the potential free energy reads [18]

$$f_{ij}^{pot} = \frac{1}{4a_{ij}}\left[\phi_i^2\phi_j^2 - m_{ij}\left(\frac{1}{3}\phi_i^3 + \phi_i^2\phi_j - \frac{1}{3}\phi_j^3 - \phi_j^2\phi_i\right)\right], \tag{3}$$

where m_{ij} is the thermodynamic driving force and $1/a_{ij}$ is the potential constant between the phases i and j.

By minimizing the local free energy the evolution equations of the phase-field order-parameters are derived [18, 19]

$$\begin{aligned}\dot{\phi_i} &= \sum_{j=1, j\neq i}^{N_p} \frac{1}{\tau_{ij}}\left(\nabla\frac{\partial}{\partial\nabla\phi_i} - \frac{\partial}{\partial\phi_i}\right)(f_{ij}^{intf} + f_{ij}^{pot}) \\ &= \sum_{j=1, j\neq i}^{N_p} \frac{1}{\tau_{ij}}\left[\epsilon_{ij}\left(\phi_j\nabla^2\phi_i - \phi_i\nabla^2\phi_j\right) - \frac{\phi_i\phi_j}{2a_{ij}}\left(\phi_j - \phi_i - 2m_{ij}\right)\right]. \end{aligned} \tag{4}$$

The parameters $\epsilon_{ij}, a_{ij}, \tau_{ij}$, and m_{ij} are now replaced by the physical material parameters,

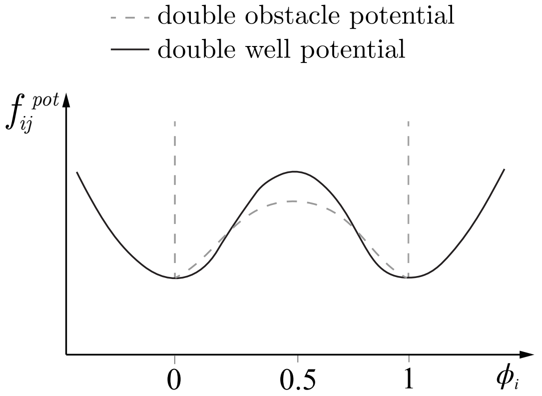

Figure 1: Double well and double obstacle potential

interface mobility μ_{ij}, interface energy σ_{ij}, interface thickness η_{ij} and the change of Gibbs energy ΔG_{ij}. Note that $\mu_{ij} = \mu_{ji}$, $\sigma_{ij} = \sigma_{ji}$ and $\eta_{ij} = \eta_{ji}$ but $\Delta G_{ij} = -\Delta G_{ji}$.

$$\tau_{ij} = \frac{\eta_{ij}}{\mu_{ij}}, \qquad a_{ij} = \frac{\eta_{ij}}{72\sigma_{ij}}, \qquad \epsilon_{ij} = \sigma_{ij}\eta_{ij}, \qquad m_{ij} = -6\Delta G_{ij} a_{ij}. \tag{5}$$

The derivation of the equations (5) using the Gibbs-Thomson equation [20] can be found in the appendix. With these results the evolution equation of the phase parameters reads

$$\dot{\phi}_i = \sum_{j=1, j\neq i}^{N_p} \mu_{ij} \left[\sigma_{ij} \left((\phi_j \nabla^2 \phi_i - \phi_i \nabla^2 \phi_j) - \frac{36}{\eta_{ij}^2} \phi_i \phi_j (\phi_j - \phi_i) \right) - \frac{6 \cdot \Delta G_{ij}}{\eta_{ij}} \phi_i \phi_j \right]. \tag{6}$$

For the lower bainitic transformation considered in this work $N_p = 3$ phases are involved:

1. bainitic ferrite (ϕ_1),
2. austenite (ϕ_2) and
3. carbide (ϕ_3).

2.2 Phase-field anisotropy

To simulate the typical slim form of bainite sheaves an anisotropic phase-field model as presented by [21] and [22] is used. The interface energy σ_{ij} is redefined as a function of the actual growth direction θ and of a predefined main growth direction called θ_0

$$\sigma_{ij} = \sigma_{ij}(\theta, \theta_0). \tag{7}$$

To be specific we use

$$\sigma_{ij}(\theta,\theta_0) = \sigma_{ij}^0 \cdot (1 + s \cdot \cos(\theta - \theta_0)), \tag{8}$$

where σ_{ij}^0 is the constant material parameter of the interface energy between phases i and j. In this approach anisotropy is only present between the ferrite and austenite phases. Therefore σ_{12} and θ read

$$\sigma_{12} = \sigma_{12}^0 \cdot (1 + s \cdot \cos(\theta - \theta_0)), \quad \text{where} \quad \theta = \arctan \frac{\frac{\partial\phi_1}{\partial y}}{\frac{\partial\phi_1}{\partial x}}. \tag{9}$$

The parameter s is used to calibrate the strength of anisotropy. Since only one sheaf shall be simulated the main growth direction θ_0 of the ferrite can be chosen arbitrary. This anisotropy approach is a simplification and an issue for further investigations.

2.3 Carbon diffusion

The diffusion of carbon is crucial for modeling carbide precipitation. The ferrite can contain considerably less carbon. For example it may only contain 0.022 wt.% carbon at about 1000 K [23]. Prior to the transformation of austenite to ferrite, the austenite may contain much more carbon, which depends on the actual alloy. During the lower bainitic transformation the transition from austenite to ferrite is too fast for the carbon to diffuse out of the austenite. That is why the carbon starts to diffuse within the supersaturated ferrite and builds accumulations of high concentration due to its lower energy level. This mechanism named uphill diffusion continues until it reaches the maximum carbon concentration of 6.67 wt.% [24]. At this stage the carbide precipitation starts.

In this case uphill diffusion cannot be described by Fick's law. Therefore we use the Cahn-Hilliard equation [25, 26, 27], which is widely used in material modeling, especially for carbon diffusion [7]. In contrast to the phase-field equation, the Cahn-Hilliard equation, describing the transport of atoms between unit cells, is a conservation law [2]. Here we use a viscous Cahn-Hilliard formulation due to its superior characteristics for homogenization [28]

$$\begin{aligned}
&1. \qquad && \underline{J} = -\phi_1 M \nabla \eta \\
&2. \qquad && \eta = a\dot{c} - b\nabla^2 c + df'(c) \\
&3. \qquad && f(c) = (X_{UG} - c)^2 (X_{OG} - c)^2 \\
&4. \qquad && f'(c) = -2(X_{UG} - c)(X_{OG} - c)^2 - 2(X_{OG} - c)(X_{UG} - c)^2.
\end{aligned} \tag{10}$$

In equation (10.1) the diffusion flux $\underline{J}$ is defined as the product of the ferrite phase parameter ϕ_1, the diffusion coefficient M and the gradient of chemical potential η. Specific in this work is the phase parameter ϕ_1. Due to the fact that it only varies between 1 and 0 it does not change the characteristics of the diffusion. The diffusion equation is coupled with the phase-field model by this parameter, because the diffusion flux can only be nonzero in an area where the ferrite ϕ_1 dominates. This model is physically reasonable because this kind of diffusion takes only place within the bainitic ferrite. The function f in equation (10.3) is a double well potential as plotted in Figure 2. It restricts the carbon concentration to remain between the upper X_{OG} and lower X_{UG} concentration limit.

Using the mass conservation law one finally obtains the evolution equation for the carbon concentration:

$$\dot{c} = -\nabla \cdot \underline{J} = \phi_1 M \nabla^2 \eta + \nabla \phi_1 M \nabla \eta. \tag{11}$$

2.4 Carbide precipitation

The precipitation of carbides occurs only at places where the local carbon concentration is at its high point $X_{OG} = 6.67\,\text{wt.\%}$. To model this physical behavior the interface mobility parameter μ_{13} between bainitic ferrite and carbide is defined as a function of the local carbon concentration. With regard to the numerical implementation a smooth step function is defined

$$\mu_{13}(c) = \mu_{13}^0 \cdot \begin{cases} 0 & \text{if } c < X_{OG} - \varepsilon \\ 1 & \text{if } c > X_{OG} \\ \frac{1}{2} + \frac{1}{2} \cdot sin(\frac{\pi}{\varepsilon} \cdot c + \frac{\pi}{2} - \frac{\pi}{\varepsilon} \cdot X_{OG}) & \text{else,} \end{cases} \tag{12}$$

where μ_{13}^0 is the constant material parameter of the interface mobility and ε governs the transition zone illustrated in Figure 3. For the simulations presented in this work $\varepsilon = 1$

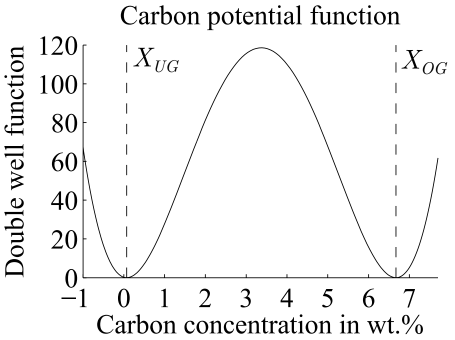

Figure 2: Double well function for the Cahn-Hilliard equation

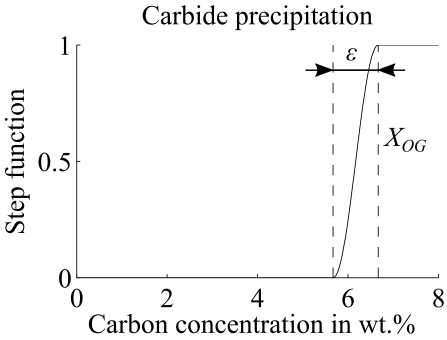

Figure 3: Step function for carbide precipitation

is used. The advantage in extending the interface mobility parameter rather than the change of Gibbs energy ΔG, is that the carbide nucleuses cannot decline to zero while the carbon concentration is low.

3 Numerical implementation

The system of partial differential equations (6), (9), (11) and (12) is solved using a finite element method in space. The resulting nonlinear system of equations is solved with Newton's method. In the two dimensional space quadrilateral elements with linear shape functions are used. The model described above has four unknowns per node: ferrite ϕ_1, austenite ϕ_2, carbide ϕ_3 and the carbon concentration c. Since the Cahn-Hilliard equation (11) has fourth-order derivatives the chemical potential η in equations (10) will also be used for discretization, thus leading to five unknowns per node: $\begin{bmatrix} c & \eta & \phi_1 & \phi_2 & \phi_3 \end{bmatrix}^T$.

The weak form of equation (6) with the test function ν_ϕ, using Gauss's theorem and homogeneous Neumann boundary conditions reads

$$\int_V \nu_\phi \dot{\phi}_i \, dV = \int_V \sum_{j=1, j\neq i}^{N_p} \mu_{ij} \Bigg[\sigma_{ij} \Bigg(\nabla \nu_\phi (\nabla \phi_j \phi_i - \nabla \phi_i \phi_j) - \frac{36}{\eta_{ij}^2} \nu_\phi \phi_i \phi_j (\phi_j - \phi_i) \Bigg) - \frac{6 \Delta G_{ij}}{\eta_{ij}} \nu_\phi \phi_i \phi_j \Bigg] \, dV. \quad (13)$$

The diffusion equation (11) can be written in weak form as

$$\int_V \nu_c \dot{c} \, dV - \int_V \nu_c \phi_1 M \nabla^2 \eta \, dV - \int_V \nu_c \nabla \phi_1 M \nabla \eta \, dV = 0, \quad (14)$$

where ν_c denotes the test function for the carbon concentration. Using Gauss's theorem and homogeneous boundary conditions we end with

$$\int_V \nu_c \dot{c} \; dV + \int_V \nabla \nu_c \phi_1 M \nabla \eta \; dV = 0. \tag{15}$$

Since the chemical potential should also be discretized the weak form of the evolution equation of η defined in equation (10.2) can be derived as

$$\int_V \nu_\eta \eta \; dV = \int_V \nu_\eta a \dot{c} + b \nabla \nu_\eta \nabla c + \nu_\eta d(\gamma c^3 + \beta c^2 + \alpha c + \xi) \; dV = 0 \tag{16}$$

with the derivative of the generalized carbon potential function

$$\begin{aligned} f'(c) &= \gamma c^3 + \beta c^2 + \alpha c + \xi \text{ , where} \\ \alpha &= -2X_{OG}^2 - 2X_{UG}^2 - 8X_{UG}X_{OG} \; , \\ \beta &= 6X_{OG} + 6X_{UG} \; , \\ \gamma &= -4 \; , \\ \xi &= 2X_{UG}X_{OG}^2 + 2X_{OG}X_{UG}^2 \; . \end{aligned} \tag{17}$$

x Nodal quantities are denoted by the superimposed hat $\hat{(\cdot)}$. The degrees of freedom at every node are $\underline{\hat{d}} = \left[\underline{\hat{c}} \;\; \underline{\hat{\eta}} \;\; \underline{\hat{\phi}_1} \;\; \underline{\hat{\phi}_2} \;\; \underline{\hat{\phi}_3}\right]^T$. The four shape functions per element are inside the row vector $\underline{N}$, so that the quantities c, η and the ϕ_i can be written as scalar products:

$$c = \underline{N}\underline{\hat{c}} \; , \qquad \eta = \underline{N}\underline{\hat{\eta}} \; , \qquad \phi_i = \underline{N}\underline{\hat{\phi}_i} \; , \quad i = 1, 2, 3. \tag{18}$$

For gradient terms the matrix $\underline{\underline{B}}$ is defined as

$$\underline{\underline{B}} = \begin{bmatrix} \underline{N}_{,x} \\ \underline{N}_{,y} \end{bmatrix}, \qquad \text{with} \qquad \underline{N}_{,x} = \frac{\partial \underline{N}}{\partial x}. \tag{19}$$

The gradients of the unknowns read

$$\nabla c = \underline{\underline{B}}\underline{\hat{c}} \; , \qquad \nabla \eta = \underline{\underline{B}}\underline{\hat{\eta}} \; , \qquad \nabla \phi_i = \underline{\underline{B}}\underline{\hat{\phi}_i} \; , \quad i = 1, 2, 3. \tag{20}$$

The test functions are formulated analogously. The time dependence is discretized with an implicit Euler method. Nodal quantities with a superscript $(\cdot)^{n-1}$ denote the solution of the last time step. The current one which is denoted by $(\cdot)^n$ is omitted for brevity.

A local residual vector can now be defined as $\underline{R} = [\underline{R}^c \;\; \underline{R}^\eta \;\; \underline{R}^{\phi_i}]^T$ with

$$\underline{R}^c = \int\limits_{\Omega_e} \frac{1}{\Delta t} \, \underline{N}^T \underline{N} \, d\Omega, \tag{21}$$

$$\begin{aligned} \underline{R}^\eta = \int\limits_{\Omega_e} a(\underline{N}^T \underline{N}) \cdot \frac{\hat{\underline{c}}^n - \hat{\underline{c}}^{n-1}}{\Delta t} + d\big(\xi + \alpha(\underline{N}^T \underline{N})\hat{\underline{c}} + \beta \underline{N}^T (\underline{N}\hat{\underline{c}})^2 \\ + \gamma \underline{N}^T (\underline{N}\hat{\underline{c}})^3\big) + b(\underline{B}^T \underline{B})\hat{\underline{c}} - (\underline{N}^T \underline{N})\hat{\underline{\eta}} \, d\Omega, \end{aligned} \tag{22}$$

$$\begin{aligned} \underline{R}^{\phi_i} = \int\limits_{\Omega_e} \underline{N}^T \underline{N} \, \frac{\hat{\underline{\phi}}_i^n - \hat{\underline{\phi}}_i^{n-1}}{\Delta t} + \sum_{j=1, j\neq i}^{N_p} \mu_{ij} \, \Bigg[\sigma_{ij}\Bigg(- (\underline{B}^T \underline{B})\hat{\underline{\phi}}_j \cdot (\underline{N}\hat{\underline{\phi}}_i) + (\underline{B}^T \underline{B})\hat{\underline{\phi}}_i \cdot (\underline{N}\hat{\underline{\phi}}_j) \\ - \frac{36}{\eta_{ij}^2} \underline{N}^T \underline{N}(\hat{\underline{\phi}}_i - \hat{\underline{\phi}}_j)(\underline{N}\hat{\underline{\phi}}_i) \cdot (\underline{N}\hat{\underline{\phi}}_j)\Bigg) + \frac{6}{\eta_{ij}} \Delta G_{ij} \underline{N}^T \cdot (\underline{N}\hat{\underline{\phi}}_i) \cdot (\underline{N}\hat{\underline{\phi}}_j)\Bigg] \, d\Omega. \end{aligned} \tag{23}$$

For Newton's method the tangent of the residual function $\underline{R}$ is needed:

$$\underline{K} = \frac{\partial \underline{R}}{\partial \hat{\underline{d}}} = \begin{bmatrix} \underline{K}^{cc} & \underline{K}^{c\eta} & \underline{K}^{c\phi_1} & \underline{0} & \underline{0} \\ \underline{K}^{\eta c} & \underline{K}^{\eta\eta} & \underline{0} & \underline{0} & \underline{0} \\ \underline{K}^{\phi_1 c} & \underline{0} & \underline{K}^{\phi_1\phi_1} & \underline{K}^{\phi_1\phi_2} & \underline{K}^{\phi_1\phi_3} \\ \underline{0} & \underline{0} & \underline{K}^{\phi_2\phi_1} & \underline{K}^{\phi_2\phi_2} & \underline{K}^{\phi_2\phi_3} \\ \underline{K}^{\phi_3 c} & \underline{0} & \underline{K}^{\phi_3\phi_1} & \underline{K}^{\phi_3\phi_2} & \underline{K}^{\phi_3\phi_3} \end{bmatrix}, \tag{24}$$

where the matrix entries are calculated as follows:

$$\begin{aligned} \underline{K}^{\phi_i\phi_i} = \frac{\partial R^{\phi_i}}{\partial \hat{\underline{\phi}}_i} = \int\limits_{\Omega_e} \underline{N}^T \underline{N} \frac{1}{\Delta t} + \sum_{j=1, j\neq i}^{N_p} \mu_{ij} \, \Bigg[\sigma_{ij}\Bigg((\underline{B}^T \underline{B})(\underline{N}\hat{\underline{\phi}}_j) \\ - (\underline{B}^T \underline{B})(\underline{N}\hat{\underline{\phi}}_i) - \frac{36}{\eta_{ij}^2} \underline{N}^T \underline{N}(\underline{N}\hat{\underline{\phi}}_j) \cdot (2 \cdot \hat{\underline{\phi}}_i - \hat{\underline{\phi}}_j)\Bigg) + \frac{6}{\eta_{ij}} \Delta G_{ij} \underline{N}^T \underline{N} \cdot (\underline{N}\hat{\underline{\phi}}_j)\Bigg] \, d\Omega, \end{aligned} \tag{25}$$

$$\begin{aligned} \underline{K}^{\phi_i\phi_j} = \frac{\partial R^{\phi_i}}{\partial \hat{\underline{\phi}}_j} = \int\limits_{\Omega_e} \mu_{ij} \, \Bigg[\sigma_{ij}\Bigg(- (\underline{B}^T \underline{B})(\underline{N}\hat{\underline{\phi}}_i) \\ + (\underline{B}^T \underline{B})\hat{\underline{\phi}}_i \cdot \underline{N} - \frac{36}{\eta_{ij}^2} \underline{N}^T \underline{N}(\underline{N}\hat{\underline{\phi}}_i) \cdot (\underline{N} \cdot (\hat{\underline{\phi}}_i - 2\hat{\underline{\phi}}_j)\Bigg) + \frac{6}{\eta_{ij}} \Delta G_{ij} \underline{N}^T \underline{N} \cdot (\underline{N}\hat{\underline{\phi}}_i)\Bigg] \, d\Omega, \end{aligned} \tag{26}$$

$$
\begin{aligned}
\underline{K}^{\phi_1 c} = \frac{\partial R^{\phi_1}}{\partial \underline{\hat{c}}} = \int\limits_{\Omega_e} \frac{\partial \mu_{13}}{\partial \underline{\hat{c}}} \Bigg[\sigma_{ij} \Bigg(&- (\underline{B}^T \underline{B}) \underline{\hat{\phi}}_3 \cdot (\underline{N} \underline{\hat{\phi}}_1) + (\underline{B}^T \underline{B}) \underline{\hat{\phi}}_1 \cdot (\underline{N} \underline{\hat{\phi}}_3) \\
&- \frac{36}{\eta_{ij}^2} \underline{N}^T \underline{N} (\underline{\hat{\phi}}_1 - \underline{\hat{\phi}}_3)(\underline{N} \underline{\hat{\phi}}_1) \cdot (\underline{N} \underline{\hat{\phi}}_3) \Bigg) + \frac{6}{\eta_{ij}} \Delta G_{ij} (\underline{N}^T \underline{N}) \underline{\hat{\phi}}_1 \cdot (\underline{N} \underline{\hat{\phi}}_3) \Bigg] \cdot \underline{N} \, d\Omega, \quad (27)
\end{aligned}
$$

$$
\begin{aligned}
\underline{K}^{\phi_3 c} = \frac{\partial R^{\phi_3}}{\partial \underline{\hat{c}}} = \int\limits_{\Omega_e} \frac{\partial \mu_{31}}{\partial \underline{\hat{c}}} \Bigg[\sigma_{ij} \Bigg(&- (\underline{B}^T \underline{B}) \underline{\hat{\phi}}_1 \cdot (\underline{N} \underline{\hat{\phi}}_3) + (\underline{B}^T \underline{B}) \underline{\hat{\phi}}_3 \cdot (\underline{N} \underline{\hat{\phi}}_1) \\
&- \frac{36}{\eta_{ij}^2} \underline{N}^T \underline{N} (\underline{\hat{\phi}}_3 - \underline{\hat{\phi}}_1)(\underline{N} \underline{\hat{\phi}}_3) \cdot (\underline{N} \underline{\hat{\phi}}_1) \Bigg) + \frac{6}{\eta_{ij}} \Delta G_{ij} (\underline{N}^T \underline{N}) \underline{\hat{\phi}}_3 \cdot (\underline{N} \underline{\hat{\phi}}_1) \Bigg] \cdot \underline{N} \, d\Omega, \quad (28)
\end{aligned}
$$

$$
\underline{K}^{cc} = \int\limits_{\Omega_e} \frac{1}{\Delta t} \cdot \underline{N}^T \underline{N} \, d\Omega, \quad (29)
$$

$$
\underline{K}^{\eta\eta} = \int\limits_{\Omega_e} -\underline{N}^T \underline{N} \, d\Omega, \quad (30)
$$

$$
\underline{K}^{c\eta} = \int\limits_{\Omega_e} M \cdot (\underline{N} \underline{\hat{\phi}}_1) \underline{B}^T \underline{B} \, d\Omega, \quad (31)
$$

$$
\begin{aligned}
\underline{K}^{\eta c} = \int\limits_{\Omega_e} \frac{a}{\Delta t} \cdot \underline{N}^T \underline{N} - b \cdot \underline{B}^T \underline{B} + d(\alpha \cdot (\underline{N}^T \underline{N}) - 2\beta \cdot (\underline{N}^T \underline{N}) \cdot (\underline{N} \underline{\hat{c}}) \\
- 3\gamma \cdot (\underline{N}^T \underline{N}) \cdot (\underline{N} \underline{\hat{c}})^2) \, d\Omega, \quad (32)
\end{aligned}
$$

$$
\underline{K}^{c\phi_1} = \frac{\partial R^c}{\partial \underline{\hat{\phi}}_1} = \int\limits_{\Omega_e} M \cdot \big(\underline{N} (\underline{B}^T \underline{B}) \big) \, \underline{\hat{\eta}} \, d\Omega. \quad (33)
$$

To evaluate the integrals a Gauss-Legendre rule is used.

4 Numerical examples

4.1 Basics

In this section three numerical examples for lower bainitic transformation are presented. The evolution of a ferrite nucleus and the ensuing diffusion of carbon within this phase are

Parameter	**Symbol**	**Value/Unit**
Strength of the anisotropy	s	0.5
Maximum carbon concentration in ferrite	X_{UG}	0.0704 wt.% [12]
Maximum carbon concentration in steel	X_{OG}	6.67 wt.% [24]
Bainitic main growth direction	θ_0	0°
Cahn-Hilliard viscosity factor	a	0.00002 s
Cahn-Hilliard balance factor	b	$0.00016\ \mathrm{µm}^2$
Cahn-Hilliard potential factor	d	$0.014\ \frac{1}{\mathrm{µm}^2}$
Diffusion coefficient in bainitic ferrite	M	$0.02\ \frac{\mathrm{µm}^2}{\mathrm{s}}$
Bainitic ferrite/austenite interface energy	σ_{12}	$0.001\ \frac{\mathrm{J}}{\mathrm{µm}^2}$
Bainitic ferrite/carbide interface energy	σ_{13}	$0.001\ \frac{\mathrm{J}}{\mathrm{µm}^2}$
Austenite/carbide interface energy	σ_{23}	$0\ \frac{\mathrm{J}}{\mathrm{µm}^2}$
Bainitic ferrite/austenite interface mobility	μ_{12}	$0.5\ \frac{\mathrm{µm}^4}{\mathrm{Js}}$
Bainitic ferrite/carbide interface mobility	μ_{13}^0	$0.5\ \frac{\mathrm{µm}^4}{\mathrm{Js}}$
Austenite/carbide interface mobility	μ_{23}	$0\ \frac{\mathrm{µm}^4}{\mathrm{Js}}$
Gibbs free energy between bainitic ferrite and austenite	ΔG_{12}	$1.07\ \frac{\mathrm{J}}{\mathrm{µm}^3}$
Gibbs free energy between bainitic ferrite and carbide	ΔG_{13}	$-0.865\ \frac{\mathrm{J}}{\mu\mathrm{m}^3}$
Gibbs free energy between austenite and carbide	ΔG_{23}	$0\ \frac{\mathrm{J}}{\mathrm{µm}^3}$
Interfacial thickness	η_{ij}	$0.17\mu\mathrm{m}$

Table 1: Material parameters for the phase-field method and the Cahn-Hilliard equation.

calculated. The precipitation of carbides completes the simulations. The first example “Low carbon” starts with initially 1.93 wt.% and the second one with 3.0 wt.%. Small randomly distributed perturbations are added to both initial conditions. The third example starts without perturbations in the carbon field and exactly 1.93 wt.% of carbon concentration. All remaining parameters do not change.

In materials science it is common sense that the bainitic nucleation is based on preformed nucleuses [29]. Therefore a small nucleus of ferrite is implemented as an initial condition. The growth of the bainitic sheaf will start at this nucleus. Furthermore very weak nucleuses (around $\phi_3 = 0.01$) of carbide are randomly distributed over the domain. The austenite phase completes to one. For physical reasons all variable fields are implemented with homogeneous Neumann boundary conditions.

Table 1 shows all required parameters for the model. Most of the them are only tentative and are an issue for further investigations. They are used as a working solution to qualitatively model lower bainitic transformations. Some of them may be determined with the CALPHAD method [12]. The parameters depend on the actual alloy and the transformation temperature (e.g. $\Delta G_{ij}(T)$). Due to the small interfacial thickness, a very fine discretization of the 3 µm × 3 µm area is needed. For the following examples a grid with 16384 elements and an edge length of 0.0234 µm is used to have at least 7 elements for the diffuse interfaces which have a width of $\eta_{ij} = 0.17\,\mu\text{m}$. The results of all three simulations show a phase transition over a period of 30 s discretized with a step size of $\Delta t = 0.05\,\text{s}$.

4.2 Example 1: Low carbon

a) Austenite

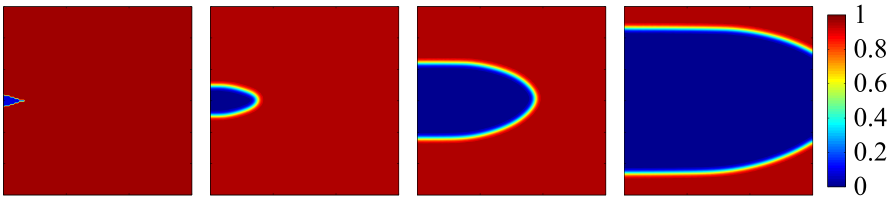

b) Bainitic ferrite

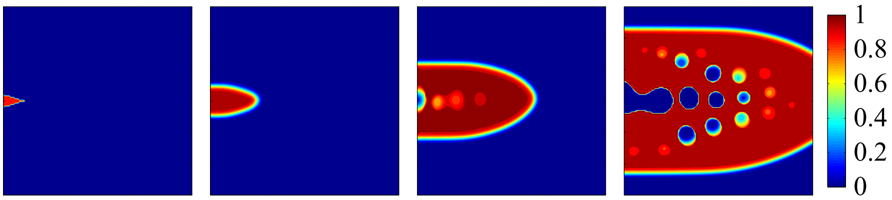

c) Carbon concentration

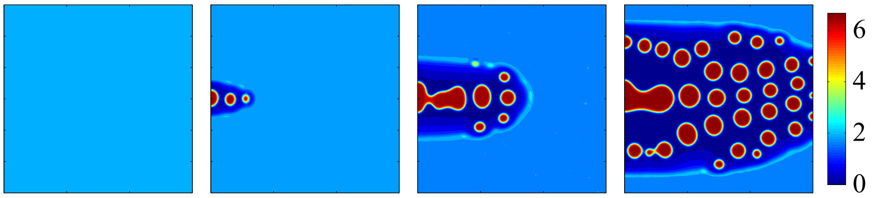

d) Carbide

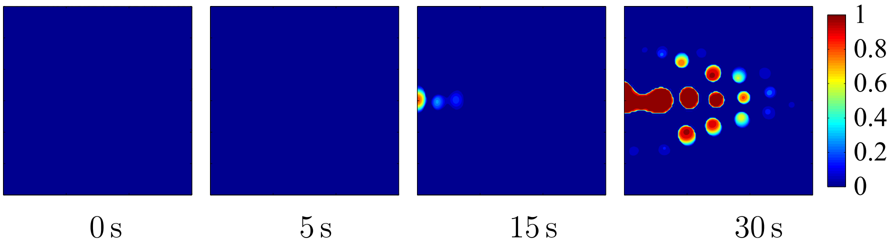

Figure 4: Example 1: Lower bainitic transformation after 0 s, 5 s, 15 s and 30 s.

Figure 4 shows the evolution of the three phases and the carbon concentration of Example 1. Part a) shows the austenite, part b) the bainitic ferrite, c) shows the carbon concentration and d) the carbide phase. The initial conditions can be seen in the left column. As described in Subsection 4.1 a small nucleus of bainitic ferrite is introduced

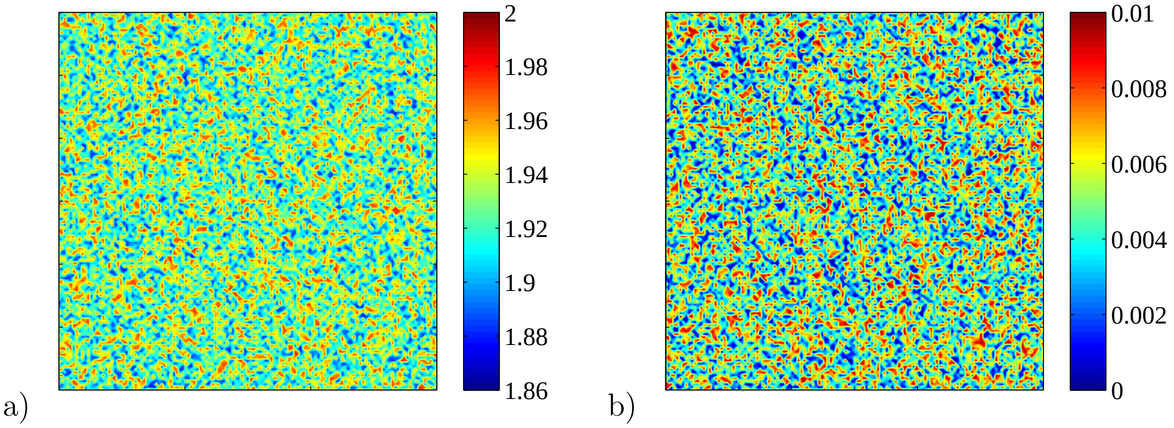

Figure 5: Example 1: Initial conditions of a) carbon concentration and b) carbide phase.

on the left side. The carbon concentration and the carbides are uniformly distributed with small randomly distributed perturbations which can be seen in Figure 5 due to the different scale. The second column of Figure 4 shows the fields after 5 s. It can be seen that the sharp interfaces of the initial conditions between the austenite and the bainitic ferrite become diffuse and the sheaf grows. The carbon starts to diffuse within the bainitic ferrite and build accumulations. These accumulations have globular or elliptical shapes. As shown in Section 2.3 the segregation of carbon can only take place within the bainitic ferrite. There are no visible changes in the carbide phase. The third column shows the results after 15 s. The bainitic sheaf grows and within the ferrite the old carbon accumulations merge to a larger one while new accumulations grow near the boundary of the sheaf. The new ones have an elliptical shape again. One carbide on the left boundary is now visible. In addition two small nucleuses of carbide grow within the bainitic sheaf at places with maximum carbon concentration. The last column in Figure 4 shows the results of the simulation after 30 s. The bainitic sheaf nearly fills the whole domain. In addition to the merged carbon accumulations there are many smaller elliptical accumulations which grow along with the moving interface. There are more carbides now. The carbides have the same shape as the carbon accumulations.

Figure 6 additionally shows the phases and the carbon concentration over time at two points. The point P_1 in Figure 6.a is located at $x = 1.5\,\mu\text{m}$, $y = 1.5\,\mu\text{m}$, point P_2 in Figure 6.b at $x = 2\,\mu\text{m}$, $y = 2\,\mu\text{m}$. The left axis is used for the carbon concentration in wt.% while the right axis is the scale for the phases varying between zero and one. The phases plotted are austenite, bainitic ferrite, carbide and the sum of all phases. The sum is just an error variable, which stays perfectly at one at all time. At the beginning austenite is the dominating phase at both points. All other phases are close to zero. The

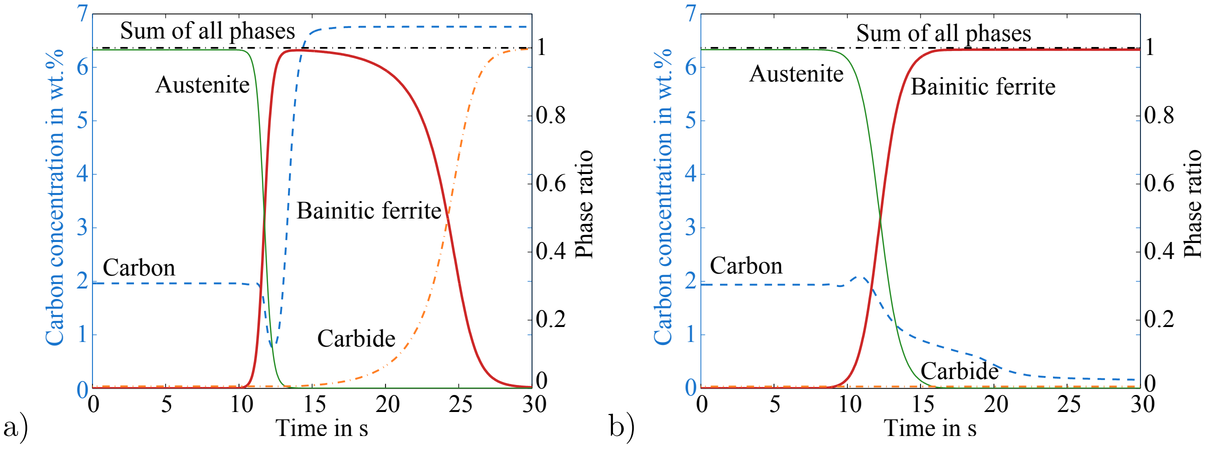

Figure 6: Example 1: Phases and carbon concentration over time at points a) P_1 ($x = 1.5\,\mu\mathrm{m}$, $y = 1.5\,\mu\mathrm{m}$) and b) P_2 ($x = 2\,\mu\mathrm{m}$, $y = 2\,\mu\mathrm{m}$)

carbon concentration has its initial condition at around 1.93 wt.%. This concentration does not change until the phase transition starts. In Figure 6.a the carbon concentration declines firstly when the bainitic phase starts to grow. However after a short time period the concentration increases. The chosen point is placed within a carbon accumulation, but not in the center of it. That is why the carbon concentration starts to decrease but than rises to its maximum value of $X_{OG} = 6.67$ wt.%. Shortly after the carbon concentration reaches the top the bainitic ferrite declines and the carbide starts to precipitate. At 30 s the phase transformation between bainitic ferrite and carbide is completed. Figure 6.b shows the evolution of the phases at a point with minimum carbon concentration. The carbon starts to diffuse right after the bainitic ferrite starts to grow but than it converges to the minimum concentration. That is why the carbide phase stays zero and the bainitic ferrite becomes the dominating phase at this local point.

4.3 Example 2: High carbon

The second example has 3.0 wt.% carbon and the initial nucleus of bainitic ferrite has a slightly different shape as can be seen in Figure 7. Here again initial conditions for the carbon concentration and the carbide phase as seen in Figure 5 are applied. After 5 s the bainitic nucleus has grown. Within this supersaturated nucleus the carbon moves to build maxima surrounded by an area with nearly no carbon left. In contrast to Example 1 the largest carbon accumulation has a lamellar shape. There are no carbides visible yet. The plots of the next instant of time show more lamellar carbon accumulations. One carbide at the left boundary and shades of more growing carbides are already visible. The last column shows the results after 30 s. Comparing the carbon field with the one at $t = 15\,\mathrm{s}$ it can be observed that some accumulations merge. The main difference between the two examples is the shape of the carbides. The initial carbon concentration differs while all other parameters, initial and boundary conditions are the same. Due to this it can be said that the initial carbon concentration influences the shape of the carbides significantly.

a) Austenite

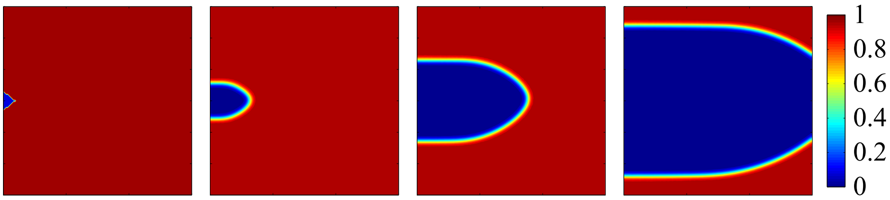

b) Bainitic ferrite

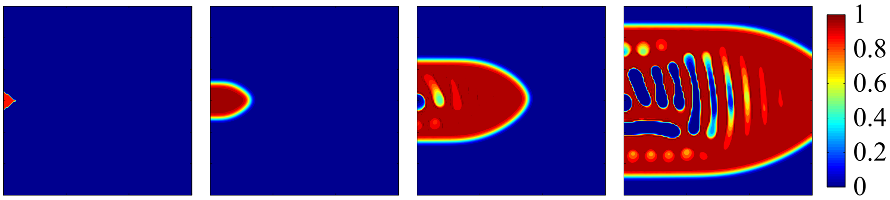

c) Carbon concentration

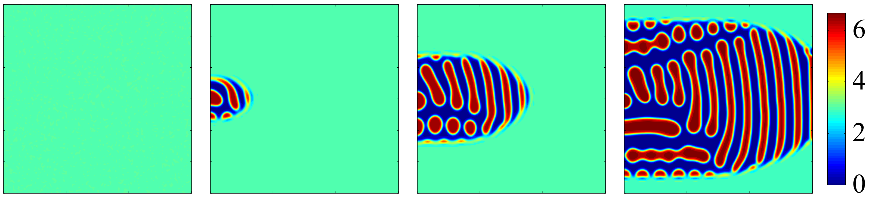

d) Carbide

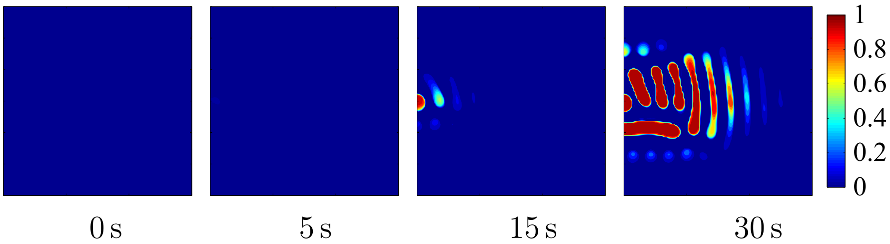

Figure 7: Example 2: Lower bainitic transformation after 0 s, 5 s, 15 s and 30 s: a) Austenite, b) Bainitic ferrite, c) Carbon concentration in wt.%, d) Carbides.

The results for two points are plotted over time in Figure 8. The diagrams show the carbon concentration, the bainitic ferrite, austenite, carbides and the sum of phases over the time measured in seconds. The scale of the carbon concentration is on the left side

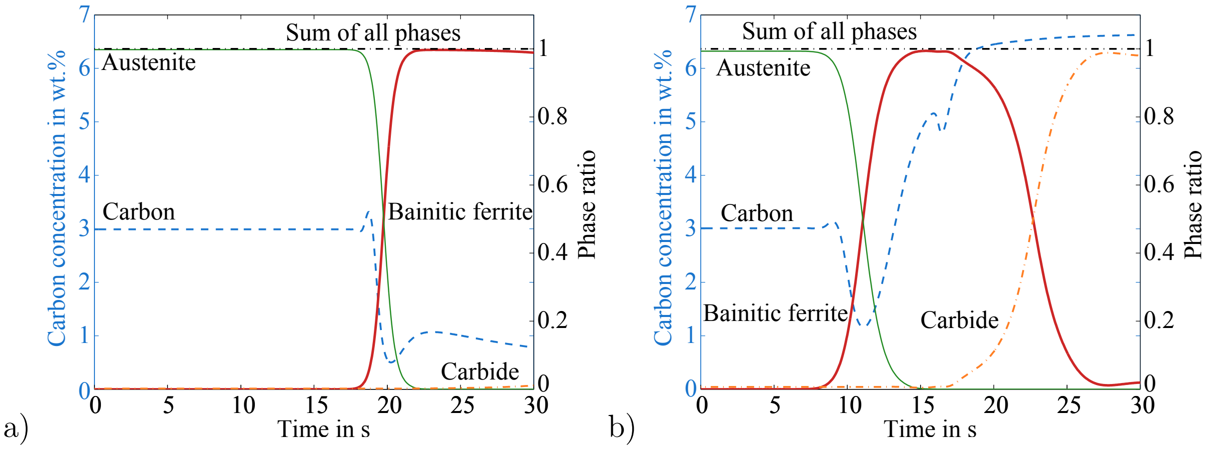

Figure 8: Example 2: Phases and carbon concentration over time at points a) P_2 ($x = 2\,\mu m$, $y = 2\,\mu m$) and b) P_3 ($x = 0.5\,\mu m$, $y = 1\,\mu m$)

and the values are given in wt.% whereas the phases are measured on the right axis. The point plotted in Figure 8.a is located in a ferrite area. After about 13 s the austenite starts to transform to bainitic ferrite. That is exactly the time when carbon starts to diffuse, because the new built ferrite is supersaturated. After a short wave, the carbon declines. Due to this, the carbide does not even start to grow at this location. It remains constant close to zero, at its initial value.

The phase transformation plotted in Figure 8.b is more complex. The bainitic transformation starts in the same way with a growing bainitic ferrite phase. Then the carbon starts to diffuse. It runs through some ups and downs until it reaches its maximum concentration $X_{OG} = 6.67\,\mathrm{wt.\%}$. Because of this the carbide phase slowly starts to grow while the bainitic ferrite decreases in the same way. At the end of the simulation this material point consists of nearly 100 % carbide. The sum of the phases is one all the time.

4.4 Example 3: Influence of the initial carbon perturbation

The results above show that the shapes of the carbides vary dependent on the average initial carbon concentration. Other numerical examples also show a dependence on the perturbation of the initial carbon concentration. In this third example the initial perturbation of the carbon is disabled. All other parameters are the same as in Example 1. Figure 9 shows the carbon concentration of Example 3 in part a) and of Example 1 in part b) at the same time. While in Example 1 the diffusion in the supersaturated ferrite starts directly, it takes about 16 s to start the diffusion without any perturbation. As a result of this the carbon accumulations are smaller, the carbides precipitate later and

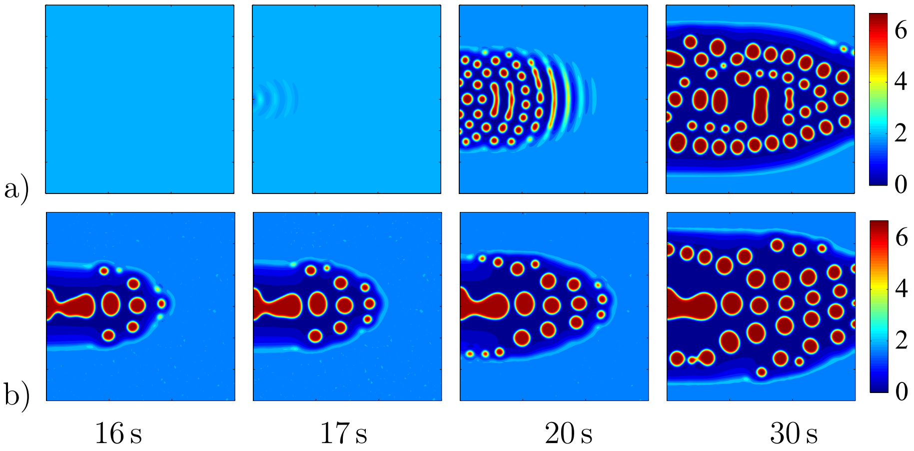

Figure 9: Carbon concentration in wt.%: a) Example 3 without and b) Example 1 with initial perturbations.

their extensions are also smaller.

5 Conclusions and outlook

In this work, a phase-field model to simulate the formation of lower bainite is presented. Simulations showing the described transformation kinetics are performed. The microstructure evolution including the coupled carbon diffusion is successfully shown. A single bainitic sheaf grows during isothermal transformation by means of the phase-field method. Within the bainitic sheaf carbon starts to diffuse governed by the Cahn-Hilliard equation. At places where the carbon concentration reaches its maximum carbides precipitate. As demonstrated in the examples the carbides may have lamellar or globular shapes.

However, parameter identification has not been taken into account in this work. This will be done in future work using the CALPHAD method. Besides it will be necessary to simulate the carbide precipitation within the residual austenite. A coupling with the mechanical problem will be introduced in further work to improve the anisotropic phase growth and goal-oriented adaptivity [30] might be a worthwhile objective.

References

[1] H. K. D. H. Bhadeshia, Bainite in steels, 2nd Edition, Maney Materials Science, 2001.

[2] M. E. Gurtin, Generalized Ginzburg-Landau and Cahn-Hilliard equations based on a microforce balance, Physica D: Nonlinear Phenomena 92 (3) (1996) 178–192.

[3] I. Steinbach, Phase-field models in materials science, Modelling and simulation in materials science and engineering 17 (7) (2009) 1–31.

[4] M. Militzer, M. Mecozzi, J. Sietsma, S. van der Zwaag, Three-dimensional phase field modelling of the austenite-to-ferrite transformation, Acta Materilia 54 (15) (2006) 3961–3972.

[5] C.-J. Huang, D. J. Browne, S. McFadden, A phase-field simulation of austenite to ferrite transformation kinetics in low carbon steels, Acta Materilia 54 (2005) 11–21.

[6] I. Steinbach, M. Apel, The influence of lattice strain on pearlite formation in fe-c, Acta Materialia 55 (14) (2007) 4817–4822.

[7] A. Yamanaka, T. Takaki, Y. Tomita, Phase-Field Simulation of Austenite to Ferrite Transformation and Widmanstätten Ferrite Formation in Fe-C Alloy, Materials Transactions 47 (11) (2006) 2725–2731.

[8] A. Yamanaka, T. Takaki, Y. Tomita, Elastoplastic phase-field simulation of self-and plastic accommodations in cubic tetragonal martensitic transformation, Materials Science and Engineering: A 491 (1) (2008) 378–384.

[9] R. Schmitt, R. Müller, C. Kuhn, H. M. Urbassek, A phase field approach for multivariant martensitic transformations of stable and metastable phases, Archive of Applied Mechanics 83 (6) (2013) 849–859.

[10] K. Ammar, Modelling and Simulation of Phase Transformation-Mechanics coupling Using a Phase Field Method, Ph.D. thesis, l'École nationale supérieure des mines de Paris (2010).

[11] T. Arif, R. Qin, A phase-field model for bainitic transformation, Computational Materials Science 77 (2013) 230–235.

[12] W. Song, U. Prahl, W. Bleck, K. Mukherjee, Phase-field simulations of bainitic phase transformation in 100cr6, TMS 2011 140th Annual Meeting and Exhibition (2011) 417–425.

[13] G. Sidhu, S. Bhole, D. Chen, E. Essadiqi, An improved model for bainite formation at isothermal temperatures, Scripta Materialia 64 (1) (2011) 73–76.

[14] R. Garrett, S. Xu, J. Lin, T. Dean, A model for predicting austenite to bainite phase transformation in producing dual phase steels, International Journal of Machine Tools and Manufacture 44 (7) (2004) 831–837.

[15] A. Lambert-Perlade, A.-F. Gourgues, A. Pineau, Austenite to bainite phase transformation in the heat-affected zone of a high strength low alloy steel, Acta Materialia 52 (8) (2004) 2337–2348.

[16] R. Mahnken, A. Schneidt, T. Antretter, U. Ehlenbröker, M. Wolff, Multi-scale modeling of bainitic phase transformation in multi-variant polycrystalline low alloy steels, International Journal of Solids and Structures 54 (2015) 156–171.

[17] R. Mahnken, A. Schneidt, S. Tschumak, H. Maier, On the simulation of austenite to bainite phase transformation, Computational Materials Science 50 (6) (2011) 1823–1829.

[18] I. Steinbach, F. Pezzolla, B. Nestler, M. Seeßelberg, R. Ptieler, G. Schmitz, J. Rezende, A phase field concept for multiphase systems, Physica D 94 (1996) 135–147.

[19] J. Tiaden, B. Nestler, H. Diepers, I. Steinbach, The multiphase-field model with an integrated concept for modelling solute diffusion, Physica D: Nonlinear Phenomena 115 (1) (1998) 73–86.

[20] M. Mecozzi, J. Sietsma, S. van der Zwaag, M. Apel, P. Schaffnit, I. Steinbach, Analysis of the $\gamma \rightarrow \alpha$ Transformation in a C-Mn Steel by Phase-Field Modeling, Metallurgical and Materials Transactions A 36A (2005) 2327–2340.

[21] G. B. McFadden, A. A. Wheeler, R. J. Braun, S. R. Coriell, R. F. Sekerkat, Phase-field models for anisotropic interfaces, Physical Review E 48 (3) (1993) 2016–2024.

[22] R. Kobayashi, Modeling and numerical simulations of dendritic crystal growth, Physica D 63 (1993) 410–423.

[23] D. Jiang, E. Carter, Carbon dissolution and diffusion in ferrite and austenite from first principles, Physical Review B 67 (21) (2003) 214103.

[24] D. Horstmann, Das Zustandsschaubild Eisen-Kohlenstoff und die Grundlagen der Wärmebehandlung der Eisenkohlenstoff-Legierungen., Stahleisen, Ddf., 1985.

[25] C. M. Elliott, D. A. French, Numerical studies of the Cahn-Hilliard equation for phase separation, IMA Journal of Applied Mathematics 38 (2) (1987) 97–128.

[26] C. M. Elliott, Z. Songmu, On the Cahn-Hilliard equation, Archive for Rational Mechanics and Analysis 96 (4) (1986) 339–357.

[27] R. L. Pego, Front migration in the nonlinear Cahn-Hilliard equation, Proceedings of the Royal Society of London. A. Mathematical and Physical Sciences 422 (1863) (1989) 261–278.

[28] W. Dreyer, C. Guhlke, Sharp limit of the viscous cahn–hilliard equation and thermodynamic consistency, Continuum Mechanics and Thermodynamics (2015) 1–22.

[29] G. Olson, H. Bhadeshia, M. Cohen, Coupled Diffusional / Displacive Transformations, Acta Metallurgica 37 (2) (1989) 381–389.

[30] R. Mahnken, Goal-oriented adaptive refinement for phase field modeling with finite elements, International Journal for Numerical Methods in Engineering 94 (4) (2013) 418–440.

Appendix

The aim of this appendix is to derive relationships between the four basic parameters $\epsilon_{ij}, a_{ij}, \tau_{ij}, m_{ij}$ of equation (4) and the physical material parameters, interface mobility μ_{ij}, interface energy σ_{ij}, interface thickness η_{ij} and the change of Gibbs energy ΔG_{ij}. The results are shown in equations (5). The change of coefficients will here be done using a two phases model for brevity. With $N_p = 2$, $\phi_j = (1-\phi_i)$ and $\nabla\phi_j = -\nabla\phi_i$ it follows from equation (4)

$$\begin{aligned}
\dot{\phi}_i &= \frac{1}{\tau_{ij}}\left[\epsilon_{ij}\big((1-\phi_i)\nabla^2\phi_i - \phi_i\nabla(-\nabla\phi_i)\big) - \frac{\phi_i(1-\phi_i)}{2a_{ij}}(1-\phi_i-\phi_i-2m_{ij})\right] \\
&= \frac{1}{\tau_{ij}}\left[\epsilon_{ij}\big(\nabla^2\phi_i - \phi_i\nabla^2\phi_i + \phi_i\nabla^2\phi_i\big) - \frac{\phi_i(1-\phi_i)}{2a_{ij}}(1-2\phi_i-2m_{ij})\right] \\
&= \frac{1}{\tau_{ij}}\left[\epsilon_{ij}\nabla^2\phi_i - \frac{\phi_i(1-\phi_i)}{a_{ij}}\left(\frac{1}{2}-\phi_i\right) + \frac{\phi_i(1-\phi_i)}{a_{ij}}m_{ij}\right] \\
&= \frac{1}{\tau_{ij}}\left[\epsilon_{ij}\nabla^2\phi_i - \frac{1}{a_{ij}}\phi_i(1-\phi_i)\left(\frac{1}{2}-\phi_i\right) + \frac{m_{ij}}{a_{ij}}\phi_i(1-\phi_i)\right]. \qquad \text{(A.1)}
\end{aligned}$$

For the next steps we define:

$$\dot{\phi} := \dot{\phi}_\alpha, \qquad \tau := \tau_{ij}, \qquad \gamma := \frac{1}{a_{ij}}, \qquad \epsilon := \epsilon_{ij}, \qquad m := \frac{m_{ij}}{a_{ij}}. \tag{A.2}$$

With equation (A.2) equation (A.1) can be written as [20, 3]

$$\tau\dot{\phi} = \epsilon\nabla^2\phi - \gamma\phi(1-\phi)\left(\frac{1}{2}-\phi\right) + m\phi(1-\phi). \tag{A.3}$$

According to [20] and [3] the stationary one-dimensional solution for equation (A.3) is

$$\phi(x) = \frac{1}{2}\tanh\left(\frac{3x}{\eta}\right) + \frac{1}{2}, \tag{A.4}$$

where the boundary values of the interface are $\phi(x = -\eta/2) \approx 0.05$ and $\phi(x = \eta/2) \approx 0.95$ as shown in Figure 10.a.

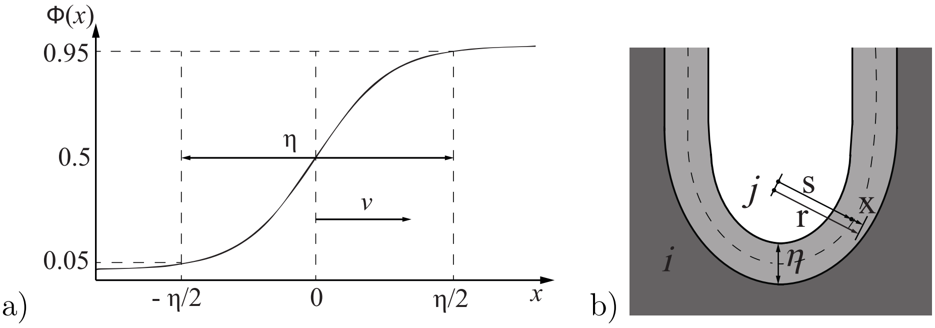

Figure 10: a) Stationary one-dimensional solution, b) two-phase model [20]

The two-phase model can be plotted schematically as shown in Figure 10.b. The two coordinates s and r are introduced. Both are parallel to the x coordinate. The current location of the interface center is described by s. The r coordinate is the corresponding cylindrical coordinate. From Figure 10 b) it is easy to see that

$$x = r - s \tag{A.5}$$

holds. The Laplacian operator in two-dimensional cylindrical coordinates is

$$\Delta\phi = \nabla^2\phi = \frac{\partial^2\phi}{\partial r^2} + \frac{1}{r}\frac{\partial\phi}{\partial r} + \frac{1}{r^2}\frac{\partial^2\phi}{\partial\varphi^2}. \tag{A.6}$$

With the assumption that the phase variable cannot change in the parallel direction to the interface (= φ direction),

$$\frac{\partial \phi}{\partial \varphi} = 0, \qquad \frac{\partial^2 \phi}{\partial \varphi^2} = 0 \tag{A.7}$$

it follows directly for equation (A.6)

$$\Delta \phi = \nabla^2 \phi = \frac{\partial^2 \phi}{\partial r^2} + \frac{1}{r}\frac{\partial \phi}{\partial r}. \tag{A.8}$$

Because x and r point to the same material point inside the interface, it follows that

$$\frac{\partial \phi}{\partial r} = \frac{\partial \phi}{\partial x}, \qquad \frac{\partial^2 \phi}{\partial r^2} = \frac{\partial^2 \phi}{\partial x^2}. \tag{A.9}$$

The equations (A.8) and (A.9) inserted into (A.3) yield

$$\tau \dot{\phi} = \epsilon \left[\frac{\partial^2}{\partial x^2} + \frac{1}{r}\frac{\partial}{\partial x} \right] \phi - \gamma \phi (1-\phi) \left(\frac{1}{2} - \phi \right) + m \phi (1-\phi). \tag{A.10}$$

The time derivative of the phase-field variable can be determined by the chain rule:

$$\dot{\phi} = \frac{\partial \phi}{\partial t} = \frac{\partial \phi}{\partial x}\frac{\partial x}{\partial t} = \frac{\partial \phi}{\partial x} v. \tag{A.11}$$

The variable v is the velocity of the interface. It is assumed that the interface thickness η is constant. With (A.11) it follows for (A.10)

$$\left[\tau v - \epsilon \frac{1}{r} \right] \frac{\partial \phi}{\partial x} - \epsilon \frac{\partial^2 \phi}{\partial x^2} = -\gamma \phi (1-\phi) \left(\frac{1}{2} - \phi \right) + m \phi (1-\phi). \tag{A.12}$$

To determine the derivatives of the stationary solution, it is firstly converted into its exponential notation

$$\phi(x) = \frac{1}{2} \tanh \left(\frac{3x}{\eta} \right) + \frac{1}{2} = \frac{e^{(6x/\eta)}}{e^{(6x/\eta)} + 1}. \tag{A.13}$$

The derivatives are then

$$\frac{\partial \phi}{\partial x} = \frac{6e^{(6x/\eta)}}{\eta\left(e^{(6x/\eta)}+1\right)^2} = \frac{6}{\eta}\,\frac{e^{(6x/\eta)}}{e^{(6x/\eta)}+1}\,\frac{1}{e^{(6x/\eta)}+1} = \frac{6}{\eta}\phi(1-\phi) \tag{A.14}$$

$$\begin{aligned}\frac{\partial^2 \phi}{\partial x^2} &= -\frac{36e^{(6x/\eta)}\left(e^{(6x/\eta)}-1\right)}{\eta^2\left(e^{(6x/\eta)}+1\right)^3} = \frac{72}{\eta^2}\,\frac{e^{(6x/\eta)}}{\left(e^{(6x/\eta)}+1\right)^2}\,\frac{-1\left(e^{(6x/\eta)}-1\right)}{2\left(e^{(6x/\eta)}+1\right)}\\ &= \frac{72}{\eta^2}\phi(1-\phi)\left(\frac{1}{2}-\phi\right)\end{aligned} \tag{A.15}$$

with

$$(1-\phi) = 1 - \frac{e^{(6x/\eta)}}{e^{(6x/\eta)}+1} = \frac{e^{(6x/\eta)}+1}{e^{(6x/\eta)}+1} - \frac{e^{(6x/\eta)}}{e^{(6x/\eta)}+1} = \frac{1}{e^{(6x/\eta)}+1} \tag{A.16}$$

and

$$\begin{aligned}\left(\frac{1}{2}-\phi\right) &= \frac{1}{2} - \frac{e^{(6x/\eta)}}{e^{(6x/\eta)}+1} = \frac{1}{2}\left(\frac{e^{(6x/\eta)}+1}{e^{(6x/\eta)}+1} - \frac{2e^{(6x/\eta)}}{e^{(6x/\eta)}+1}\right) = \frac{1}{2}\left(\frac{-e^{(6x/\eta)}+1}{e^{(6x/\eta)}+1}\right)\\ &= -\frac{1}{2}\left(\frac{e^{(6x/\eta)}-1}{e^{(6x/\eta)}+1}\right).\end{aligned} \tag{A.17}$$

The equations (A.14) and (A.15) inserted in (A.12) deliver

$$\left[\tau v - \epsilon\frac{1}{r}\right]\frac{6}{\eta} = \left(\epsilon\frac{72}{\eta^2}-\gamma\right)\left(\frac{1}{2}-\phi\right) + m. \tag{A.18}$$

Equation (A.18) becomes independent of ϕ once the product

$$\left(\epsilon\frac{72}{\eta^2}-\gamma\right)\left(\frac{1}{2}-\phi\right) = 0. \tag{A.19}$$

This will be the case if the condition

$$\gamma = \epsilon\frac{72}{\eta^2} \tag{A.20}$$

is fulfilled. Thus equation (A.18) simplifies to

$$v = \frac{\eta}{\tau}\left[\frac{\epsilon}{\eta}\,\frac{1}{r} + \frac{m}{6}\right]. \tag{A.21}$$

According to [3] the Gibbs-Thomson equation is

$$v = \mu \left[\sigma \kappa - \Delta f \right] \tag{A.22}$$

with the already known physical coefficients. The comparison of equation (A.21) with equation (A.22) allows one to obtain relationships between the phase-field parameters ($\epsilon_{ij}, a_{ij}, \tau_{ij}$ and m_{ij}) and the physical material parameters (μ_{ij}, σ_{ij}, η_{ij} and ΔG_{ij}):

$$\mu = \frac{\eta}{\tau}, \qquad \sigma = \frac{\epsilon}{\eta}, \qquad \kappa = \frac{1}{r}, \qquad \Delta f = -\frac{m}{6}. \tag{A.23}$$

After transposing and with equation (A.19) it follows

$$\epsilon = \sigma \eta \,, \qquad \gamma = 72 \frac{\sigma}{\eta} \,, \qquad \tau = \frac{\eta}{\mu} \,, \qquad m = -6 \Delta f \ . \tag{A.24}$$

The back substitution with equation (A.2) yields

$$\tau_{ij} = \frac{\eta_{ij}}{\mu_{ij}} \,, \qquad a_{ij} = \frac{\eta_{ij}}{72 \sigma_{ij}} \,, \qquad \epsilon_{ij} = \sigma_{ij} \eta_{ij} \,, \qquad m_{ij} = -6 \Delta G_{ij} a_{ij} \,, \tag{A.25}$$

where

$$\Delta f_{ij} = \Delta G_{ij} \tag{A.26}$$

and due to the symmetry

$$\epsilon_{ij} = \epsilon_{ji}, \qquad a_{ij} = a_{ji}, \qquad m_{ij} = -m_{ji}, \qquad \sigma_{ij} = \sigma_{ji}, \qquad \Delta G_{ij} = -\Delta G_{ji} \tag{A.27}$$

hold.

Paper B

M. Düsing and R. Mahnken

A thermodynamic framework for coupled multiphase Ginzburg-Landau/Cahn-Hilliard systems for simulation of lower bainitic transformation

Archive of Applied Mechanics 86 (12), 1947–1964, 2016

A thermodynamic framework for coupled multiphase Ginzburg–Landau/Cahn–Hilliard systems for simulation of lower bainitic transformation

Martin Düsing and Rolf Mahnken

Chair of Engineering Mechanics, Paderborn University,

Warburger Str. 100, 33098 Paderborn, Germany

Abstract

A thermodynamic framework for a coupled Ginzburg-Landau and Cahn-Hilliard system is presented in this work. It is based on the concept of generalized stresses and microforce balances as introduced by Gurtin (1996). His concept is extended to compute phase changes and diffusion simultaneously on the same domain and adding coupling terms between the quantities. The resulting thermodynamic framework distinguishes between basic balance laws which are universal and constitutive equations which depend on the specific material. As an application the transformation of austenite to lower bainite is simulated in this work. The multiphase field model describes the evolution of bainitic ferrite and the precipitation of carbides while the Cahn-Hilliard equation governs the carbon diffusion within the bainitic ferrite.

Keywords: Multiphase field method, Cahn-Hilliard diffusion, Lower bainitic transformation, Thermodynamic framework, Microforce balance

1 Introduction

The phase field method is widely used in materials science to model phase transformations [12, 26]. There are several approaches describing for example Widmanstätten formation

[30], austenite-to-martensite transformations [31, 23], austenite-to-ferrite [19, 14] and austenite-to-perlite transitions [27]. Phase-field approaches for the bainitic transformation are presented in [5, 25], however they do not consider the precipitation of carbides and are not based on a thermodynamic framework.

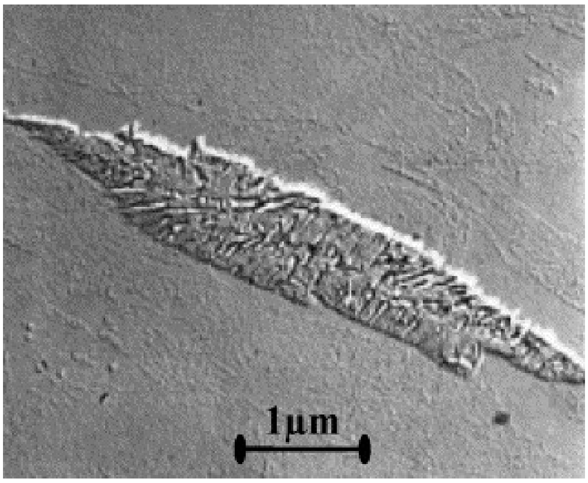

Figure 1: Lower bainite TEM image obtained by isothermal heat treated at 350 °C [22]. Reprinted from [22], © 2007 Elsevier B.V., with permission from Elsevier.

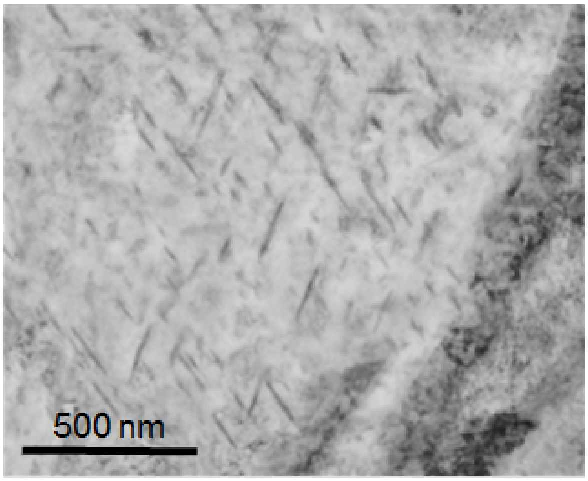

Figure 2: Lower bainite BFTEM micrograph. © Chair of Materials Science, Paderborn University.

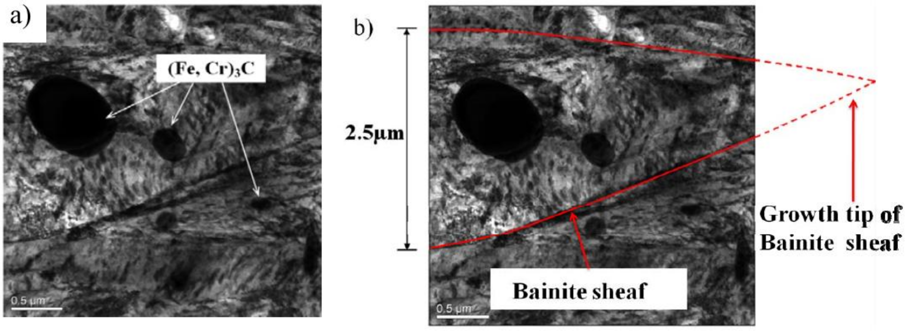

Figure 3: HRTEM micrograph of 100Cr6 isothermally heat treated at 260°C for 2500 s [25]. Reprinted from [25], © 2011 by The Minerals, Metals, & Materials Society, John Wiley & Sons, Inc., with permission from John Wiley & Sons, Inc.

The bainitic transformation starts with austenite and a uniformly distributed carbon concentration. During the isothermal heat treatment a phase called bainitic ferrite grows which can contain less carbon as austenite in its equilibrium state. The nuclei are called bainitic sheaves and consist of subunits. After the displacive transformation from austenite to bainitic ferrite at low temperatures, the ferrite is supersaturated with carbon, which therefore begins to diffuse [7]. Due to separation kinetics the carbon starts to build accumulations where subsequently carbides precipitate. All these processes are running within the bainitic ferrite phase while only a few carbides precipitate between the bainitic sheaves. This transformation is called lower bainitic transformation.

At higher temperatures the carbon can diffuse out of the bainitic ferrite and carbides precipitate within the austenite phase. The corresponding microstructure is called upper bainite, however not considered in this paper.

Figure 1 shows a micrograph of a lower bainitic sheaf transformed at 350 °C [22]. The sheaf has a typical plate-like form. The dark needles are small lenticular carbides at an angle of about $55° - 60°$ to the main growth direction of the sheaf [22]. They tend to adopt a single crystallographic variant [7]. Figure 2 presents a BFTEM micrograph at a smaller scale. Needle-like carbides within the bainitic sheaf can be seen here. Figure 3 shows an HRTEM micrograph of 100Cr6 isothermally heat treated at 260°C for 2500 s [25]. In contrast to Figures 1 and 2 there are rather large carbides with globular shapes within the lower bainite sheaf. More TEM micrographs can be found in the literature e.g. in [6, 15].

A continuum thermodynamic framework for Ginzburg-Landau and Cahn-Hilliard equations based on fundamental balance laws is proposed by Gurtin and Fried [10, 12] to derive a two-phase field model and a conservative diffusion model. In addition to balance laws of classical continuum mechanics they introduce a balance law for microforces considering generalized stresses, external forces and internal forces. These microforces perform work in conjunction with the time derivative of an order parameter ϕ which characterizes the configuration of atoms, for example a specific microstructure or phase. A multiphase field model coupled with deformation is introduced in [11]. The motivation lies in the strict separation between basic balance laws and constitutive equations as it is common in continuum mechanics. While constitutive equations may change for different materials the balance laws and especially the dissipation inequality must hold in any case. In other works [3, 2] the generalized Ginzburg-Landau formulation for a two-phase field model is extended with a diffusion equation by means of Fick's law.

The objective of this work is to extend the thermodynamic framework of [3, 2, 12] for a coupled Ginzburg-Landau – Cahn-Hilliard system considering an arbitrary number of phases. Our framework is based on the concept of generalized stresses, where microforces and microstresses for every phase and the concentration are introduced. In a prototype model the lower bainitic transformation, as described above, will be simulated using the thermodynamic framework. We consider an isothermal transformation from austenite to lower bainite, neglecting other phases like pearlite or martensite which may occur during a more complex cooling down process. Furthermore we neglect the influence of stresses and strains. The characteristic precipitation of carbides within the bainitic ferrite is modeled here, while the precipitation of carbides within the austenite, which is significant for upper bainite, is neglected. All these aspects are parts of future work.

This work is organized as follows. Section 2 describes the thermodynamic framework. It begins with the balances of microforces and the conservation of energy. Afterwards a Clausius-Duhem inequality is introduced to formulate restrictions for constitutive equations. Finally evolution equations are presented. In Section 3 a prototype model with corresponding constitutive equations is proposed to simulate the lower bainitic transformation. Especially the coupling between diffusion and phase transformation is applied. Section 4 gives an insight into the numerical implementation. Finally, Section 5 shows two representative examples for the coupled phase field - diffusion system to model the lower bainitic transformation and compares the results with the micrographs in Figures 1 - 3.

2 Thermodynamic framework

2.1 Balances of forces and conservation of energy

We introduce order parameters $\phi_i, i = 1, .., N_p$, to identify N_p different configurations of atoms which are denoted as phases. In order to describe the balance laws for the related multiphase field model a system of generalized forces with N_p *vector phase stresses* $\boldsymbol{\xi}_i$, *internal scalar phase forces* π_i and *external scalar phase forces* γ_i over the volume B is proposed. Given an arbitrary control volume V as a subregion of B the integrals

$$\int_V -\boldsymbol{\xi}_i \cdot \nabla\dot{\phi}_i \; dV, \quad \int_V \pi_i\dot{\phi}_i \; dV, \quad \int_V \gamma_i\dot{\phi}_i \; dV, \qquad i = 1, ..., N_p \tag{1}$$

characterize the power performed on the atomic configurations within V, which is an extension of the concept by Gurtin [12] and Ammar *et al.* [4] for one phase.

Over the volume B a concentration field c and its gradient ∇c are defined. In order to perform power, in the same manner as in terms (1), a *scalar internal diffusion force* ω and a *vector diffusion stress* $\boldsymbol{\lambda}$ are introduced

$$\int_V -\boldsymbol{\lambda} \cdot \nabla\dot{c} \; dV, \quad \int_V \omega\dot{c} \; dV. \tag{2}$$

Note, that an external force is not needed to derive the diffusion equation and therefore is skipped for brevity. The phase forces in (1) and the diffusion forces in (2) are also referred to as microforces. The stresses are referred to as microstresses in literature [12, 3]. The system of microforces and microstresses in (1) and (2) shall be consistent with the microforce balance for each control volume V

$$\sum_{i=1}^{N_p} \left(- \int_V \boldsymbol{\xi}_i \cdot \nabla \dot{\phi}_i \; dV + \int_V \pi_i \dot{\phi}_i \; dV + \int_V \gamma_i \dot{\phi}_i \; dV \right) - \int_V \boldsymbol{\lambda} \cdot \nabla \dot{c} \; dV + \int_V \omega \dot{c} \; dV = 0. \tag{3}$$

Using Gauss theorem renders

$$\begin{aligned} \sum_{i=1}^{N_p} \left(- \int_{\partial V} \boldsymbol{\xi}_i \cdot \dot{\phi}_i \;\; \cdot \boldsymbol{n} \; dA + \int_V \nabla \cdot \boldsymbol{\xi}_i \cdot \dot{\phi}_i \; dV + \int_V \pi_i \dot{\phi}_i \; dV + \int_V \gamma_i \dot{\phi}_i \; dV \right) & \\ - \int_{\partial V} \boldsymbol{\lambda} \cdot \dot{c} \;\; \cdot \boldsymbol{n} \; dA + \int_V \nabla \cdot \boldsymbol{\lambda} \cdot \dot{c} \; dV + \int_V \omega \dot{c} \; dV = 0, & \end{aligned} \tag{4}$$

where $\boldsymbol{n}$ is the outward unit normal vector to ∂V. Transforming equation (4) leads to

$$\begin{aligned} \sum_{i=1}^{N_p} \left(- \int_{\partial V} \boldsymbol{\xi}_i \cdot \dot{\phi}_i \;\; \cdot \boldsymbol{n} \; dA + \int_V \left(\nabla \cdot \boldsymbol{\xi}_i \cdot + \pi_i + \gamma_i \right) \dot{\phi}_i \; dV \right) & \\ - \int_{\partial V} \boldsymbol{\lambda} \cdot \dot{c} \;\; \cdot \boldsymbol{n} \; dA + \int_V \left(\nabla \cdot \boldsymbol{\lambda} + \omega \right) \dot{c} \; dV = 0. & \end{aligned} \tag{5}$$

Equation (5) is satisfied for any fields $\dot{\phi}_i$ and $\dot{c}$ if and only if

$$\nabla \cdot \boldsymbol{\xi}_i + \pi_i + \gamma_i = 0 \;\; \text{in} \;\; V \quad \text{for} \;\; i = 1, ..., N_p, \tag{6}$$

$$\nabla \cdot \boldsymbol{\lambda} + \omega = 0 \;\; \text{in} \;\; V, \tag{7}$$

$$\boldsymbol{\xi}_i \cdot \boldsymbol{n} = 0 \;\; \text{on} \;\; \partial V \quad \text{for} \;\; i = 1, ..., N_p, \tag{8}$$

$$\boldsymbol{\lambda} \cdot \boldsymbol{n} = 0 \;\; \text{on} \;\; \partial V. \tag{9}$$

The equations (6) and (7) express the *local microforce balances* while the equations (8) and (9) represent the Neumann boundary conditions.

According to the principle of conservation of energy and neglecting kinetic energy, the time derivative of the internal energy $\mathcal{E}$ is equal to the external power $\mathcal{P}^{\text{ext}}$

$$\dot{\mathcal{E}} = \mathcal{P}^{\text{ext}}. \tag{10}$$

The internal energy rate $\dot{\mathcal{E}}$ is related to a local internal energy rate $\dot{e}$ as

$$\dot{\mathcal{E}} = \int_V \dot{e}\; dV. \tag{11}$$

Following [2] the external power $\mathcal{P}^{\text{ext}}$ is equal to the negative internal power $\mathcal{P}^{\text{int}}$

$$\mathcal{P}^{\text{ext}} = -\mathcal{P}^{\text{int}}, \tag{12}$$

which is the sum of all powers on atoms of V with internal contribution in (1) and (2)

$$\mathcal{P}^{\text{int}} = \int_V \left(\omega \dot{c} - \boldsymbol{\lambda} \cdot \nabla \dot{c} + \sum_{i=1}^{N_p} (\pi_i \dot{\phi}_i - \boldsymbol{\xi}_i \cdot \nabla \dot{\phi}_i) \right) \; dV. \tag{13}$$

Inserting equations (11)-(13) into equation (10) leads to the following local internal energy rate:

$$\dot{e} = \boldsymbol{\lambda} \cdot \nabla \dot{c} - \omega \dot{c} + \sum_{i=1}^{N_p} \left(\boldsymbol{\xi}_i \cdot \nabla \dot{\phi}_i - \dot{\phi}_i \pi_i \right). \tag{14}$$

2.2 Dissipation inequality/entropy principle

The second law of thermodynamics can be formulated as the Clausius-Duhem inequality [1, 20, 24] in global form

$$\int_V \dot{s}\; dV \geq - \int_{\partial V} \boldsymbol{\Phi} \;\cdot \boldsymbol{n}\; dA, \tag{15}$$

where s is the local entropy density and $\boldsymbol{\Phi}$ the vector entropy flux, defined as, [2, 29]

$$\boldsymbol{\Phi} = -\mu \frac{\boldsymbol{J}}{T}. \tag{16}$$

This definition introduces three additional quantities: The absolute temperature T, the scalar chemical potential μ and the chemical flux $\boldsymbol{J}$ which describes the flux of the concentration c. A mass conservation renders

$$\dot{c} = -\nabla \cdot \boldsymbol{J}. \tag{17}$$

Inserting equation (16) into the inequality (15) and using Gauss's theorem leads to a local form of inequality (15)

$$T\dot{s} - \nabla \cdot (\mu \boldsymbol{J}) \geq 0. \tag{18}$$

The Helmholtz energy ψ is obtained from the internal energy e by a Legendre transformation with respect to the temperature T and the entropy s

$$\psi = e - Ts. \tag{19}$$

The energy equation (14) and the entropy inequality (18) can be linked using the time derivative of the Helmholtz energy equation (19). For the isothermal case and with the mass conservation (17) this leads to the *local dissipation inequality*

$$-\dot{\psi} + \boldsymbol{\lambda} \cdot \nabla \dot{c} - \omega \dot{c} + \mu \dot{c} - \boldsymbol{J} \cdot \nabla \mu + \sum_{i=1}^{N_p} \left(\boldsymbol{\xi}_i \cdot \nabla \dot{\phi}_i - \pi_i \dot{\phi}_i \right) \geq 0. \tag{20}$$

2.3 Restrictions to constitutive equations imposed by the second law of thermodynamics

The local dissipation inequality (20) is used next to formulate restrictions to constitutive equations. To this end, in the first step we choose *constitutive variables* based on the work of Gurtin [12]. He allows the constitutive equations to depend on the order parameter ϕ and its derivatives $\nabla\phi$ and $\dot{\phi}$ to model capillarity and transition kinetics [12]. Further generalizations by means of more constitutive variables and especially higher order derivatives of the order parameter are possible. However this is not within the scope of this paper since it is not needed for our prototype example.

Our framework should be capable of describing N_p phases. Therefore the order parameters ϕ_i and its derivatives range from $i = 0$ to $i = N_p$. Furthermore, $c, \nabla c$ and $\dot{c}$ are appended to the constitutive variables together with the chemical potential μ and its gradient $\nabla\mu$ for the diffusion process as described by Gurtin [12]. For convenience all *constitutive variables* are combined in the vector

$$\boldsymbol{z} = [c,\ \nabla c,\ \dot{c},\ \mu,\ \nabla \mu,\ \{\phi_i,\ \nabla \phi_i,\ \dot{\phi}_i\}_{i=1}^{N_p}]. \tag{21}$$

The second step is to define the remaining quantities in the local dissipation inequality (20) by use of *constitutive equations*. In detail these are the Helmholtz energy ψ, the stresses $\boldsymbol{\xi}_i, \boldsymbol{\lambda}$, the internal forces π_i, ω and the chemical flux $\boldsymbol{J}$, which, for the time being, are assumed to be dependent on the vector $\boldsymbol{z}$ and combined as a vector

$$\boldsymbol{Z}(\boldsymbol{z}) = [\hat{\psi}(\boldsymbol{z}),\ \hat{\boldsymbol{J}}(\boldsymbol{z}),\ \hat{\omega}(\boldsymbol{z}),\ \hat{\boldsymbol{\lambda}}(\boldsymbol{z}),\ \{\hat{\pi}_i(\boldsymbol{z}),\ \hat{\boldsymbol{\xi}}_i(\boldsymbol{z})\}_{i=1}^{N_p}], \quad N_Z = 4 + 2N_p \tag{22}$$

with the dimension N_Z.

In the next step the time derivative of the Helmholtz energy

$$\begin{aligned}\dot{\psi} = {} & \frac{\partial\hat{\psi}(\boldsymbol{z})}{\partial c}\frac{\partial c}{\partial t} + \frac{\partial\hat{\psi}(\boldsymbol{z})}{\partial\nabla c}\frac{\partial\nabla c}{\partial t} + \frac{\partial\hat{\psi}(\boldsymbol{z})}{\partial\dot{c}}\frac{\partial\dot{c}}{\partial t} + \frac{\partial\hat{\psi}(\boldsymbol{z})}{\partial\mu}\frac{\partial\mu}{\partial t} + \frac{\partial\hat{\psi}(\boldsymbol{z})}{\partial\nabla\mu}\frac{\partial\nabla\mu}{\partial t} \\ & + \sum_{i=1}^{N_p}\left(\frac{\partial\hat{\psi}(\boldsymbol{z})}{\partial\phi_i}\frac{\partial\phi_i}{\partial t} + \frac{\partial\hat{\psi}(\boldsymbol{z})}{\partial\nabla\phi_i}\frac{\partial\nabla\phi_i}{\partial t} + \frac{\partial\hat{\psi}(\boldsymbol{z})}{\partial\dot{\phi}_i}\frac{\partial\dot{\phi}_i}{\partial t}\right)\end{aligned} \tag{23}$$

is inserted into the dissipation inequality (20):

$$\begin{aligned}&\left(\mu - \hat{\omega}(\boldsymbol{z}) - \frac{\partial\hat{\psi}(\boldsymbol{z})}{\partial c}\right)\dot{c} + \left(\hat{\boldsymbol{\lambda}}(\boldsymbol{z}) - \frac{\partial\hat{\psi}(\boldsymbol{z})}{\partial\nabla c}\right)\nabla\dot{c} - \frac{\partial\hat{\psi}(\boldsymbol{z})}{\partial\dot{c}}\ddot{c} - \frac{\partial\hat{\psi}(\boldsymbol{z})}{\partial\mu}\dot{\mu} - \frac{\partial\hat{\psi}(\boldsymbol{z})}{\partial\nabla\mu}\nabla\dot{\mu} \\ & - \nabla\mu\cdot\hat{\boldsymbol{J}}(\boldsymbol{z}) + \sum_{i=1}^{N_p}\left[\left(\hat{\boldsymbol{\xi}}_i(\boldsymbol{z}) - \frac{\partial\hat{\psi}(\boldsymbol{z})}{\partial\nabla\phi_i}\right)\nabla\dot{\phi}_i - \left(\hat{\pi}_i(\boldsymbol{z}) + \frac{\partial\hat{\psi}(\boldsymbol{z})}{\partial\phi_i}\right)\dot{\phi}_i - \frac{\partial\hat{\psi}(\boldsymbol{z})}{\partial\dot{\phi}_i}\ddot{\phi}_i\right] \geq 0.\end{aligned} \tag{24}$$

From the requirement that the inequality (24) must hold for arbitrary values of $\boldsymbol{z}$ and the higher order derivatives $\nabla\dot{c}, \ddot{c}, \dot{\mu}, \nabla\dot{\mu}, \ddot{\phi}_i, \nabla\dot{\phi}_i$ which appear in inequality (24) at any time and any material point one can conclude certain restrictions. As outlined next, three groups of terms in the inequality (24) may be distinguished.

The first group contains all products with the derivatives $\ddot{c}, \dot{\mu}, \nabla\dot{\mu}$ and $\ddot{\phi}_i$ in inequality (24). The characteristic property of these quantities is that they are not constitutive variables of the vector $\boldsymbol{z}$ and thus they appear linearly in (24). Therefore, one could easily find values for $\boldsymbol{z}$ and the higher order derivatives which would violate (24) and consequently it follows as necessary conditions

$$\frac{\partial\hat{\psi}(\boldsymbol{z})}{\partial\dot{c}} = 0, \quad \frac{\partial\hat{\psi}(\boldsymbol{z})}{\partial\mu} = 0, \quad \frac{\partial\hat{\psi}(\boldsymbol{z})}{\partial\nabla\mu} = 0, \quad \frac{\partial\hat{\psi}(\boldsymbol{z})}{\partial\dot{\phi}_i} = 0, \quad \text{for } i = 1, ..., N_p. \tag{25}$$

The equations (25) indicate that the Helmholtz energy function $\hat{\psi}(\boldsymbol{z})$ does not depend on

$\dot{c}$, μ, $\nabla\mu$ and $\dot{\phi}_i$ but only on the variables $\tilde{\boldsymbol{z}}$, resulting into

$$\hat{\psi}(\tilde{\boldsymbol{z}}), \quad \text{where} \quad \tilde{\boldsymbol{z}} = [c, \nabla c, \{\phi_i, \nabla\phi_i\}_{i=1}^{N_p}]. \tag{26}$$

The second group consists of those terms containing $\nabla\dot{\phi}_i$ or $\nabla\dot{c}$ in inequality (24). As for group one, the related higher order derivatives are not constitutive variables of the vector $\boldsymbol{z}$ and thus they appear linearly in (24). In contrast to group one, the corresponding factors are composed of additive terms. Again $\nabla\dot{\phi}_i$ and $\nabla\dot{c}$ could be chosen to violate inequality (24). Thus it can be stated without loss of generality that the factors have to be zero as necessary conditions, leading to

$$\hat{\boldsymbol{\lambda}}(\boldsymbol{z}) = \frac{\partial\hat{\psi}(\tilde{\boldsymbol{z}})}{\partial\nabla c} \quad \text{and} \quad \hat{\boldsymbol{\xi}}_i(\boldsymbol{z}) = \frac{\partial\hat{\psi}(\tilde{\boldsymbol{z}})}{\partial\nabla\phi_i} \quad \text{for} \;\; i = 1, ..., N_p. \tag{27}$$

The restrictions (27) define relations between constitutive equations (22) and therefore reduce its number to $3 + N_p < N_Z$. These results show that the constitutive equations $\boldsymbol{\xi}_i$ and $\boldsymbol{\lambda}$ are no longer independent but directly dependent on the choice of $\hat{\psi}(\tilde{\boldsymbol{z}})$.

With the results (26) and (27) the dissipation inequality (24) reduces to

$$-\nabla\mu \cdot \hat{\boldsymbol{J}}(\boldsymbol{z}) - \left(\hat{\omega}(\boldsymbol{z}) + \frac{\partial\hat{\psi}(\tilde{\boldsymbol{z}})}{\partial c} - \mu\right)\dot{c} - \sum_{i=1}^{N_p}\left(\hat{\pi}_i(\boldsymbol{z}) + \frac{\partial\hat{\psi}(\tilde{\boldsymbol{z}})}{\partial\phi_i}\right)\dot{\phi}_i \geq 0. \tag{28}$$

All remaining terms occurring in inequality (28) are part of group three. The characteristic property is that $\nabla\mu, \dot{c}$ and $\dot{\phi}_i$ are constitutive variables of the vector $\boldsymbol{z}$ and therefore may appear linearly or nonlinearly in inequality (28). Since it is not known whether the terms violate the inequality, they cannot be set to zero as a necessary condition. Instead the inequality (28) can be written as a reduced dissipation

$$\mathcal{D} = -\nabla\mu \cdot \hat{\boldsymbol{J}}(\boldsymbol{z}) - \omega^{dis}\dot{c} - \sum_{i=1}^{N_p}\pi_i^{dis}\dot{\phi}_i \geq 0 \tag{29}$$

with additional quantities

$$\omega^{dis} = \hat{\omega}(\boldsymbol{z}) + \frac{\partial\hat{\psi}(\tilde{\boldsymbol{z}})}{\partial c} - \mu, \tag{30}$$

$$\pi_i^{dis} = \hat{\pi}_i(\boldsymbol{z}) + \frac{\partial\hat{\psi}(\tilde{\boldsymbol{z}})}{\partial\phi_i}, \quad i = 1, ..., N_p\;. \tag{31}$$

They are chosen as

$$\omega^{dis} = -\tau(\boldsymbol{z})\dot{c}, \tag{32}$$

$$\pi_i^{dis} = -\beta_i(\boldsymbol{z})\dot{\phi}_i, \quad i = 1, ..., N_p, \tag{33}$$

where $\tau(\boldsymbol{z})$ and $\beta_i(\boldsymbol{z})$ are *constitutive moduli.* The chemical flux is chosen as

$$\hat{\boldsymbol{J}}(\boldsymbol{z}) = -\boldsymbol{A}(\boldsymbol{z})\nabla\mu, \tag{34}$$

where $\boldsymbol{A}(\boldsymbol{z})$ is the second order *mobility tensor* [12]. Inserting the definitions (30)-(34) into the dissipation inequality (29) renders

$$\mathcal{D} = \nabla\mu \cdot \boldsymbol{A}(\boldsymbol{z})\nabla\mu + \tau(\boldsymbol{z})\dot{c}^2 + \sum_{i=1}^{N_p} \beta_i(\boldsymbol{z})\dot{\phi}_i^{\,2} \geq 0. \tag{35}$$

The inequality (35) holds for any choice of $\nabla\mu, \dot{c}$ and $\dot{\phi}_i$ if and only if

$$\tau(\boldsymbol{z}) \geq 0, \quad \beta_i(\boldsymbol{z}) \geq 0, \quad \boldsymbol{s} \cdot \boldsymbol{A}(\boldsymbol{z})\boldsymbol{s} \geq 0 \;\; \forall \boldsymbol{s}. \tag{36}$$

In conclusion we are left with $3 + N_p$ constitutive equations describing the Helmholtz energy $\psi(\tilde{\boldsymbol{z}})$, the constitutive moduli $\beta_i(\boldsymbol{z})$, $\tau(\boldsymbol{z})$ and the mobility tensor $\boldsymbol{A}(\boldsymbol{z})$. They have to fulfill the criteria of (26) and (36). Every set of functions that satisfies these restrictions is in accordance with the microforce balance equations (6) and (7), mass conservation (17), the first (10) and the second law of thermodynamics (15).

[7, S. 5ff]

2.4 Evolution equations

Combining equations (30) and (32) with the force balance (7) and equation (27) yields an expression for the chemical potential

$$\mu = \frac{\partial\hat{\psi}(\tilde{\boldsymbol{z}})}{\partial c} - \nabla \cdot \frac{\partial\hat{\psi}(\tilde{\boldsymbol{z}})}{\partial\nabla c} + \tau(\boldsymbol{z})\dot{c}. \tag{37}$$

Inserting equation (34) with (37) for the chemical potential into the mass conservation law (17) one obtains the viscous Cahn-Hilliard equation [8]

$$\dot{c} = \nabla \cdot (\boldsymbol{A}(\boldsymbol{z})\nabla\mu) = \nabla \cdot \left(\boldsymbol{A}(\boldsymbol{z})\nabla \left(\frac{\partial\hat{\psi}(\tilde{\boldsymbol{z}})}{\partial c} - \nabla \cdot \frac{\partial\hat{\psi}(\tilde{\boldsymbol{z}})}{\partial\nabla c} + \tau(\boldsymbol{z})\dot{c} \right) \right). \tag{38}$$

Remark 1: Setting $\tau(\boldsymbol{z}) = 0$, $\hat{\psi}_c(c, \nabla c) = f(c) + \frac{1}{2}\rho|\nabla c|^2$ and $\boldsymbol{A}(\boldsymbol{z}) = \kappa\mathbf{1}$ in equation (38) leads to the standard Cahn-Hilliard equation

$$\dot{c} = \kappa\Delta\left(f'(c) - \rho\Delta c\right). \tag{39}$$

Alternatively, choosing $\hat{\psi}_c(c, \nabla c) = \frac{1}{2}c^2$ leads to Fick's second law of diffusion

$$\dot{c} = \kappa\Delta c. \tag{40}$$

The evolution equations for the multiphase field can be formulated with equations (31) and (33), the microforce balance (6) and equation (27)

$$\dot{\phi}_i = \frac{1}{\beta_i(\boldsymbol{z})} \left(\nabla \cdot \frac{\partial\hat{\psi}(\tilde{\boldsymbol{z}})}{\partial\nabla\phi_i} - \frac{\partial\hat{\psi}(\tilde{\boldsymbol{z}})}{\partial\phi_i} + \gamma_i \right), \quad i = 1, ..., N_p. \tag{41}$$

Remark 2: The evolution equation (41) is the most general partial differential equation for a multiphase field model. With the choice $N_p = 1$, $\beta(\boldsymbol{z}) = \text{const.} > 0$, $\hat{\psi}(\boldsymbol{z}) = f(\phi) + \frac{1}{2}r|\nabla\phi|^2$ and $\gamma = 0$ it leads to the classical GINZBURG-LANDAU equation

$$\beta\dot{\phi} = r\Delta\phi - f'(\phi). \tag{42}$$

3 A prototype model for lower bainite

3.1 Helmholtz energy

The framework of Section 2 is now specialized to simulate the lower bainitic transformation with three phases ($N_p = 3$) and the evolution of the carbon concentration c. Therefore the phases

1. bainitic ferrite (ϕ_1),
2. austenite (ϕ_2) and

3. carbide (ϕ_3)

are introduced where the corresponding order parameters ϕ_1, ϕ_2, ϕ_3 vary between 0 and 1.

$$\hat{\psi}(\tilde{\boldsymbol{z}}) = \hat{\psi}_c(c, \nabla c) + \hat{\psi}_\phi(\phi_1, \phi_2, \phi_3, \nabla\phi_1, \nabla\phi_2, \nabla\phi_3) \tag{43}$$

where $\hat{\psi}_c(c, \nabla c)$ and $\hat{\psi}_\phi(\phi_1, \phi_2, \phi_3, \nabla\phi_1, \nabla\phi_2, \nabla\phi_3)$ are Helmholtz energies for diffusion and phase fields, respectively. The diffusion part $\hat{\psi}_c(c, \nabla c)$ required for the viscous Cahn-Hilliard equation (38) is proposed as

$$\hat{\psi}_c(c, \nabla c) = f(c) + \frac{1}{2}\rho|\nabla c|^2, \quad \text{where} \quad f(c) = d(c_{\text{eq}} - c)^2(c_{\text{carb}} - c)^2, \tag{44}$$

where ρ is the diffusion gradient energy coefficient and $f(c)$ is a potential free energy density function. It is a double well potential with roots at c_{eq} and c_{carb}. Due to this definition the carbon concentration varies between the maximal carbon concentration in equilibrium bainitic ferrite $c_{\text{eq}} = 0.0704\,\text{wt.\%}$ [25] which is also the effective minimum carbon concentration of the overall model and the carbon concentration of carbide $c_{\text{carb}} = 6.67\,\text{wt.\%}$ [13].

The equations (44) only consider the diffusion within the bainitic ferrite, because the characteristic separation of carbon takes place within this phase. Consequently, this separation leads to the precipitation of carbides within the bainitic ferrite. Additionally, diffusion of carbon within austenite occurs. However, this effect is regarded as negligible, compared to the diffusion within the bainitic ferrite phase.

For the multiphase field part in equation (43) we choose

$$\hat{\psi}_\phi(\phi_1, \phi_2, \phi_3, \nabla\phi_1, \nabla\phi_2, \nabla\phi_3) = \sum_{i=1}^{N_p}\sum_{j>i}^{N_p} \frac{1}{q_{ij}} \left[h_{ij}(\phi_i, \phi_j, \nabla\phi_i, \nabla\phi_j) + g_{ij}(\phi_i, \phi_j)\right] \tag{45}$$

with the interfacial energy density $h_{ij}(\phi_i, \phi_j, \nabla\phi_i, \nabla\phi_j)$ and the potential energy $g_{ij}(\phi_i, \phi_j)$ between two phases i and j. The phase energy coefficients are denoted by q_{ij}. The interfacial energy density is chosen, following [28], as

$$h_{ij}(\phi_i, \phi_j, \nabla\phi_i, \nabla\phi_j) = \frac{1}{2}\alpha_{ij}(\phi_i\nabla\phi_j - \phi_j\nabla\phi_i)^2 \tag{46}$$

with the phase gradient energy coefficient α_{ij}. The potential or chemical energy density

g_{ij} between two phases i and j is chosen as a simple double well potential

$$g_{ij}(\phi_i, \phi_j) = \frac{1}{4a_{ij}} \phi_i^2 \phi_j^2, \tag{47}$$

where a_{ij} is the potential constant. The potential energy density functions (47) describe double well potentials to separate areas with high or low densities or different phases.

A coupling between the phase fields and the carbon concentration is not defined within this Helmholtz energy term. This could be achieved using the mobility tensor $\boldsymbol{A}(\boldsymbol{z})$, the constitutive moduli $\beta_i(\boldsymbol{z})$, $\tau(\boldsymbol{z})$ and the external scalar forces γ_i.

3.2 Constitutive moduli and evolution equations

In this subsection we provide proposals for the constitutive moduli τ, β_i and the mobility tensor $\boldsymbol{A}$ introduced in equations (32)-(34). The constitutive moduli $\tau(\boldsymbol{z})$ in equation (32) and $\beta_i(\boldsymbol{z})$ in equation (33) are chosen as constant material parameters

$$\tau(\boldsymbol{z}) = \tau \ = const. \ , \tag{48}$$

$$\beta_i(\boldsymbol{z}) = \beta_i = const. \tag{49}$$

In order to describe the diffusion of carbon within the bainitic ferrite a simple choice for the second-order mobility tensor $\boldsymbol{A}(\boldsymbol{z})$ in equation (34) is

$$\boldsymbol{A}(\boldsymbol{z}) = \boldsymbol{A}(\phi_1) = \phi_1 \cdot \kappa \mathbf{1}, \tag{50}$$

where κ is a constant. In this way the flux $\boldsymbol{J}$ will be zero if ϕ_1, representing the bainite phase, is zero, otherwise the carbon will diffuse. This constitutes an important coupling between the phase field and the diffusion model.

From equations (37), (43) and (44) we obtain for the chemical potential

$$\mu = \frac{\partial f(c)}{\partial c} - \rho \Delta c + \tau \dot{c}. \tag{51}$$

The evolution equation (38) for the diffusion reads with equation (50):

$$\begin{aligned} \dot{c} &= \phi_1 \kappa \Delta \mu + \nabla \phi_1 \kappa \nabla \mu \\ &= \phi_1 \kappa \Delta \left(\frac{\partial f(c)}{\partial c} - \rho \Delta c + \tau \dot{c} \right) + \nabla \phi_1 \kappa \nabla \left(\frac{\partial f(c)}{\partial c} - \rho \Delta c + \tau \dot{c} \right). \end{aligned} \tag{52}$$

The evolution equations (41) for the specific constitutive laws (43), (45)-(47) and (49) become

$$\dot{\phi}_i = \sum_{j=1,j\neq i}^{N_p} \frac{1}{\beta_i q_{ij}} \left(\alpha_{ij} \left(\phi_j \Delta\phi_i - \phi_i \Delta\phi_j \right) - \frac{\phi_i \phi_j}{2a_{ij}} (\phi_j - \phi_i) \right) + \gamma_i, \qquad \text{for} \;\; i = 1, ..., N_p \; . \quad (53)$$

Details on the derivatives of the Helmholtz energy $\hat{\psi}(\tilde{\boldsymbol{z}})$ in (45)-(47) can be found in [28].

3.3 Change of parameters

For a better physical interpretation of the phase field model, all material parameters of the phase field evolution equations (53) are changed according to [18].

The phase gradient energy coefficients α_{ij}, the potential constants a_{ij}, the phase energy coefficients q_{ij} and the dissipative moduli β_i are replaced by the physical material parameters, interface mobilities ζ_{ij}, interface energies σ_{ij} and interface thicknesses η_{ij}

$$\beta_i q_{ij} = \frac{\eta_{ij}}{\zeta_{ij}}, \qquad a_{ij} = \frac{\eta_{ij}}{72\sigma_{ij}}, \qquad \alpha_{ij} = \sigma_{ij}\eta_{ij}. \quad (54)$$

The derivation of the equations (54) using the Gibbs-Thomson equation [18] can be found in the appendix of [9].

The external microforces γ_i for the phase field are specified on the basis of [28] as a sum of external forces γ_{ij} which perform work on the phase transition only between the phases i and j

$$\gamma_i = \sum_{j=1,j\neq i}^{N_p} \gamma_{ij} = - \sum_{j=1,j\neq i}^{N_p} \frac{6\zeta_{ij} \cdot \Delta G_{ij}(\boldsymbol{z})}{\eta_{ij}} \, \phi_i \; \phi_j, \quad (55)$$

where ΔG_{ij} are the change of Gibbs energies which may be a function of $\boldsymbol{z}$. The arbitrary factor 6 has been introduced to be consistent with the evolution equations of [9, 18]. Note the relations $\zeta_{ij} = \zeta_{ji}$, $\sigma_{ij} = \sigma_{ji}$ and $\eta_{ij} = \eta_{ji}$ but $\Delta G_{ij} = -\Delta G_{ji}$.

With equations (55) and (54) the evolution equation (53) reads

$$\dot{\phi}_i = \sum_{j=1,j\neq i}^{N_p} \zeta_{ij} \left[\sigma_{ij} \left((\phi_j \Delta\phi_i - \phi_i \Delta\phi_j) - \frac{36}{\eta_{ij}^2} \phi_i \phi_j (\phi_j - \phi_i) \right) - \frac{6 \cdot \Delta G_{ij}(\boldsymbol{z})}{\eta_{ij}} \phi_i \phi_j \right] \qquad \text{for} \;\; i = 1, ..., N_p. \quad (56)$$

3.4 Carbide precipitation

The formation of carbides is a central mechanism of the lower bainitic transformation since it influences significantly the macroscopic material characteristics of bainite. However the simulation of this precipitation process yields several challenges. Firstly the phase field equation (56) does not provide the growth of any phase ϕ_i whose value is zero over the whole domain. To avoid this difficulty nuclei of carbides are defined as initial conditions. Secondly the formation of carbide is a process which starts after the phase transformation of austenite-to-bainitic ferrite and the ensuing carbon diffusion. During this process the nuclei of carbide converge to zero, so that they are not able to grow any more. This difficulty has been tackled in our paper [9] by defining the interface mobility ζ_{ij} as a function of the carbon concentration. The interface mobility is zero while the carbon concentration is low. In this way the nuclei of carbide are prevented to vanish.

However the approach of [9] cannot be integrated easily in the presented concept of generalized forces. Therefore we present an alternative approach based on changes of Gibbs energies

$$\Delta G_{ij}(\boldsymbol{z}) = \Delta G_{ij}^0 \; v(\phi_i, \phi_j, c) \tag{57}$$

where

$$v(\phi_i, \phi_j, c) = \begin{cases} \dfrac{w(c)}{\phi_3^2} & \text{for } i = 3 \vee j = 3 \\ 1 & \text{otherwise} \end{cases} \tag{58}$$

and ΔG_{ij}^0 is a constant material parameter. The function $w(c)$ is a smooth unit step function used in [9]

$$w(c) = \begin{cases} 0 & \text{for } c < c_{\text{carb}} - \varepsilon \\ 1 & \text{for } c > c_{\text{carb}} \\ \frac{1}{2} + \frac{1}{2} \cdot \sin(\frac{\pi}{\varepsilon} \cdot c + \frac{\pi}{2} - \frac{\pi}{\varepsilon} \cdot c_{\text{carb}}) & \text{otherwise,} \end{cases} \tag{59}$$

where the parameter ε governs the transition zone between $\varepsilon = 1$ for high carbon and $\varepsilon = 0$ for low carbon concentration.

The equations (57) - (59) do not change the transformation kinetics between austenite (ϕ_2) and bainitic ferrite (ϕ_1). For phase transitions involving carbide (ϕ_3) the thermodynamic driving force will be zero if the carbon concentration is low. Carbides will precipitate in supersaturated steel if the local carbon concentration is at $c_{\text{carb}} = 6.67\,\text{wt.\%}$ [13]. This is governed by the step function w. The function v ensures that the carbide phase can grow even if the nuclei have become very small in time.

Remark 3: In our previous approach [9] we implemented the carbide precipitation by defining the interface mobility

$$\zeta_{ij}(c) = \begin{cases} 0 & \text{for } c < c_{\text{carb}} - \varepsilon \\ 1 & \text{for } c > c_{\text{carb}} \\ \frac{1}{2} + \frac{1}{2} \cdot \sin(\frac{\pi}{\varepsilon} \cdot c + \frac{\pi}{2} - \frac{\pi}{\varepsilon} \cdot c_{\text{carb}}) & \text{otherwise,} \end{cases}$$

which is identical to the function in (59). In the new approach of this work the step function $w(c)$ is integrated into the external scalar forces γ_i which are transfered to the changes of Gibbs energies $\Delta G_{ij}(\boldsymbol{z})$ by equation (55).

3.5 Anisotropic phase growth

The characteristic slim shapes of the bainite sheaves are modeled using an anisotropic extension of the phase-field model as presented by [17] and [16] and used in [9]. The interface energy parameters σ_{ij} are manipulated depending on the local gradient $\nabla\phi_i$ and a predefined growth direction θ_0

$$\sigma_{ij} = \sigma_{ij}(\theta(\nabla\phi_i), \theta_0). \tag{60}$$

In lower bainite the transformation from austenite to bainitic ferrite shows an anisotropic behavior. Therefore only σ_{12} needs to be defined as

$$\sigma_{12} = \sigma_{12}^0 \cdot (1 + r \cdot \cos(\theta - \theta_0)), \quad \text{with} \quad \theta = \arctan \frac{\frac{\partial\phi_1}{\partial y}}{\frac{\partial\phi_1}{\partial x}}, \tag{61}$$

where σ_{12}^0 is the isotropic interface energy and r is a measure of the strength of anisotropy. The main growth direction θ_0 of the ferrite which could be chosen arbitrary. Here it is set to $\theta_0 = 0°$.

4 Numerical implementation

Numerical solutions for the evolution equations (52) and (56) are obtained with the finite element method for two dimensional problems. For time discretization an implicit Euler scheme is implemented. The resulting nonlinear system of equations is solved iteratively with Newton's method. The implementation is straightforward as described in [9].

For the finite element method quadrilateral elements with linear shape functions are used. The equation (51) for the chemical potential μ will be discretized, because the Cahn-Hilliard equation (52) has fourth-order derivatives. Due to this procedure the model has five unknowns per node: $\begin{bmatrix} c & \mu & \phi_1 & \phi_2 & \phi_3 \end{bmatrix}^T$. The diffusion equation (52) can be written in weak form as

$$\int_V \nu_c \dot{c}\ dV - \int_V \nu_c \phi_1 \kappa \Delta\mu\ dV - \int_V \nu_c \nabla\phi_1 \kappa \nabla\mu\ dV = 0, \tag{62}$$

where ν_c denotes the test function for the carbon concentration. Using Gauss's theorem and homogeneous boundary conditions we obtain

$$\int_V \nu_c \dot{c}\ dV + \int_V \nabla\nu_c \phi_1 \kappa \nabla\mu\ dV = 0. \tag{63}$$

Since the chemical potential μ should also be discretized, the weak form for the evolution equation of μ in equation (51) can be derived as

$$\int_V \nu_\mu \tau \dot{c} + \rho \nabla\nu_\mu \nabla c + \nu_\mu (qc^3 + pc^2 + oc + l) - \nu_\mu \mu\ dV = 0 \tag{64}$$

with the derivative of the generalized carbon potential function

$$\begin{aligned} f'(c) &= d(qc^3 + pc^2 + oc + l)\ , \text{where} \\ o &= 2c_{\text{carb}}^2 + 2c_{\text{eq}}^2 + 8c_{\text{eq}}c_{\text{carb}}\ , \\ p &= -6c_{\text{carb}} - 6c_{\text{eq}}\ , \\ q &= 4\ , \\ l &= -2c_{\text{eq}}c_{\text{carb}}^2 - 2c_{\text{carb}}c_{\text{eq}}^2\ . \end{aligned} \tag{65}$$

The weak form of the phase field evolution equation (56) with test function ν_ϕ, again using Gauss's theorem and homogeneous Neumann boundary conditions, reads

$$\int_V \nu_\phi \dot{\phi}_i \, dV = \int_V \sum_{j=1, j\neq i}^{N_p} \zeta_{ij} \Bigg[\sigma_{ij} \Bigg(\nabla \nu_\phi (\nabla \phi_j \phi_i - \nabla \phi_i \phi_j) - \frac{36}{\eta_{ij}^2} \nu_\phi \phi_i \phi_j (\phi_j - \phi_i) \Bigg) \\ - \frac{6 \Delta G_{ij}(\boldsymbol{z})}{\eta_{ij}} \nu_\phi \phi_i \phi_j \Bigg] \, dV. \quad (66)$$

The degrees of freedom at every node, which are denoted by the superimposed hat $\hat{(\cdot)}$, are $\underline{\hat{d}} = \begin{bmatrix} \underline{\hat{c}} & \underline{\hat{\mu}} & \underline{\hat{\phi}}_1 & \underline{\hat{\phi}}_2 & \underline{\hat{\phi}}_3 \end{bmatrix}^T$. The row vector $\underline{N}$ contains the shape functions, such that the quantities c, μ and the ϕ_i can be written as scalar products:

$$c = \underline{N}\underline{\hat{c}} \ , \qquad \mu = \underline{N}\underline{\hat{\mu}} \ , \qquad \phi_i = \underline{N}\underline{\hat{\phi}_i} \ , \quad i = 1, 2, 3. \quad (67)$$

The matrix $\underline{B}$ used for gradient terms is defined as

$$\underline{B} = \begin{bmatrix} \underline{N}_{,x} \\ \underline{N}_{,y} \end{bmatrix}, \qquad \text{with} \qquad \underline{N}_{,x} = \frac{\partial \underline{N}}{\partial x}. \quad (68)$$

The gradients read

$$\nabla c = \underline{B}\underline{\hat{c}} \ , \qquad \nabla \mu = \underline{B}\underline{\hat{\mu}} \ , \qquad \nabla \phi_i = \underline{B}\underline{\hat{\phi}_i} \ , \quad i = 1, 2, 3. \quad (69)$$

In the same manner the shape functions are used for the test functions ν_ϕ, ν_c and ν_μ. As mentioned above the time dependence is discretized with an implicit Euler method. The superscript $(\cdot)^n$ signals the time step of the solution. The actual time step is denoted by n, which is in most cases omitted for brevity.

The residuum vector is defined as $\underline{R} = [\underline{R}^c \;\; \underline{R}^\mu \;\; \underline{R}^{\phi_i}]^T$ with

$$\underline{R}^c = \int\limits_{\Omega_e} (\underline{N}^T \underline{N}) \cdot \frac{\underline{\hat{c}}^n - \underline{\hat{c}}^{n-1}}{\Delta t} + \kappa \cdot (\underline{N} \hat{\boldsymbol{\phi}}_1) \underline{B}^T \underline{B} \underline{\hat{\mu}} \, d\Omega, \quad (70)$$

$$\underline{R}^\mu = \int\limits_{\Omega_e} \tau (\underline{N}^T \underline{N}) \cdot \frac{\underline{\hat{c}}^n - \underline{\hat{c}}^{n-1}}{\Delta t} + d \big(\underline{N}^T l + o (\underline{N}^T \underline{N}) \underline{\hat{c}} + p \underline{N}^T (\underline{N}\underline{\hat{c}})^2 \\ + q \underline{N}^T (\underline{N}\underline{\hat{c}})^3 \big) + \rho (\underline{B}^T \underline{B}) \underline{\hat{c}} - (\underline{N}^T \underline{N}) \underline{\hat{\mu}} \, d\Omega, \quad (71)$$

$$\underline{R}^{\phi_i} = \int\limits_{\Omega_e} \underline{N}^T \underline{N} \, \frac{\hat{\underline{\phi}}_i^{n} - \hat{\underline{\phi}}_i^{n-1}}{\Delta t} + \sum_{j=1, j \neq i}^{N_p} \zeta_{ij} \, \Bigg[\sigma_{ij} \Bigg(- (\underline{B}^T \underline{B}) \hat{\underline{\phi}}_j \cdot (\underline{N} \hat{\underline{\phi}}_i) + (\underline{B}^T \underline{B}) \hat{\underline{\phi}}_i \cdot (\underline{N} \hat{\underline{\phi}}_j) \\ - \frac{36}{\eta_{ij}^2} \underline{N}^T \underline{N} (\hat{\underline{\phi}}_i - \hat{\underline{\phi}}_j) (\underline{N} \hat{\underline{\phi}}_i) \cdot (\underline{N} \hat{\underline{\phi}}_j) \Bigg) + \frac{6}{\eta_{ij}} \Delta G_{ij}(\boldsymbol{z}) \underline{N}^T \cdot (\underline{N} \hat{\underline{\phi}}_i) \cdot (\underline{N} \hat{\underline{\phi}}_j) \Bigg] \, d\Omega. \qquad (72)$$

The integrals are calculated with a Gauss-Legendre rule. To solve the system of algebraic equations Newton's method is used. Therefore the tangent of the residual function $\underline{R}$ is needed

$$\underline{K} = \frac{\partial \underline{R}}{\partial \hat{\underline{d}}} = \begin{bmatrix} \underline{K}^{cc} & \underline{K}^{c\mu} & \underline{K}^{c\phi_1} & \underline{0} & \underline{0} \\ \underline{K}^{\mu c} & \underline{K}^{\mu\mu} & \underline{0} & \underline{0} & \underline{0} \\ \underline{K}^{\phi_1 c} & \underline{0} & \underline{K}^{\phi_1\phi_1} & \underline{K}^{\phi_1\phi_2} & \underline{K}^{\phi_1\phi_3} \\ \underline{K}^{\phi_2 c} & \underline{0} & \underline{K}^{\phi_2\phi_1} & \underline{K}^{\phi_2\phi_2} & \underline{K}^{\phi_2\phi_3} \\ \underline{K}^{\phi_3 c} & \underline{0} & \underline{K}^{\phi_3\phi_1} & \underline{K}^{\phi_3\phi_2} & \underline{K}^{\phi_3\phi_3} \end{bmatrix}, \qquad (73)$$

with the following matrix entries

$$\underline{K}^{\phi_i\phi_i} = \frac{\partial R^{\phi_i}}{\partial \hat{\underline{\phi}}_i} = \int\limits_{\Omega_e} \underline{N}^T \underline{N} \frac{1}{\Delta t} + \sum_{j=1, j \neq i}^{N_p} \zeta_{ij} \, \Bigg[\sigma_{ij} \Bigg((\underline{B}^T \underline{B}) (\underline{N} \hat{\underline{\phi}}_j) - (\underline{B}^T \underline{B}) \hat{\underline{\phi}}_j \cdot \underline{N} \\ - \frac{36}{\eta_{ij}^2} \underline{N}^T \underline{N} (\underline{N} \hat{\underline{\phi}}_j) \cdot \underline{N} (2 \hat{\underline{\phi}}_i - \hat{\underline{\phi}}_j) \Bigg) \\ + \frac{6}{\eta_{ij}} \Bigg(\Delta G_{ij}(\boldsymbol{z}) \underline{N}^T \underline{N} \cdot (\underline{N} \hat{\underline{\phi}}_j) + \frac{\partial \Delta G_{ij}(\boldsymbol{z})}{\partial \hat{\underline{\phi}}_i} \underline{N}^T \cdot (\underline{N} \hat{\underline{\phi}}_i) \cdot (\underline{N} \hat{\underline{\phi}}_j) \Bigg) \Bigg] \, d\Omega, \qquad (74)$$

$$\underline{K}^{\phi_i\phi_j} = \frac{\partial R^{\phi_i}}{\partial \hat{\underline{\phi}}_j} = \int\limits_{\Omega_e} \zeta_{ij} \, \Bigg[\sigma_{ij} \Bigg(- (\underline{B}^T \underline{B}) (\underline{N} \hat{\underline{\phi}}_i) + (\underline{B}^T \underline{B}) \hat{\underline{\phi}}_i \cdot \underline{N} - \frac{36}{\eta_{ij}^2} \underline{N}^T \underline{N} (\underline{N} \hat{\underline{\phi}}_i) \cdot \underline{N} (\hat{\underline{\phi}}_i - 2 \hat{\underline{\phi}}_j) \Bigg) \\ + \frac{6}{\eta_{ij}} \Bigg(\Delta G_{ij}(\boldsymbol{z}) \underline{N}^T \underline{N} \cdot (\underline{N} \hat{\underline{\phi}}_i) + \frac{\partial \Delta G_{ij}(\boldsymbol{z})}{\partial \hat{\underline{\phi}}_j} \underline{N}^T \cdot (\underline{N} \hat{\underline{\phi}}_i) \cdot (\underline{N} \hat{\underline{\phi}}_j) \Bigg) \Bigg] \, d\Omega, \qquad (75)$$

$$\underline{K}^{\phi_i c} = \frac{\partial R^{\phi_i}}{\partial \underline{\hat{c}}} = \int\limits_{\Omega_e} \sum_{j=1,j\neq i}^{N_p} \zeta_{ij} \frac{6}{\eta_{ij}} \frac{\partial \Delta G_{ij}(\boldsymbol{z})}{\partial \underline{\hat{c}}} \underline{N}^T \cdot (\underline{N}\underline{\hat{\phi}}_i) \cdot (\underline{N}\underline{\hat{\phi}}_j) \; d\Omega. \tag{76}$$

$$\underline{K}^{cc} = \int\limits_{\Omega_e} \frac{1}{\Delta t} \cdot \underline{N}^T \underline{N} \; d\Omega, \tag{77}$$

$$\underline{K}^{\mu\mu} = \int\limits_{\Omega_e} -\underline{N}^T \underline{N} \; d\Omega, \tag{78}$$

$$\underline{K}^{c\mu} = \int\limits_{\Omega_e} \kappa \cdot (\underline{N}\hat{\boldsymbol{\phi}}_1) \underline{B}^T \underline{B} \; d\Omega, \tag{79}$$

$$\underline{K}^{\mu c} = \int\limits_{\Omega_e} \frac{\tau}{\Delta t} \cdot \underline{N}^T \underline{N} + \rho \cdot \underline{B}^T \underline{B} + d(o \cdot (\underline{N}^T \underline{N}) + 2p \cdot (\underline{N}^T \underline{N}) \cdot (\underline{N}\underline{\hat{c}}) + 3q \cdot (\underline{N}^T \underline{N}) \cdot (\underline{N}\underline{\hat{c}})^2) \; d\Omega, \tag{80}$$

$$\underline{K}^{c\phi_1} = \frac{\partial R^c}{\partial \underline{\hat{\phi}}_1} = \int\limits_{\Omega_e} \kappa \cdot (\underline{B}^T \underline{B}) \underline{\hat{\mu}} \underline{N} \; d\Omega. \tag{81}$$

5 Representative numerical examples

5.1 Preliminary remarks

The results of two example calculations of the prototype model for lower bainite are presented in this section. They give an impression of possible applications of the thermodynamic framework derived in this work.

As initial conditions nuclei of bainitic ferrite and carbide are generated. While the ferrite nucleus is strong ($\phi_1 = 1$) and concentrated at a single location, carbide nuclei are spread over the whole domain and are very weak ($\max(\phi_3) = 0.01$). The distribution and the strength of the carbide nuclei are random. This approach is supported by the fact that the bainitic nucleation is based on preformed nuclei [21]. The carbon concentration has a constant initial condition of 1.87 wt.% with small randomly distributed perturbations. All equations are implemented with homogeneous Neumann boundary conditions.

The first example “slower diffusion” uses a diffusion coefficient of $\kappa = 0.008$ µm^2/s whereas the second example exhibits a rather “faster diffusion” with $\kappa = 0.02$ µm^2/s. Different values for the diffusion coefficient may occur due to different cooling temperatures.

Parameter	**Symbol**	**Value/Unit**
Strength of the anisotropy	r	0.5
Maximum carbon concentration in ferrite	c_{eq}	0.0704 wt.% [25]
Maximum carbon concentration in steel	c_{carb}	6.67 wt.% [13]
Bainitic main growth direction	θ_0	0°
Cahn-Hilliard viscosity factor	τ	0.00002 s
Cahn-Hilliard balance factor	ρ	0.00016 μm^2
Cahn-Hilliard potential factor	d	0.014 $\frac{1}{\mu\text{m}^2}$
Bainitic ferrite/Austenite interface energy	σ_{12}	0.001 $\frac{\text{J}}{\mu\text{m}^2}$
Bainitic ferrite/Carbide interface energy	σ_{13}	0.001 $\frac{\text{J}}{\mu\text{m}^2}$
Austenite/Carbide interface energy	σ_{23}	0 $\frac{\text{J}}{\mu\text{m}^2}$
Bainitic ferrite/Austenite interface mobility	ζ_{12}	0.5 $\frac{\mu\text{m}^4}{\text{Js}}$
Bainitic ferrite/Carbide interface mobility	ζ_{13}^0	0.5 $\frac{\mu\text{m}^4}{\text{Js}}$
Austenite/Carbide interface mobility	ζ_{23}	0 $\frac{\mu\text{m}^4}{\text{Js}}$
Gibbs energy between Bainitic ferrite and Austenite	ΔG_{12}	-0.0755 $\frac{\text{J}}{\mu\text{m}^3}$
Gibbs energy between bainitic ferrite and carbide	ΔG_{13}	0.061 $\frac{\text{J}}{\mu m^3}$
Gibbs energy between austenite and carbide	ΔG_{23}	0 $\frac{\text{J}}{\mu\text{m}^3}$
Interfacial thickness	η	0.17μm
Step function width	ε	0.1

Table 1: Material parameters

However the values here are hypothetical and used to show how the shapes of the carbides vary depending on the diffusion coefficient. Both calculations run over a period of 30 s with a time step size of $\Delta t = 0.05\,\text{s}$.

All other values for the parameters introduced in the previous sections can be found in Table 1. They are an issue of further investigations since most of them are tentative. The mesh of the finite element method used to solve the problem divides the $3\,\mu\text{m} \times 3\,\mu\text{m}$ domain into 16384 elements. This fine grid ensures that at least 7 elements describe the diffuse interface between two phases with the given interface width of $\eta_{ij} = 0.17\,\mu\text{m}$.

a) Austenite

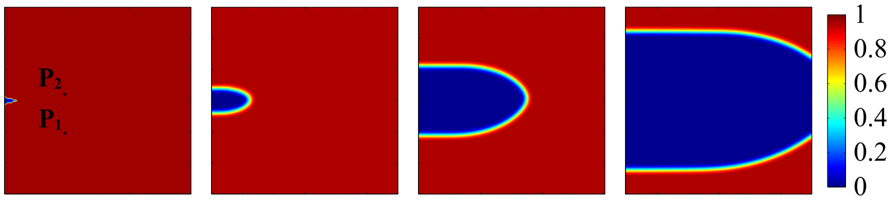

b) Bainitic ferrite

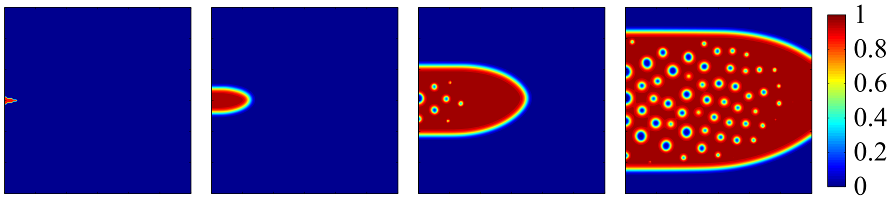

c) Carbide

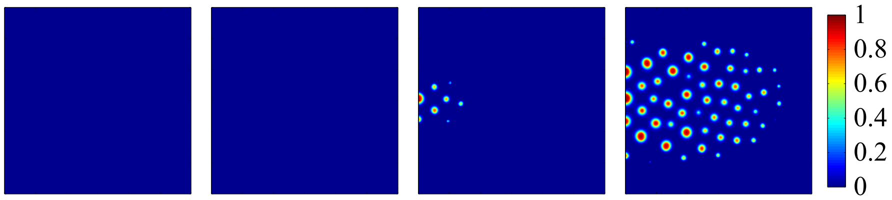

d) Carbon concentration

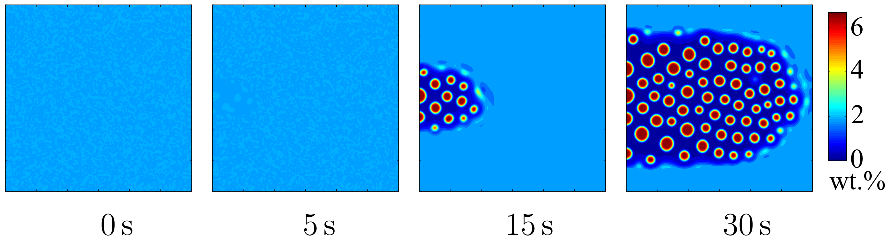

Figure 4: Slower diffusion: Lower bainitic transformation after 0 s, 5 s, 15 s and 30 s.

5.2 Example 1: Slower diffusion

The evolution of the three phases and the motion of the carbon is shown in Figure 4. From top to bottom we have: austenite, bainitic ferrite, carbide and carbon concentration with corresponding initial conditions in first column. One can see the initial bainitic ferrite nucleus on the left boundary. The small nuclei of the carbide cannot be seen due to the chosen scaling. The perturbations of the initial carbon concentration can be hardly seen, either. For further information see [9]. The next columns depict the corresponding evolutions after 5 s, 15 s and 30 s, respectively. After 5 s the bainitic ferrite grows and has its typical slim shape. There are still no carbides and the carbon concentration field shows only very little change within the area of the bainitic ferrite. At 15 s accumulations of carbon are visible while the surrounding field declines to the minimum concentration. This is the typical diffusion process of lower bainite. The ferrite can contain much less carbon than the austenite. Due to the fact that the ferrite sheaf grows too fast, the carbon cannot diffuse out of it instead it starts to build accumulations within the phase. Carbides precipitate at the places of the carbon accumulations. The carbides closer to the left boundary are larger, because the bainitic sheaf growth from left to right. Furthermore it can be seen that the diffusion process is slower than the phase transformation, because the carbon concentration changes only in about half of the ferrite area. The last column shows the results after 30 s. The carbides have globular or elliptical shapes. The difference between the conserved diffusion of the carbon and the non-conserved phase evolution can be seen in this figure.

The lenticular shape of the sheaf in Figure 4 can be compared with the micrographs in Figures 1 and 3. The distribution of the carbides is similar those in the micrograph in Figure 2. However the carbides do not show the expected shape and orientation. This is part of further investigations.

a) Austenite

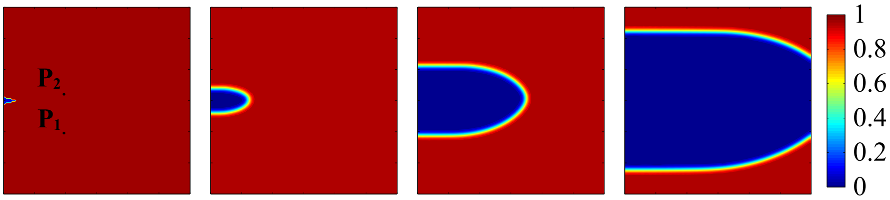

b) Bainitic ferrite

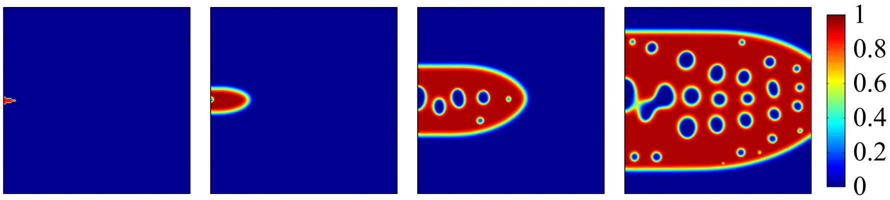

c) Carbide

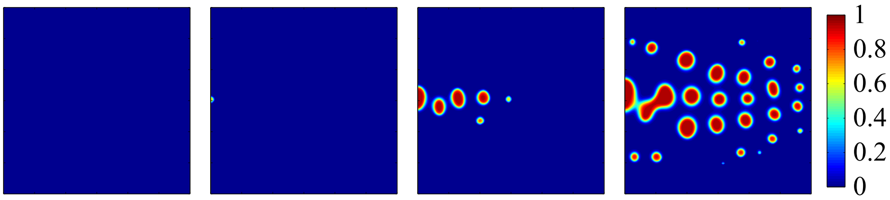

d) Carbon concentration

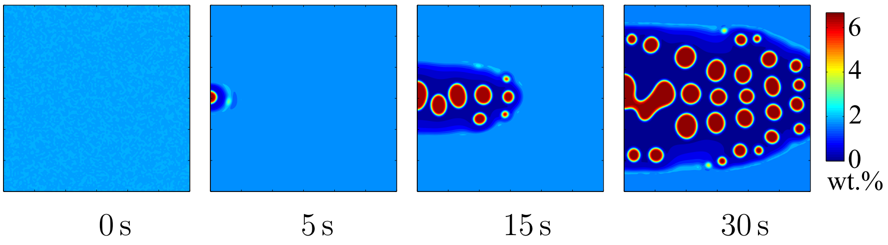

Figure 5: Faster diffusion: Lower bainitic transformation after 0 s, 5 s, 15 s and 30 s.

5.3 Example 2: Faster diffusion

Figure 5 shows the results of the second example with a higher diffusion coefficient κ. It is structured in the same way as Figure 4. In comparison with Example 1 the carbon starts to move earlier which can be seen in part d) of Figure 4 and 5 after 5 s. While the concentration field in the first example hardly changes at all, the field in the second example shows already a maximum. The more important consequence of the higher diffusion coefficient is that the size of the accumulations increase and thereby the carbide precipitations are larger, too. The results of this example also show the characteristics of globular and rather large carbides as in the micrograph in Figure 3.

5.4 Comparison of results with different diffusion coefficients

Figure 6 shows two plots of the different fields over the time. The left axis has a scale for the carbon concentration in wt.%. with a range from 0 wt.% to 7 wt.%. The scale on the right axis of both diagrams represents the phase field order parameters. They vary between 0 and 1. The solid lines show results from Example 1 with a low diffusion coefficient and the dashed lines show the results of the second example with faster diffusion.

The data plotted in Figure 6.a are calculated for the point P_1 ($x = 0.98438\,\mu\text{m}$, $y = 0.98438\,\mu\text{m}$) as marked in Figures 4.a and 5.a. The carbon concentration is at around 1.87 wt.% and austenite is the dominating microstructure, which is not plotted here for clarity. While in both situations the initial status is the same, evolutions of the fields differ from the instant on when the bainitic ferrite phase starts to grow. The beginning of the phase transformation between austenite and bainitic ferrite marks the instant when diffusion of the carbon starts, because the bainitic ferrite can contain much less carbon than austenite. One can see that while the faster diffusion (dashed line) directly starts to move the carbon, the slower diffusion almost does not change the concentration at all. It starts about 5 s later. The ups and downs of the carbon field are due to spacial interactions with neighboring points. It can be reasoned that the point is not in the middle of a carbon accumulation. The transformation from bainitic ferrite to carbide starts very rapidly, when the carbon reaches maximum concentration. This can be observed for the slow (solid line) diffusion. The rather soft transformation for the faster one is also reasoned by spacial interactions. There are already carbides at neighboring points.

Diagram 6.b shows results from Point P_2 ($x = 0.98438\,\mu\text{m}, y = 1.5938\,\mu\text{m}$) as marked in Figures 4.a and 5.a. Here the phenomena can be seen even better, because directly when the bainitic ferrite lines crosses those of the carbon concentration, the concentration

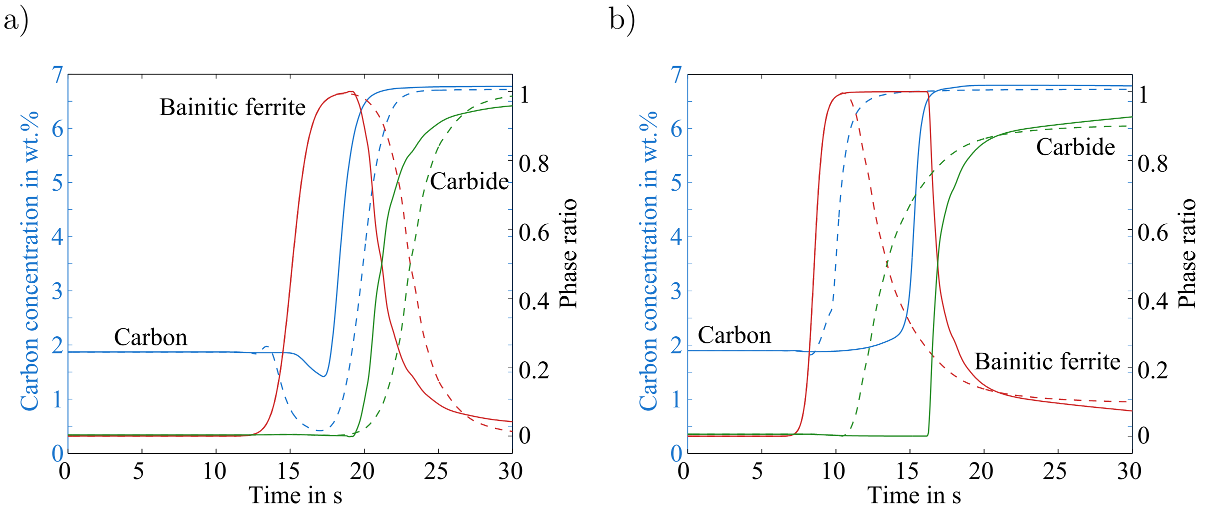

Figure 6: Phases and carbon concentration over time at a) P_1 and b) P_2 as marked in Figures 4 and 5. Solid lines denote slower diffusion, dashed lines faster diffusion.

with the faster diffusion coefficient changes rapidly and increases to its maxima. The concentration of carbon in Example 1 does not change for the next few seconds before it starts to move slowly. However the mean increase of carbon is almost in parallel, showing that now the diffusion is similarly fast.

6 Conclusion

The thermodynamical framework presented in this work can be used to develop constitutive equations for many kinds of phase transformations between several phases. The transformations may be coupled to a diffusion process. The Cahn-Hilliard equation used in this framework provides a wide area of diffusion models. It includes the classical Cahn-Hilliard, a viscous Cahn-Hilliard and Fick's Law. Basic universal laws, such as the microforce balances, the energy conservation law, the mass conversation law and the entropy inequality are strictly separated from constitutive laws which depend on the specific material. As a prototype application of the framework the simulation of the lower bainitic transformation is presented. Within this specific formulation the coupling between different phase order parameters and the diffusion model can be seen. In future work we plan to extend the framework to deformable continua.

Acknowledgements

We thank Prof. M. Schaper and Dr. O. Grydin from the Chair of Materials Science, Paderborn University for helpful discussions and providing the micrograph in Figure 2.

References

[1] Altenbach, H.: Kontinuumsmechanik: Einführung in die materialunabhängigen und materialabhängigen Gleichungen. Springer Berlin Heidelberg (2012)

[2] Ammar, K.: Modelling and Simulation of Phase Transformation-Mechanics coupling Using a Phase Field Method. Ph.D. thesis, l'École nationale supérieure des mines de Paris (2010)

[3] Ammar, K., Appolaire, B., Cailletaud, G., Feyel, F., Forest, S.: Finite element formulation of a phase field model based on the concept of generalized stresses. Computational materials science **45**(3), 800–805 (2009)

[4] Ammar, K., Appolaire, B., Cailletaud, G., Forest, S.: Combining phase field approach and homogenization methods for modelling phase transformation in elastoplastic media. European Journal of Computational Mechanics/Revue Européenne de Mécanique Numérique **18**(5-6), 485–523 (2009)

[5] Arif, T., Qin, R.: A phase-field model for bainitic transformation. Computational Materials Science **77**, 230–235 (2013)

[6] Babu, S.S., Specht, E.D., David, S.A., Karapetrova, E., Zschack, P., Peet, M., Bhadeshia, H.: In-situ observations of lattice parameter fluctuations in austenite and transformation to bainite. Metallurgical and Materials Transactions A **36**(12), 3281–3289 (2005)

[7] Bhadeshia, H.K.D.H.: Bainite in steels, 2nd edn. Maney Materials Science (2001)

[8] Dreyer, W., Guhlke, C.: Sharp limit of the viscous Cahn-Hilliard equation and thermodynamic consistency. Continuum Mechanics and Thermodynamics pp. 1–22 (2015). DOI 10.1007/s00161-015-0434-5

[9] Düsing, M., Mahnken, R.: Simulation of lower bainitic transformation with the phase-field method considering carbide formation. Computational Materials Science **111**, 91–100 (2016). DOI 10.1016/j.commatsci.2015.08.043

[10] Fried, E., Gurtin, M.E.: Continuum theory of thermally induced phase transitions based on an order parameter. Physica D: Nonlinear Phenomena **68**(3), 326–343 (1993)

[11] Fried, E., Gurtin, M.E.: Dynamic solid-solid transitions with phase characterized by an order parameter. Physica D: Nonlinear Phenomena **72**(4), 287–308 (1994)

[12] Gurtin, M.E.: Generalized Ginzburg-Landau and Cahn-Hilliard equations based on a microforce balance. Physica D: Nonlinear Phenomena **92**(3), 178–192 (1996)

[13] Horstmann, D.: Das Zustandsschaubild Eisen-Kohlenstoff und die Grundlagen der Wärmebehandlung der Eisenkohlenstoff-Legierungen. Stahleisen, Ddf. (1985)

[14] Huang, C.J., Browne, D.J., McFadden, S.: A phase-field simulation of austenite to ferrite transformation kinetics in low carbon steels. Acta Materilia **54**, 11–21 (2005)

[15] Kang, M., Sun, J., Yang, Q.: High-temperature transmission electron microscopy in situ study of lower bainite carbide precipitation. Metallurgical Transactions A **21**(3), 853–858 (1990)

[16] Kobayashi, R.: Modeling and numerical simulations of dendritic crystal growth. Physica D **63**, 410–423 (1993)

[17] McFadden, G.B., Wheeler, A.A., Braun, R.J., Coriell, S.R., Sekerkat, R.F.: Phase-field models for anisotropic interfaces. Physical Review E **48**(3), 2016–2024 (1993)

[18] Mecozzi, M., Sietsma, J., van der Zwaag, S., Apel, M., Schaffnit, P., Steinbach, I.: Analysis of the $\gamma \rightarrow \alpha$ Transformation in a C-Mn Steel by Phase-Field Modeling. Metallurgical and Materials Transactions A **36A**, 2327–2340 (2005)

[19] Militzer, M., Mecozzi, M., Sietsma, J., van der Zwaag, S.: Three-dimensional phase field modelling of the austenite-to-ferrite transformation. Acta Materilia **54**(15), 3961–3972 (2006)

[20] Müller, I., Weiss, W.: Entropy and Energy: A Universal Competition. Interaction of Mechanics and Mathematics. Springer Berlin Heidelberg (2006)

[21] Olson, G., Bhadeshia, H., Cohen, M.: Coupled Diffusional / Displacive Transformations. Acta Metallurgica **37**(2), 381–389 (1989)

[22] Sajjadi, S.A., Zebarjad, S.M.: Isothermal transformation of austenite to bainite in high carbon steels. Journal of Materials Processing Technology **189**(1), 107–113 (2007)

[23] Schmitt, R., Müller, R., Kuhn, C., Urbassek, H.M.: A phase field approach for multivariant martensitic transformations of stable and metastable phases. Archive of Applied Mechanics **83**(6), 849–859 (2013)

[24] Silhavy, M.: The Mechanics and Thermodynamics of Continuous Media. Theoretical and Mathematical Physics. Springer Berlin Heidelberg (2013)

[25] Song, W., Prahl, U., Bleck, W., Mukherjee, K.: Phase-field simulations of bainitic phase transformation in 100cr6. TMS 2011 140th Annual Meeting and Exhibition pp. 417–425 (2011)

[26] Steinbach, I.: Phase-field models in materials science. Modelling Simul. Mater. Sci. Eng. **17** (2009)

[27] Steinbach, I., Apel, M.: The influence of lattice strain on pearlite formation in fe-c. Acta Materialia **55**(14), 4817–4822 (2007)

[28] Steinbach, I., Pezzolla, F., Nestler, B., Seeßelberg, M., Ptieler, R., Schmitz, G., Rezende, J.: A phase field concept for multiphase systems. Physica D **94**, 135–147 (1996)

[29] Villani, A., Busso, E.P., Ammar, K., Forest, S., Geers, M.: A fully coupled diffusional-mechanical formulation: numerical implementation, analytical validation, and effects of plasticity on equilibrium. Archive of Applied Mechanics **84**(9-11), 1647–1664 (2014)

[30] Yamanaka, A., Takaki, T., Tomita, Y.: Phase-Field Simulation of Austenite to Ferrite Transformation and Widmanstätten Ferrite Formation in Fe-C Alloy. Materials Transactions **47**(11), 2725–2731 (2006)

[31] Yamanaka, A., Takaki, T., Tomita, Y.: Elastoplastic phase-field simulation of self-and plastic accommodations in cubic tetragonal martensitic transformation. Materials Science and Engineering: A **491**(1), 378–384 (2008)

Paper C

M. Düsing and R. Mahnken

A coupled phase field/diffusion model for upper and lower bainitic transformation

International Journal of Solids and Structures 135, 172–183, 2018

A coupled phase field/diffusion model for upper and lower bainitic transformation

Martin Düsing and Rolf Mahnken

Chair of Engineering Mechanics, Paderborn University,

Warburger Str. 100, 33098 Paderborn, Germany

Abstract

Bainite is a steel microstructure consisting of three phases, bainitic ferrite, austenite and carbides. It forms in two different morphologies, upper and lower bainite, where different diffusion mechanisms are dominant. The aim of this work is to simulate both transformations within a unified model. To this end, we extend an own previously published model for lower bainite with diffusion across the phase interface. As a central idea we introduce weighted Helmholtz energy functions and a weighted mobility tensor, respectively. The individual Helmholtz energy functions and mobility terms are related to the different diffusion mechanisms which are responsible for the formation of both morphologies. Two representative examples illustrate the capability of the coupled phase field/diffusion model and show the expected behaviour.

Keywords: Coupled phase field/diffusion model, bainite, multiphase field method, Cahn-Hilliard diffusion, diffusion across the interface, lower bainitic transformation, upper bainitic transformation, thermodynamic framework, microforce balance

1 Introduction

The bainitic microstructure of steel shows two different morphologies, upper and lower bainite. The transformation of both morphologies starts with a displacive austenite-to-bainitic-ferrite transition at preformed nuclei as observed by Olson et al. [1]. The bainitic ferrite grows in wedge-shaped sheaves, which are divided in sub-units. Subsequently (not simultaneously) carbon starts to move, where however the pertinent diffusion mechanisms are significantly different.

In lower bainite carbon undergoes a separation process within a supersaturated bainitic ferrite phase [2]. It builds accumulations of carbon, where carbides precipitate. This transformation mechanism is noticed e.g. by Bhadeshia who also showed that carbides in lower bainite precipitate directly from the bainitic ferrite [3]. Only a small amount of carbon diffuses across the interface into the austenite.

Upper bainite grows at temperatures between the pearlite formation and the lower bainite formation. The transformation from austenite to bainitic ferrite is comparable to the lower bainite formation. After this transformation most of the carbon within the supersaturated bainitic ferrite diffuses across the interface into the austenite. This movement is particularly strong near the interface and stops when the equilibrium concentration is reached. In between two sheaves the concentration of carbon may become very high, which leads to precipitation of carbides out of the austenite. Depending on other alloying elements, like Silicon or Chromium, the precipitation of carbides is suppressed such that the austenite phase does not transform and remains as residual or retained austenite.

The displacive growth of the ferritic sub-units is accompanied by invariant-plane strain deformation arising from a strain energy [2]. The resulting permanent strain is called transformation plasticity [2]. Furthermore, the austenite-to-bainitic-ferrite transition cannot be caused only by cooling to a certain temperature but also by applying stress or a combination of both [2]. The transformation plasticity can cause anisotropic changes in shape without an applied stress.

In the literature there are several models simulating phase transformations in steel [4], for example austenite-to-ferrite by Militzer et al. [5], Huang et al. [6], Mecozzi et al. [7], austenite-to-pearlite by Steinbach and Apel [8], austenite-to-martensite transformations by Yamanaka et al, Schmitt et al. [9, 10] and Widmanstätten formation by Yamanaka et al. [11]. However, only a few models are able to describe phenomena of the bainitic transformation. Arif and Qin [12] show the autocatalysis event between two sub-units and Song at al. [13] describe the growth of upper bainitic ferrite neglecting the formation of carbides. A model concept for the lower bainitic transformation is proposed in [14] and [15] considering carbon separation within the bainitic ferrite and the precipitation of carbides. It is thereafter applied in [16]. In [17] a multi-scale model for the bainitic transformation considering multi-variant polycristallines is presented. To the authors best knowledge, a model accounting for upper and lower bainitic transformation is not available so far.

This work focuses on the isothermal simulation of upper and lower bainite growth. We model a displacive transformation from austenite to bainitic ferrite, the subsequent (not simultaneous) diffusion of carbon and the resulting precipitation of carbides. We point out that we do not consider any cooperative or diffusion controlled growth as it is known for pearlite. The transformation is modelled with a coupled phase-field/diffusion approach, which is based on a coupled Ginzburg-Landau/Cahn-Hilliard system of equations. The thermodynamic framework developed in [15] for a lower bainite model with a simpler carbon diffusion is used. It is based on generalized forces and stresses as introduced by Gurtin and Fried [18, 19, 20]. In order to account for both, upper and lower bainitic transformation, within a unified model we extend the lower bainitic simulation of [15] with diffusion across the phase interface as presented by Wheeler et al. [21]. As a central idea we introduce weighted Helmholtz energy functions and a weighted mobility tensor, respectively. The individual Helmholtz energy functions and mobility terms are related to the different diffusion mechanisms which are responsible for the formation of the two different morphologies. The weighting is achieved by individual scalar functions depending on the temperature. At high temperatures, these functions guarantee diffusion across the interface and balancing diffusion within the bulk phases of the corresponding interface. The lower transformation model presented here is an extension of [15]. Due to the weighting functions the model shows a strong carbon separation process within the bainitic ferrite and additionally diffusion across the interface. Furthermore the precipitation of carbides within the austenite can be described with the proposed diffusion model. The anisotropic phase growth is modelled with a phase field based scheme [22]. A coupling with strain and stress effects is not part of this work. We plan to extend our thermodynamic framework in [15] to consider the related strain energy in future work.

An outline of this work is as follows: In Section 2 the three diffusion mechanisms required to model the bainite transformation are described in detail. Section 3 recalls the thermodynamic framework for coupled Ginzburg-Landau/Cahn-Hilliard systems based on generalized stresses [15]. In Section 4 a prototype model for upper and lower bainite is introduced. The corresponding constitutive equations include various Helmholtz energy functions, dissipation moduli and diffusion mobility terms. The section ends with evolution equations for order parameters and carbon concentration. Section 5 briefly describes the finite element implementation of the unified bainite transformation model. The resulting algebraic system of equations mirrors the coupling of the different physical phenomena. In Section 6 numerical examples for upper and lower bainite are presented and discussed. The last section is a conclusion summarizing the outcome of this paper and giving an outlook for further investigations.

Notations: Vectors $\boldsymbol{a}$ and second-order tensors $\boldsymbol{A}$ are bold and matrices $\underline{B}$ are underlined. In the three-dimensional Cartesian coordinate system, the gradient and the Laplacian, respectively, of a scalar field $\alpha(\boldsymbol{x})$ are given by

$$1.\ \nabla\alpha(\boldsymbol{x}) = \sum_{i=1}^{3} \frac{\partial\alpha(\boldsymbol{x})}{\partial x_i}\boldsymbol{e}_i \qquad 2.\ \Delta\alpha(\boldsymbol{x}) = \nabla\cdot\nabla\alpha(\boldsymbol{x}) = \sum_{i=1}^{3} \frac{\partial^2\alpha(\boldsymbol{x})}{\partial x_i^2}. \tag{1}$$

where $\boldsymbol{e}_i, i = 1, 2, 3$ are standard unit vectors and x_i are the coordinates of $\boldsymbol{x}$. The divergence of a vector field $\boldsymbol{a}(\boldsymbol{x})$ reads

$$\nabla\cdot\boldsymbol{a}(\boldsymbol{x}) = \sum_{i=1}^{3} \frac{\partial a_i}{\partial x_i}. \tag{2}$$

2 Diffusion mechanisms in upper and lower bainite

The main challenge of this work is the modelling of carbon diffusion to account for different movements of carbon within the various phases and morphologies. To this end as a model assumption, we introduce three different diffusion processes which are involved for both, upper and lower bainite, as illustrated in Figure 1 and henceforth denoted as Type I, Type II and Type III, respectively. In Figure 1 two phases are coloured in red and yellow, respectively, with a diffuse interface in between. Moreover the interface regions are illustrated by black dashed lines.

I. *Separation within a phase*: The separation diffusion process leads to accumulations of carbon at a high concentration limit within a bulk area of carbon at a low concentration limit. According to the schematic diagram in Figure 1.I, the separation takes place only within one phase. The carbon atoms, illustrated as dots, accumulate at certain places, while there are almost no atoms left in between.

II. *Accumulation within an interface*: This diffusion process governs the movement of the carbon in the diffuse interface region between two phases. As illustrated in Figure 1.II, initially uniformly distributed carbon atoms are transported to one specific side of the diffuse interface, thus resulting into a non-uniform distribution.

III. *Balancing within the phases*: The balancing mechanism distributes the atoms over a certain domain, e.g. a phase, such that the concentration of the solute is uniformly distributed as shown in Figure 1.III within both phases. It may also be referred as Fick's type diffusion. The concentrations in different phases may differ. For the specific case in Figure 1.III, the balancing process especially moves carbon atoms which are accumulated within the interface but close to the bulk phase, into the bulk phase, while on the other side of the interface it pushes atoms into the empty interface.

Accumulation within an interface (Type II) in combination with the balancing process (Type III) moves atoms from one phase into the other, henceforth denoted as *diffusion across the interface* (Type II + Type III), see Figure 1.

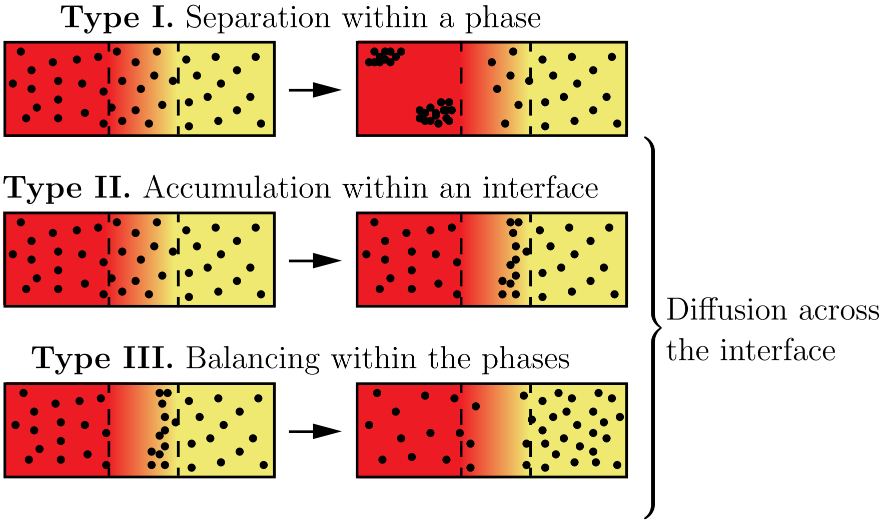

Figure 1: Schematics of three diffusion mechanisms

Table 1 links the above three diffusion processes to the phases and morphologies of upper and lower bainite. In upper bainite there is no separation process within a phase, but an accumulation within the diffuse interface (Type II) and a balancing process (Type III) which assists the diffusion across the interface between bainitic ferrite and austenite. Separation works also between bainitic ferrite and carbide in upper bainite. The nucleating carbides attract surrounding carbon to stabilize itself and grow faster.

In lower bainitic ferrite, the most significant diffusion mechanism is the separation process (Type I), which takes place only within bainitic ferrite as documented in Table 1. Additionally, there is an accumulation process within the interface between bainitic ferrite and austenite, but at a much weaker level than in upper bainite. The transported carbon can diffuse into the whole austenite region with the balancing mechanism which does not occur within the bainitic ferrite where the separation process governs the flow to the interface.

For both morphologies, upper and lower bainite, the carbon concentration influences especially the precipitation of carbides. The phase transformation from austenite to bainitic ferrite is displacive. Consequently the phase transformation is independent from the carbon diffusion which is a subsequent process governing the precipitation of carbides and the growth of residual austenite.

Type I and Type III describe diffusion processes within phases and therefore are independent of any model to simulate or identify the phases. In this work the phase field method is chosen to simulate the phases. This method uses non-sharp but diffuse interfaces between phases. Therefore we choose diffusion Type II to simulate the movement of carbon within the diffuse interface. Due to computational limits the interface width of the representative examples in Section 6 is oversized and therefore a rather crude approximation for the real process.

	Bainitic ferrite		Austenite		Carbide	
Diffusion mechanisms	upper	lower	upper	lower	upper	lower
I. Separation within a phase		$*$				
II. Accumulation within an interface	$\bullet$	$*$	$\bullet$	$*$	$\bullet$	
III. Balancing within the phases	$\bullet$		$\bullet$	$*$		

Table 1: Carbon diffusion processes within different phases and morphologies of bainite: symbol $\bullet$ marks diffusion mechanisms occurring in upper bainite and symbol $*$ those occurring in lower bainite.

3 Coupled Ginzburg-Landau/Cahn-Hilliard framework

In this work phase transformations are modelled with a multiphase Ginzburg-Landau equation which is coupled to a Cahn-Hilliard type diffusion equation. A thermodynamic framework for such a coupled problem is derived in [15]. It is based on generalized stresses and forces proposed over a volume B with an arbitrary control volume V as a subregion of B and the boundary ∂V with outward normal unit vector $\boldsymbol{n} \in \mathbb{R}^3$. All underlying constitutive variables of the model are summarized in the vector

$$\boldsymbol{z} = [c,\ \nabla c,\ \dot{c},\ \mu,\ \nabla\mu,\ \{\phi_i,\ \nabla\phi_i,\ \dot{\phi}_i\}_{i=1}^{N_p}], \tag{3}$$

where c denotes the concentration of a solute, μ is the corresponding chemical potential, ϕ_i are the phase order parameters satisfying $0 \le \phi_i \le 1, \sum_{i=1}^{N_p} \phi_i = 1$ and N_p is the number of phases.

Generally, constitutive equations may depend on the constitutive variables $\boldsymbol{z}$. However, as extensively discussed in [15] and [18] the Helmholtz energy function

$$\psi = \hat{\psi}(\tilde{\boldsymbol{z}}) \tag{4}$$

depends only on the reduced constitutive variables

$$\tilde{\boldsymbol{z}} = [c, \nabla c, \{\phi_i, \nabla\phi_i\}_{i=1}^{N_p}]. \tag{5}$$

The boundary value problem for the chemical potential reads

$$\mu = \frac{\partial\hat{\psi}(\tilde{\boldsymbol{z}})}{\partial c} - \nabla\cdot\frac{\partial\hat{\psi}(\tilde{\boldsymbol{z}})}{\partial\nabla c} + \tau(\boldsymbol{z}) \ \text{ on } \ V, \tag{6}$$

$$\nabla\mu\cdot\boldsymbol{n} = \bar{\mu} \ \text{ on } \ \partial V, \tag{7}$$

with constitutive modulus $\tau(\boldsymbol{z}) \geq 0$ and prescribed out-flux $\bar{\mu}$. The initial boundary value problem for the diffusion of a solute in [15] reads

$$\dot{c} = \nabla\cdot(\boldsymbol{A}(\boldsymbol{z})\cdot\nabla\mu) \ \text{ on } \ V, \tag{8}$$

$$c(t=0) = c_0 \ \text{ on } \ V, \tag{9}$$

$$\nabla c\cdot\boldsymbol{n} = \bar{c} \ \text{ on } \ \partial V, \tag{10}$$

with positive semi-definite second-order mobility tensor $\boldsymbol{A}(\boldsymbol{z})$, prescribed initial value c_0 and prescribed out-flux $\bar{c}$ on the boundary. Phase transformations are described by the phase order parameters ϕ_i satisfying the initial boundary value problem

$$\dot{\phi}_i = \frac{1}{\beta_i(\boldsymbol{z})}\left(\nabla\cdot\frac{\partial\hat{\psi}(\tilde{\boldsymbol{z}})}{\partial\nabla\phi_i} - \frac{\partial\hat{\psi}(\tilde{\boldsymbol{z}})}{\partial\phi_i} + \gamma_i\right), \quad i = 1, ..., N_p \ \text{ on } \ V, \tag{11}$$

$$\phi_i(t=0) = \phi_{i0} \ \text{ on } \ V, \tag{12}$$

$$\nabla\phi_i\cdot\boldsymbol{n} = \bar{\phi}_i \ \text{ on } \ \partial V. \tag{13}$$

Here γ_i are external phase forces, $\beta_i(\boldsymbol{z}) \geq 0$ are constitutive moduli and ϕ_{i0} and $\bar{\phi}_i$ are prescribed initial values and out-fluxes, respectively. Please recall, that equation (8) together with (6) constitutes a conservative fourth order Cahn-Hilliard differential equation, whereas equation (11) governing multiphase transformations is a non-conservative second-order Ginzburg-Landau equation.

4 A prototype model for upper and lower bainite

This section specifies the governing equations of the thermodynamic framework in Section 3. Thereby, to account for upper and lower bainite we provide an extension of the governing equations in [15]. The prototype model developed in this paper describes the growth of $N_p = 3$ phases

1. bainitic ferrite (ϕ_1),
2. austenite (ϕ_2) and
3. carbide (ϕ_3)

to simulate upper and lower bainite formation. Moreover, c introduced in equation (3) represents the carbon concentration.

4.1 Weighted Helmholtz energy

The Helmholtz energy function is a key ingredient to capture the different diffusion mechanisms of Table 1 for bainite. As a specification of equation (4) it is postulated as a sum of two energies

$$\hat{\psi}(\tilde{\boldsymbol{z}}) = \hat{\psi}_c(c, \nabla c) + \hat{\psi}_\phi(c, \phi_1, \phi_2, \phi_3, \nabla\phi_1, \nabla\phi_2, \nabla\phi_3), \tag{14}$$

with a purely diffusive part $\hat{\psi}_c$ and a phase-field part $\hat{\psi}_\phi$ with coupling terms. The diffusive part is again a sum of two energies

$$\hat{\psi}_c(c, \nabla c) = w_f(\theta)\hat{\psi}_f(c) + w_s(\theta)\hat{\psi}_s(c, \nabla c). \tag{15}$$

Here the energy term $\hat{\psi}_f(c)$ accounts for the balancing diffusion (Type III) according to Figure 1.III, which will result into Fick's type of diffusion and $\hat{\psi}_s(c, \nabla c)$ governs the separation of carbon (Type I) according to Figure 1.I. As explained in Section 2 the carbon in upper bainite diffuses across the interface Type II+III) into the austenite phase while in lower bainite the diffusion across the interface is of minor importance compared to the separation Type I). In equation (15) this combined effect is accounted for by weighting functions w_f and w_s, respectively, which weight the different diffusion mechanism to

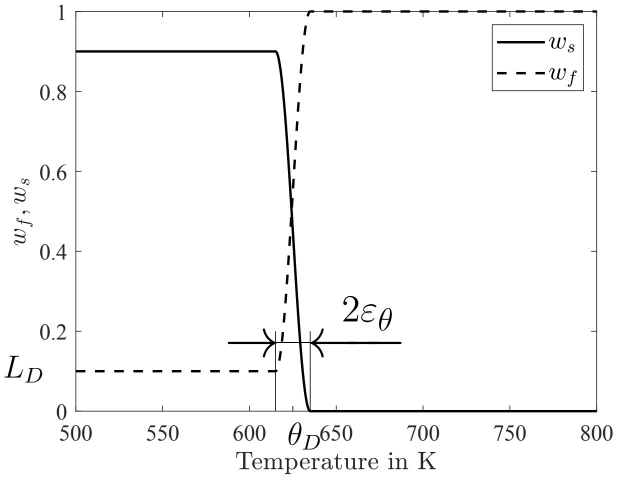

Figure 2: Weighting functions for different diffusion processes

distinguish upper from lower bainite and therefore are dependent on the temperature θ. Figure 2 illustrates both weighting functions versus the temperature θ defined as

$$w_f(\theta) = \begin{cases} 0 & \text{for } \theta < \theta_D - \varepsilon_\theta \\ 1 & \text{for } \theta > \theta_D + \varepsilon_\theta \\ \frac{1}{2} + \frac{L_D}{2} + \left(\frac{1}{2} - \frac{L_D}{2}\right) \sin\left(\pi \left(\frac{\theta - \theta_D}{2\varepsilon_\theta} + 2\right)\right) & \text{otherwise} \end{cases} \tag{16}$$

and

$$w_s(\theta) = \begin{cases} 1 & \text{for } \theta < \theta_D - \varepsilon_\theta \\ 0 & \text{for } \theta > \theta_D + \varepsilon_\theta \\ \frac{1}{2} - \frac{L_D}{2} + \left(\frac{1}{2} - \frac{L_D}{2}\right) \sin\left(\pi \left(\frac{\theta - \theta_D}{2\varepsilon_\theta} + 1\right)\right) & \text{otherwise.} \end{cases} \tag{17}$$

Here θ is the temperature of the isothermal transformation, θ_D is the transition temperature marking the boundary between upper and lower bainite, ε_θ is a factor to soften the sharp boundary for better numerical characteristics and L_D ensures the coaction of both diffusion mechanisms. Note, that both functions w_f and w_s satisfy the completeness condition

$$w_f(\theta) + w_s(\theta) = 1. \tag{18}$$

On one hand, for the separation (Type I) in lower bainite according to Table 1 a

Cahn-Hilliard equation is formulated. A suitable Helmholtz energy is postulated as

$$\hat{\psi}_s(c, \nabla c) = f(c) + \frac{1}{2}\rho|\nabla c|^2, \tag{19}$$

$$f(c) = d(c_{\text{eq}} - c)^2(c_{\text{carb}} - c)^2. \tag{20}$$

where ρ is a Cahn-Hilliard balance factor, $f(c)$ is a double well energy function, c_{eq} is the equilibrium carbon concentration in bainitic ferrite and c_{carb} is the carbon concentration of the carbides. These two concentrations define the limits of the separation process.

On the other hand, for the balancing Fick's diffusion (Type III) required for the diffusion across the interface, we introduce

$$\hat{\psi}_f(c) = \frac{c_{\text{eq}}\ln(c_{\text{eq}} - c) - c_{\text{carb}}\ln(c_{\text{carb}} - c) + c\ln(\frac{c_{\text{carb}}-c}{c_{\text{eq}}-c})}{c_{\text{eq}} - c_{\text{carb}}}. \tag{21}$$

Remarks 1:

1. Equation (21) is a modification of Wheeler et al. [21], where the original bounds 0 and 1 are replaced with c_{carb} and c_{eq}.

2. The balancing diffusion mechanism tackled in equation (21) is important for the upper bainitic transformation, however has minor significance for the lower bainitic transformation. This can be reflected by a high weighting of the separation ($w_s = 0.9$) and a low weighting of the diffusion across the interface ($w_f = 0.1$) for $\theta < \theta_D$. Alternatively, the intensity of the different diffusion mechanisms can be governed by the diffusion coefficients introduced in the next subsection.

3. It is not obvious that equation (21) leads to Fick's type diffusion within the framework used in this work. For clarification, a detailed mathematical justification is provided in Appendix A.

The Helmholtz energy for the phase transformation in equation (14) is proposed as

$$\hat{\psi}_\phi(c, \phi_1, \phi_2, \phi_3, \nabla\phi_1, \nabla\phi_2, \nabla\phi_3) = \sum_{i=1}^{N_p}\sum_{j>i}^{N_p}\frac{1}{q_{ij}}\left[h_{ij}(\phi_i, \phi_j, \nabla\phi_i, \nabla\phi_j) + (1 + c\ s_{ij}\ w_f)\ g_{ij}(\phi_i, \phi_j)\right] \tag{22}$$

with the interfacial energy density $h_{ij}(\phi_i, \phi_j, \nabla\phi_i, \nabla\phi_j)$ and the potential energy $g_{ij}(\phi_i, \phi_j)$ between two phases i and j. The phase energy coefficients are denoted by q_{ij}. Compared to [15] we introduce the additional term $c\ s_{ij}\ w_f$, where s_{ij} are interface diffusion factors which govern the accumulation of carbon within the interface (Type II) between phases i and j according to Figure 1.II. The interfacial energy density is chosen, following [23], as

$$h_{ij}(\phi_i, \phi_j, \nabla\phi_i, \nabla\phi_j) = \frac{1}{2}\alpha_{ij}(\phi_j\nabla\phi_i - \phi_i\nabla\phi_j)^2 \tag{23}$$

with the phase gradient energy coefficient α_{ij}. The potential or chemical energy density g_{ij} between two phases i and j is chosen as a simple double well potential

$$g_{ij}(\phi_i, \phi_j) = \frac{1}{4a_{ij}}\phi_i^2\phi_j^2, \tag{24}$$

where a_{ij} are potential constants.

4.2 Evolution equations

The constitutive moduli τ, β_i and the mobility tensor $\boldsymbol{A}$ introduced in equations (6), (11) and (8), respectively, have to be specified, in order to gain the evolution equations for the concentration field c and the phase order parameters ϕ_i. We postulate the constant moduli

$$\tau(\boldsymbol{z}) = \tau w_s = \text{const.}, \tag{25}$$

$$\beta_i(\boldsymbol{z}) = \beta_i = \text{const.} \tag{26}$$

In order to account for both, separation within a phase (Type I) and diffusion across the interface (Type II + Type III), the mobility tensor $\boldsymbol{A}$ is postulated as the sum of two terms, weighted by w_f and w_s introduced in equations (16) and (17),

$$\boldsymbol{A}(\boldsymbol{z}) = (w_f D_f(\phi) f_q(c) + w_s D_s(\phi))\,\mathbf{1}, \tag{27}$$

where

$$D_f(\phi) = \sum_{i=1}^{N_p} \phi_i D_{fi}, \tag{28}$$

$$D_s(\phi) = \sum_{i=1}^{N_p} \phi_i D_{si} \tag{29}$$

$$f_q(c) = (c - c_{\text{eq}})(c_{\text{carb}} - c). \tag{30}$$

In equations (28) and (29) D_{fi} and D_{si} are diffusion coefficients for diffusion across the interface and Cahn-Hilliard diffusion, respectively.

Remarks 2:

1. The function f_q in equation (30) is required to limit the accumulation process within the interface (Figure 1.II) with an upper and lower bound, c_{carb} and c_{eq}, respectively.
2. As shown in equation (A.4) of Appendix A the function f_q affects also the balancing diffusion (Figure 1.III) which is additionally needed to model diffusion across the interface as discussed in Section 2. In order to preserve Fick's type diffusion, the corresponding Helmholtz energy (21) is postulated to fulfil

$$f_q(c)\frac{\partial^2\hat{\psi}_f(c)}{\partial c^2} = 1. \tag{31}$$

Further details on this approach are explained in Appendix A.

Having specified all constitutive equations, the evolution equations can be assembled based on the thermodynamic framework in Section 3. To derive the concentration evolution equation, the chemical potential is needed. Inserting the Helmholtz energy equation (14) and the dissipation modulus (25) into equation (6) render a weighted chemical potential

$$\mu = w_f\mu_f + w_s\mu_s, \tag{32}$$

where

$$\mu_f = \frac{\partial\hat{\psi}_f(c)}{\partial c} + \sum_{i=1}^{N_p}\sum_{j>i}^{N_p} v_{ij}\phi_i^2\phi_j^2, \tag{33}$$

$$\mu_s = \frac{\partial f}{\partial c} - \rho\Delta c + \tau\dot{c}. \tag{34}$$

and for brevity

$$v_{ij} = \frac{s_{ij}}{4a_{ij}q_{ij}}. \tag{35}$$

The next equation describes the concentration field c. Inserting equation (32) into the evolution equation (8) leads to

$$\dot{c} = \nabla\cdot(w_f \boldsymbol{A}(\boldsymbol{z})\nabla\mu_f) + \nabla\cdot(w_s \boldsymbol{A}(\boldsymbol{z})\nabla\mu_s). \tag{36}$$

The next natural step would be to insert μ_f (33) and μ_s (34) into equation (36). However, to avoid fourth order derivatives in the evolution equation of the concentration c, the separation part μ_s of the chemical potential (34) is not inserted into equation (36) which would lead to difficulties for the finite element implementation, described in the next section. Therefore only μ_f from equation (33) is inserted into equation (36).

The product of $\boldsymbol{A}(\boldsymbol{z}) \cdot \nabla\mu_f$ leads to simplifications of the resulting evolution equation. The lengthy algebra describing the steps in detail can be found in Appendix A. The evolution equation of the concentration field c reads

$$\begin{aligned}
\dot{c} = {} & w_f^2 \nabla D_f(\phi) \cdot \nabla c + w_f^2 D_f(\phi)\Delta c + w_s w_f \nabla D_s(\phi) \frac{\partial^2 \hat{\psi}_f(c)}{\partial c^2} \nabla c \\
& + w_s w_f D_s(\phi) \frac{\partial^3 \hat{\psi}_f(c)}{\partial c^3} (\nabla c)^2 + w_s w_f D_s(\phi) \frac{\partial^2 \hat{\psi}_f(c)}{\partial c^2} \Delta c \\
& + \left(w_f^2 \nabla D_f(\phi) f_q(c) + w_f^2 D_f(\phi) \frac{\partial f_q(c)}{\partial c} \nabla c + w_s w_f \nabla D_s(\phi) \right) \\
& \cdot \sum_{i=1}^{N_p} \sum_{j>i}^{N_p} v_{ij} \left(2\phi_i \phi_j^2 \nabla\phi_i + 2\phi_j \phi_i^2 \nabla\phi_j \right) \\
& + \left(w_f^2 D_f(\phi) f_q(c) + w_s w_f D_s(\phi) \right) \\
& \sum_{i=1}^{N_p} \sum_{j>i}^{N_p} 2v_{ij} \left(\nabla\phi_i \phi_j^2 \nabla\phi_i + \nabla\phi_j \phi_i^2 \nabla\phi_j + 4\phi_i\phi_j \nabla\phi_i \nabla\phi_j + \phi_j \phi_i^2 \Delta\phi_j + \phi_i \phi_j^2 \Delta\phi_i \right) \\
& + \left(w_s w_f \nabla D_f(\phi) f_q(c) + w_s w_f D_f(\phi) \frac{\partial f_q(c)}{\partial c} \nabla c + w_s^2 \nabla D_s(\phi) \right) \cdot \nabla\mu_s \\
& + \left(w_s w_f D_f(\phi) f_q(c) + w_s^2 D_s(\phi) \right) \Delta\mu_s
\end{aligned} \tag{37}$$

The evolution equation for the phase order parameters ϕ_i is derived by inserting the Helmholtz energy equation (14) into equation (11)

$$\dot{\phi_i} = \sum_{j=1, j\neq i}^{N_p} \frac{1}{\beta_i q_{ij}} \left(\alpha_{ij} \left(\phi_j \Delta\phi_i - \phi_i \Delta\phi_j \right) - \frac{\phi_i \phi_j \cdot (1 + c\ s_{ij}\ w_f)}{2a_{ij}} (\phi_j - \phi_i) \right) + \gamma_i, \quad \text{for} \quad i = 1, ..., N_p\ . \tag{38}$$

According to [7] the material parameters of equation (38), namely the phase gradient energy coefficients α_{ij}, the potential constants a_{ij}, the phase energy coefficients q_{ij} and the dissipative moduli β_i are replaced by the interface mobilities ζ_{ij}, interface energies σ_{ij} and interface thicknesses η_{ij}

$$\beta_i q_{ij} = \frac{\eta_{ij}}{\zeta_{ij}}, \qquad a_{ij} = \frac{\eta_{ij}}{72\sigma_{ij}}, \qquad \alpha_{ij} = \sigma_{ij}\eta_{ij}. \tag{39}$$

Details of this parameter change (39) using the Gibbs-Thomson equation [7] can be found in the appendix of [14].

Furthermore we postulate the external forces γ_i of equation (38) as sums over all phases N_p which perform work on the phase transition between two phases i and j

$$\gamma_i = \sum_{j=1, j\neq i}^{N_p} \gamma_{ij} = -\sum_{j=1, j\neq i}^{N_p} \frac{6\zeta_{ij}\Delta G_{ij}(\boldsymbol{z})}{\eta_{ij}}\, \phi_i\, \phi_j. \tag{40}$$

In equation (40) ΔG_{ij} describe the change of Gibbs energies between the phases i and j. The arbitrary factor 6 has been introduced to be consistent with the evolution equations of [14, 7]. Note the relations $\zeta_{ij} = \zeta_{ji}$, $\sigma_{ij} = \sigma_{ji}$ and $\eta_{ij} = \eta_{ji}$ but $\Delta G_{ij} = -\Delta G_{ji}$.

The evolution equation for the phase order parameters (38) is finally written as

$$\dot{\phi}_i = \sum_{j=1, j\neq i}^{N_p} \zeta_{ij} \Bigg[\sigma_{ij} \left((\phi_j \Delta\phi_i - \phi_i \Delta\phi_j) - \frac{36}{\eta_{ij}^2}(1 + c\ s_{ij}\ w_f)\phi_i\phi_j(\phi_j - \phi_i) \right) - \frac{6\Delta G_{ij}(\boldsymbol{z})}{\eta_{ij}}\phi_i\phi_j \Bigg] \quad \text{for} \quad i = 1, ..., N_p. \tag{41}$$

To model anisotropy a widely used approach by Kobayashi [22] and G.B. McFadden et al. [24] is implemented. The interface energy parameters σ_{ij} depend on the local gradient $\nabla\phi_i$ and a predefined growth direction θ_0 [15]

$$\sigma_{ij} = \sigma_{ij}(\theta(\nabla\phi_i), \theta_0). \tag{42}$$

The anisotropic transformation from austenite to bainitic ferrite is modelled with

$$\sigma_{12} = \sigma_{12}^0 \cdot (1 + r \cdot \cos(\theta - \theta_0)), \quad \text{where} \quad \theta = \arctan\frac{\frac{\partial\phi_1}{\partial y}}{\frac{\partial\phi_1}{\partial x}}. \tag{43}$$

In the sequel, the strength of anisotropy is set to $r = 0.5$, the main growth direction is $\theta_0 = 0°$ and σ_{12}^0 is the isotropic interface energy [15].

To model the precipitation of carbides as described in Section 1 and Section 2 we provide the following set of equations for the Gibbs energy, as presented in [15]:

$$\Delta G_{ij}(\boldsymbol{z}) = \Delta G^0_{ij}\; v(\phi_i, \phi_j, c) \tag{44}$$

where

$$v(\phi_i, \phi_j, c) = \begin{cases} \frac{w(c)}{\phi_3^2+\varepsilon_\phi} & \text{for } i = 3 \vee j = 3 \\ 1 & \text{otherwise} \end{cases} \tag{45}$$

and ΔG^0_{ij} are constant material parameters describing the differences in Gibbs energy between phases i and j. Furthermore $w(c)$ is a smooth unit step function, defined as

$$w(c) = \begin{cases} 0 & \text{for } c < c_{\text{carb}} - \varepsilon \\ 1 & \text{for } c > c_{\text{carb}} \\ \frac{1}{2} + \frac{1}{2}\sin(\frac{\pi}{\varepsilon}c + \frac{\pi}{2} - \frac{\pi}{\varepsilon}c_{\text{carb}}) & \text{otherwise,} \end{cases} \tag{46}$$

where the parameter ε describes the width of the smooth step.

The idea of equations (44)-(46) is that the carbide phase will grow only if the carbon concentration at the certain place is high enough. To be specific, it must reach $c_{\text{carb}} = 6.67\,\text{wt.\%}$ [25], to start the formation of carbides.

Remarks 3:

1. In general the Gibbs energy $\Delta G_{ij}(\boldsymbol{z})$ is a function of the temperature and the carbon concentration. The model presented in this paper considers only isothermal processes such that the temperature dependence can be neglected. Furthermore the transformation from austenite (ϕ_2) to bainitic ferrite (ϕ_1) is displacive, which means that it does not depend on the local concentration of carbon, which is constant over the process at the transformation places.

2. In equation (45) we introduce a very small numerical perturbation $\varepsilon_\phi > 0$ to prevent a division by zero in the case that $\phi_3 = 0$. The divisor ϕ_3^2 guarantees a growth of the ϕ_3 phase even if the current value of ϕ_3 is close to zero.

5 Numerical implementation

In this section information about the numerical implementation is provided. The system of partial differential equations (34), (37) and (41) is solved with the finite element method in a two dimensional space. Quadrilateral elements with linear shape functions are used for the finite element formulation. For time discretization the backward Euler method is used. The resulting algebraic system of equations is solved with Newton's method.

As already mentioned in Section 4.2 the chemical potential μ_s for the lower bainitic transformation is not inserted into the evolution equation of the concentration (37), instead it will be handled as a separate degree of freedom to avoid fourth order derivatives. Taking three phases into account leads to five unknowns $c, \mu_s, \phi_1, \phi_2, \phi_3$ per finite element node. A possibility to avoid the chemical potential μ_s as an additional degree of freedom is given by the isogeometric finite element method [26, 27], which is therefore considered for future work.

The weak formulation of the lower chemical potential (34) reads

$$\int_V \nu_\mu \tau \dot{c} + \rho \nabla \nu_\mu \nabla c + \nu_\mu \frac{\partial f(c)}{\partial c} - \nu_\mu \mu_s \; dV = 0. \tag{47}$$

where ν_μ denotes the test function for the lower chemical potential. The weak formulation of the diffusion equation (37) reads

$$
\begin{aligned}
\int_V \nu_c \dot{c}\ dV = \int_V \nu_c w_f^2 \nabla D_f(\phi) \nabla c\ dV + \int_V \nu_c w_f^2 D_f(\phi) \Delta c\ dV \\
+ \int_V \nu_c w_s w_f \nabla D_s(\phi) \frac{\partial^2 \hat{\psi}_f(c)}{\partial c^2} \nabla c\ dV + \int_V \nu_c w_s w_f D_s(\phi) \frac{\partial^3 \hat{\psi}_f(c)}{\partial c^3} (\nabla c)^2\ dV \\
+ \int_V \nu_c w_s w_f D_s(\phi) \frac{\partial^2 \hat{\psi}_f(c)}{\partial c^2} \Delta c\ dV \\
+ \int_V \nu_c \left(w_f^2 \nabla D_f(\phi) f_q(c) + w_f^2 D_f(\phi) \nabla f_q(c) + w_s w_f \nabla D_s(\phi) \right) \\
\cdot \sum_{i=1}^{N_p} \sum_{j>i}^{N_p} 2 v_{ij} (\nabla \phi_i \phi_i \phi_j^2 + \phi_i^2 \phi_j \nabla \phi_j)\ dV + \int_V \nu_c \left(w_f^2 D_f(\phi) f_q(c) + w_s w_f D_s(\phi) \right) \\
\sum_{i=1}^{N_p} \sum_{j>i}^{N_p} 2 v_{ij} (\Delta \phi_i \phi_i \phi_j^2 + (\nabla \phi_i)^2 \phi_j^2 + 4 \nabla \phi_i \phi_i \phi_j \nabla \phi_j + \Delta \phi_j \phi_i^2 \phi_j + (\nabla \phi_j)^2 \phi^2)\ dV \\
+ \int_V \nu_c (w_f w_s \nabla D_f(\phi) f_q(c) + w_f w_s D_f(\phi) \nabla f_q(c) + w_s^2 \nabla D_s(\phi)) \cdot \nabla \mu_s\ dV \\
+ \int_V \nu_c (w_f w_s D_f(\phi) f_q(c) + w_s^2 D_s(\phi)) \Delta \mu_s\ dV, \quad (48)
\end{aligned}
$$

where ν_c is the test function needed for the finite element formulation.

The weak formulation of the phase field evolution equations (41) with its ν_ϕ and already applied Gauss theorem and homogeneous Neumann boundary conditions read

$$
\begin{aligned}
\int_V \nu_\phi \dot{\phi}_i\ dV = \int_V \sum_{j=1, j \neq i}^{N_p} \zeta_{ij} \Bigg[\sigma_{ij} \Bigg(\nabla \nu_\phi (\nabla \phi_j \phi_i - \nabla \phi_i \phi_j) \\
- \frac{36}{\eta_{ij}^2} \nu_\phi \phi_i \phi_j (1 + c\ s_{ij}\ w_f)(\phi_j - \phi_i) \Bigg) - \frac{6 \Delta G_{ij}(\boldsymbol{z})}{\eta_{ij}} \nu_\phi \phi_i \phi_j \Bigg]\ dV. \quad (49)
\end{aligned}
$$

For the matrix formulation we denote the degrees of freedom at every node with the superimposed hat $\hat{(\cdot)}$ and introduce a row vector $\underline{N}$ containing the shape function values. As a result the following scalar products can be used:

$$
c = \underline{N} \underline{\hat{c}}\ , \qquad \mu_s = \underline{N} \underline{\hat{\mu}_s}\ , \qquad \phi_i = \underline{N} \underline{\hat{\phi}_i}\ , \quad i = 1, 2, 3. \qquad (50)
$$

The gradient terms are described by

$$
\nabla c = \underline{B} \underline{\hat{c}}\ , \qquad \nabla \mu_s = \underline{B} \underline{\hat{\mu}_s}\ , \qquad \nabla \phi_i = \underline{B} \underline{\hat{\phi}_i}\ , \quad i = 1, 2, 3. \qquad (51)
$$

where

$$\underline{B} = \begin{bmatrix} \underline{N}_{,x} \\ \underline{N}_{,y} \end{bmatrix}, \qquad \text{with} \qquad \underline{N}_{,x} = \frac{\partial \underline{N}}{\partial x}. \tag{52}$$

The relations in equations (50) and (51) can be formulated for the test functions ν_ϕ, ν_c and ν_μ respectively. The actual time step is described by the superimposed n, which is only used inside the backward Euler terms and omitted for brevity in other parts.

In the following the element residual terms are presented based on the weak formulations (47), (48) and (49). All terms are obtained using Gauss's theorem and homogeneous Neumann boundary conditions $\bar{c} = 0, \bar{\phi}_i = 0$ in equations (10) and (13)

$$\begin{aligned} \underline{R}^c = \int\limits_{\Omega_e} \underline{N}^T \underline{N} \frac{\underline{\hat{c}}^n - \underline{\hat{c}}^{n-1}}{\Delta t} + \underline{B}^T \underline{B\hat{c}} \left(w_f^2 D_f(\phi) + w_f w_s D_s(\phi) \frac{\partial^2 \hat{\psi}_f(c)}{\partial c^2} \right) \\ + \underline{B}^T (w_f^2 D_f(\phi) f_q(\underline{\hat{c}}) + w_s w_f D_s(\phi)) \\ \sum_{i=1}^{N_p} \sum_{j>i}^{N_p} 2 v_{ij} \left((\underline{N}\underline{\hat{\phi}}_i)(\underline{N}\underline{\hat{\phi}}_j)^2 \underline{B}\underline{\hat{\phi}}_i + \underline{N}\underline{\hat{\phi}}_j (\underline{N}\underline{\hat{\phi}}_i)^2 \underline{B}\underline{\hat{\phi}}_j) \right) \\ + \underline{B}^T \underline{B}\underline{\hat{\mu}}_l \left(w_f w_s D_f(\phi) f_q(\underline{\hat{c}}) + w_s^2 D_s(\phi) \right) \, d\Omega, \end{aligned} \tag{53}$$

$$\underline{R}^{\mu_s} = \int\limits_{\Omega_e} \tau (\underline{N}^T \underline{N}) \frac{\underline{\hat{c}}^n - \underline{\hat{c}}^{n-1}}{\Delta t} + \underline{N}^T \frac{\partial f(\underline{N}\hat{c})}{\partial c} + \rho (\underline{B}^T \underline{B}) \underline{\hat{c}} - (\underline{N}^T \underline{N}) \underline{\hat{\mu}_s} \, d\Omega, \tag{54}$$

$$\begin{aligned} \underline{R}^{\phi_i} = \int\limits_{\Omega_e} \underline{N}^T \underline{N} \, \frac{\underline{\hat{\phi}}_i^n - \underline{\hat{\phi}}_i^{n-1}}{\Delta t} + \sum_{j=1, j\neq i}^{N_p} \zeta_{ij} \Bigg[\sigma_{ij} \Bigg(- (\underline{B}^T \underline{B}) \underline{\hat{\phi}}_j (\underline{N}\underline{\hat{\phi}}_i) + (\underline{B}^T \underline{B}) \underline{\hat{\phi}}_i (\underline{N}\underline{\hat{\phi}}_j) \\ - \frac{36}{\eta_{ij}^2} \underline{N}^T (1 + s_{ij} w_f(\underline{N\hat{c}})) \underline{N} (\underline{\hat{\phi}}_i - \underline{\hat{\phi}}_j) \left((\underline{N}\underline{\hat{\phi}}_i)(\underline{N}\underline{\hat{\phi}}_j) \right) \Bigg) \\ + \frac{6}{\eta_{ij}} \Delta G_{ij}(\boldsymbol{z}) \underline{N}^T (\underline{N}\underline{\hat{\phi}}_i)(\underline{N}\underline{\hat{\phi}}_j) \Bigg] \, d\Omega. \end{aligned} \tag{55}$$

The integrals are numerically computed with a Gauss-Legendre rule. As described above Newton's method is used to solve the non-linear system of equations. Hence the derivatives of the residual function $\underline{R} = [\underline{R}^c \quad \underline{R}^{\mu_s} \quad \underline{R}^{\phi_i}]^T$ with respect to all unknown variables

$\underline{\hat{d}} = [\underline{\hat{c}} \;\; \underline{\hat{\mu}} \;\; \underline{\hat{\phi}_i}]^T$ are needed

$$\underline{K} = \frac{\partial \underline{R}}{\partial \underline{\hat{d}}} = \begin{bmatrix} \underline{K}^{cc} & \underline{K}^{c\mu_s} & \underline{K}^{c\phi_o} & \underline{K}^{c\phi_p} \\ \underline{K}^{\mu_s c} & \underline{K}^{\mu_s\mu_s} & \underline{0} & \underline{0} \\ \underline{K}^{\phi_o c} & \underline{0} & \underline{K}^{\phi_o\phi_o} & \underline{K}^{\phi_o\phi_p} \\ \underline{K}^{\phi_p c} & \underline{0} & \underline{K}^{\phi_p\phi_o} & \underline{K}^{\phi_p\phi_p} \end{bmatrix}, \tag{56}$$

with the matrices

$$\begin{aligned} \underline{K}^{\phi_i\phi_i} = \frac{\partial \underline{R}^{\phi_i}}{\partial \underline{\hat{\phi}}_i} = \int\limits_{\Omega_e} \underline{N}^T \underline{N} \frac{1}{\Delta t} + \sum_{j=1, j\neq i}^{N_p} \zeta_{ij} \Bigg[\sigma_{ij} \Bigg(& (\underline{B}^T \underline{B})(\underline{N}\underline{\hat{\phi}}_j) - (\underline{B}^T \underline{B})\underline{\hat{\phi}}_j \underline{N} \\ & - \frac{36}{\eta_{ij}^2} \underline{N}^T \underline{N}(1 + s_{ij} w_f(\underline{N}\underline{\hat{c}}))(\underline{N}\underline{\hat{\phi}}_j)\underline{N}(2\underline{\hat{\phi}}_i - \underline{\hat{\phi}}_j) \Bigg) \\ & + \frac{6}{\eta_{ij}} \Bigg(\Delta G_{ij}(\boldsymbol{z}) \underline{N}^T \underline{N}(\underline{N}\underline{\hat{\phi}}_j) + \frac{\partial \Delta G_{ij}(\boldsymbol{z})}{\partial \underline{\hat{\phi}}_i} \underline{N}^T (\underline{N}\underline{\hat{\phi}}_i)(\underline{N}\underline{\hat{\phi}}_j) \Bigg) \Bigg] \, d\Omega, \end{aligned} \tag{57}$$

$$\begin{aligned} \underline{K}^{\phi_i\phi_j} = \frac{\partial \underline{R}^{\phi_i}}{\partial \underline{\hat{\phi}}_j} = \int\limits_{\Omega_e} \zeta_{ij} \Bigg[\sigma_{ij} \Bigg(& - (\underline{B}^T \underline{B})(\underline{N}\underline{\hat{\phi}}_i) + (\underline{B}^T \underline{B})\underline{\hat{\phi}}_i \underline{N} \\ & - \frac{36}{\eta_{ij}^2} \underline{N}^T \underline{N}(1 + s_{ij} w_f(\underline{N}\underline{\hat{c}}))(\underline{N}\underline{\hat{\phi}}_i)\underline{N}(\underline{\hat{\phi}}_i - 2\underline{\hat{\phi}}_j) \Bigg) \\ & + \frac{6}{\eta_{ij}} \Bigg(\Delta G_{ij}(\boldsymbol{z}) \underline{N}^T \underline{N}(\underline{N}\underline{\hat{\phi}}_i) + \frac{\partial \Delta G_{ij}(\boldsymbol{z})}{\partial \underline{\hat{\phi}}_j} \underline{N}^T (\underline{N}\underline{\hat{\phi}}_i)(\underline{N}\underline{\hat{\phi}}_j) \Bigg) \Bigg] \, d\Omega, \end{aligned} \tag{58}$$

$$\begin{aligned} \underline{K}^{\phi_i c} = \frac{\partial \underline{R}^{\phi_i}}{\partial \underline{\hat{c}}} = \int\limits_{\Omega_e} \sum_{j=1, j\neq i}^{N_p} \zeta_{ij} \Bigg[& - \frac{36\sigma_{ij}}{\eta_{ij}^2} \underline{N}^T \underline{N} s_{ij} w_f \underline{N}(\underline{\hat{\phi}}_i - \underline{\hat{\phi}}_j) \Big((\underline{N}\underline{\hat{\phi}}_i)(\underline{N}\underline{\hat{\phi}}_j) \Big) \\ & + \frac{6}{\eta_{ij}} \frac{\partial \Delta G_{ij}(\boldsymbol{z})}{\partial \underline{\hat{c}}} \underline{N}^T (\underline{N}\underline{\hat{\phi}}_i)(\underline{N}\underline{\hat{\phi}}_j) \Bigg] \, d\Omega, \end{aligned} \tag{59}$$

$$
\begin{aligned}
\underline{K}^{cc} = \frac{\partial \underline{R}^c}{\partial \underline{\hat{c}}} = \int_{\Omega_e} & \frac{1}{\Delta t}\underline{N}^T\underline{N} + \underline{B}^T\underline{B}\left(w_f^2 D_f(\phi) + w_f w_s D_s(\phi)\frac{\partial^2 \hat{\psi}_u(\underline{N}\underline{\hat{c}})}{\partial c^2}\underline{N}\right) \\
& + \underline{B}^T w_f^2 D_f(\phi)\frac{\partial f_q(\underline{\hat{N}c})}{\partial c}\underline{N}\sum_{i=1}^{N_p}\sum_{j>i}^{N_p} 2v_{ij}\left((\underline{N}\underline{\hat{\phi}}_i)(\underline{N}\underline{\hat{\phi}}_j)^2\underline{B}\underline{\hat{\phi}}_i + \underline{N}\underline{\hat{\phi}}_j(\underline{N}\underline{\hat{\phi}}_i)^2\underline{B}\underline{\hat{\phi}}_j)\right) \\
& + (\underline{B}^T\underline{B})\underline{\hat{c}}w_f w_s D_s(\phi)\frac{\partial^3 \hat{\psi}_u(\underline{N}\underline{\hat{c}})}{\partial c^3} + (\underline{B}^T\underline{B})\underline{\hat{\mu}}_l w_f w_s D_f(\phi)\frac{\partial f_q(\underline{\hat{N}c})}{\partial c}\underline{N}\; d\Omega, \qquad (60)
\end{aligned}
$$

$$
\underline{K}^{\mu_s\mu_s} = \frac{\partial \underline{R}^{\mu_s}}{\partial \underline{\hat{\mu}_s}} = \int_{\Omega_e} -\underline{N}^T\underline{N}\; d\Omega, \qquad (61)
$$

$$
\underline{K}^{c\mu_s} = \frac{\partial \underline{R}^{c}}{\partial \underline{\hat{\mu}_s}} = \int_{\Omega_e} \underline{B}^T\underline{B}(w_f w_s D_f(\phi) f_q(\underline{N}\underline{\hat{c}}) + w_s^2 D_s(\phi))\; d\Omega, \qquad (62)
$$

$$
\underline{K}^{\mu_s c} = \frac{\partial \underline{R}^{\mu_s}}{\partial \underline{\hat{c}}} = \int_{\Omega_e} \frac{\tau}{\Delta t}\underline{N}^T\underline{N} + \rho\underline{B}^T\underline{B} + \underline{N}^T\frac{\partial^2 f(c)}{\partial c^2}\underline{N}\; d\Omega, \qquad (63)
$$

$$
\begin{aligned}
\underline{K}^{c\phi_i} = \frac{\partial \underline{R}^c}{\partial \underline{\hat{\phi}_i}} = \int_{\Omega_e} & \underline{B}^T\underline{B\hat{c}}\left(w_f^2\frac{\partial D_f(\phi)}{\partial \underline{\hat{\phi}}_i}\underline{N} + w_f w_s\frac{\partial D_s(\phi)}{\partial \underline{\hat{\phi}}_i}\underline{N}\frac{\partial^2 \hat{\psi}_u(\underline{N}\underline{\hat{c}})}{\partial c^2}\right) \\
& + \underline{B}^T(w_f^2 D_f(\phi) f_q(\underline{\hat{c}}) + w_s w_f D_s(\phi)) \\
\sum_{j=1, j\neq i}^{N_p} & 2v_{ij}\left(\underline{B}(\underline{N}\underline{\hat{\phi}}_i)(\underline{N}\underline{\hat{\phi}}_j)^2 + (\underline{B}\underline{\hat{\phi}}_i)\underline{N}(\underline{N}\underline{\hat{\phi}}_j)^2 + 2(\underline{B}\underline{\hat{\phi}}_j)(\underline{N}\underline{\hat{\phi}}_j)(\underline{N}\underline{\hat{\phi}}_i)\underline{N})\right) \\
& + \underline{B}^T\left(w_f^2\frac{\partial D_f(\phi)}{\partial \underline{\hat{\phi}}_i} f_q(\underline{\hat{c}}) + w_s w_f\frac{\partial D_s(\phi)}{\partial \underline{\hat{\phi}}_i}\right) \\
& \sum_{k=1}^{N_p}\sum_{j>k}^{N_p} 2v_{kj}\left((\underline{N}\underline{\hat{\phi}}_k)(\underline{N}\underline{\hat{\phi}}_j)^2\underline{B}\underline{\hat{\phi}}_k + \underline{N}\underline{\hat{\phi}}_j(\underline{N}\underline{\hat{\phi}}_k)^2\underline{B}\underline{\hat{\phi}}_j)\right) \\
& + \underline{B}^T\underline{B}\underline{\hat{\mu}}_l\left(w_f w_s\frac{\partial D_f(\phi)}{\partial \underline{\hat{\phi}}_i} f_q(\underline{\hat{c}})\underline{N} + w_s^2\frac{\partial D_s(\phi)}{\partial \underline{\hat{\phi}}_i}\underline{N}\right)\; d\Omega. \qquad (64)
\end{aligned}
$$

6 Representative examples

In this section we present two examples to illustrate upper and lower bainitic transformations, respectively, on a 3 µm × 3 µm domain. As described in Section 5 the system of partial differential equations is solved with a finite element method. Therefore the domain is discretized into 16384 quadrilateral elements. Homogeneous Neumann boundary

Parameter	**Symbol**	**Value/Unit**
Lower diffusion-across-the-interface parameter	L_D	0.5
Maximum carbon concentration in ferrite	c_{eq}	0.0704 wt.% [13]
Maximum carbon concentration in steel	c_{carb}	6.67 wt.% [25]
Bainitic main growth direction	θ_0	0°
Cahn-Hilliard viscosity factor	τ	0.00002 s
Cahn-Hilliard balance factor	ρ	0.00016 $\mu\mathrm{m}^2$
Cahn-Hilliard potential factor	d	0.014 $\frac{1}{(\mathrm{wt.\%})^2}$
Bainitic ferrite/Austenite interface energy	σ_{12}	0.001 $\frac{\mathrm{J}}{\mu\mathrm{m}^2}$
Bainitic ferrite/Carbide interface energy	σ_{13}	0.001 $\frac{\mathrm{J}}{\mu\mathrm{m}^2}$
Austenite/Carbide interface energy	σ_{23}	0.001 $\frac{\mathrm{J}}{\mu\mathrm{m}^2}$
Bainitic ferrite/Austenite interface mobility	ζ_{12}	200 $\frac{\mu\mathrm{m}^4}{\mathrm{Js}}$
Bainitic ferrite/Carbide interface mobility	ζ_{13}^0	500 $\frac{\mu\mathrm{m}^4}{\mathrm{Js}}$
Austenite/Carbide interface mobility	ζ_{23}	500 $\frac{\mu\mathrm{m}^4}{\mathrm{Js}}$
Gibbs energy between Bainitic ferrite and Austenite	ΔG_{12}^0	-0.045529 $\frac{\mathrm{J}}{\mu\mathrm{m}^3}$
Gibbs energy between bainitic ferrite and carbide	ΔG_{13}^0	0.1210588 $\frac{\mathrm{J}}{\mu\mathrm{m}^3}$
Gibbs energy between austenite and carbide	ΔG_{23}^0	0.1210588 $\frac{\mathrm{J}}{\mu\mathrm{m}^3}$
Interfacial thickness	η	0.17μm
Step function width	ε	0.1
Transition temperature	θ_D	350°C
Temperature step function width	ε_θ	1 K
Interface diffusion coefficient bainitic ferrite → austenite	s_{12}	1.224$\frac{1}{\mathrm{wt.\%}}$
Interface diffusion coefficient bainitic ferrite → carbide	s_{13}	1.44$\frac{1}{\mathrm{wt.\%}}$
Interface diffusion coefficient austenite → carbide	s_{23}	0$\frac{1}{\mathrm{wt.\%}}$
Cahn-Hilliard diffusion coefficient within bainitic ferrite	D_{s1}	20$\frac{\mu\mathrm{m}^2}{\mathrm{s}}$
Cahn-Hilliard diffusion coefficient within austenite	D_{s2}	0$\frac{\mu\mathrm{m}^2}{\mathrm{s}}$
Cahn-Hilliard diffusion coefficient within carbide	D_{s3}	0$\frac{\mu\mathrm{m}^2}{\mathrm{s}}$
Fick's diffusion coefficient within bainitic ferrite	D_{f1}	1$\frac{\mu\mathrm{m}^2}{\mathrm{s}}$
Fick's diffusion coefficient within austenite	D_{f2}	1$\frac{\mu\mathrm{m}^2}{\mathrm{s}}$
Fick's diffusion coefficient within carbide	D_{f3}	0$\frac{\mu\mathrm{m}^2}{\mathrm{s}}$

Table 2: Material parameters

(a) Austenite

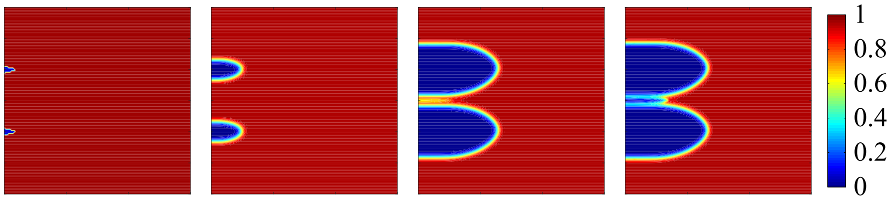

(b) Bainitic ferrite

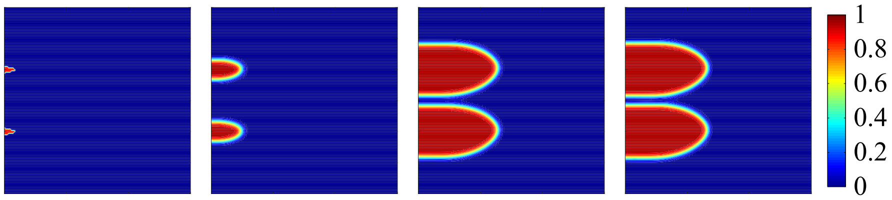

(c) Carbide

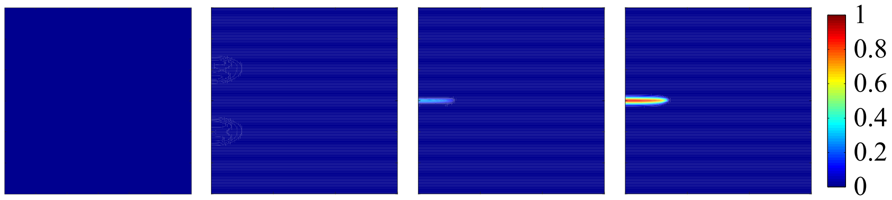

(d) Carbon concentration

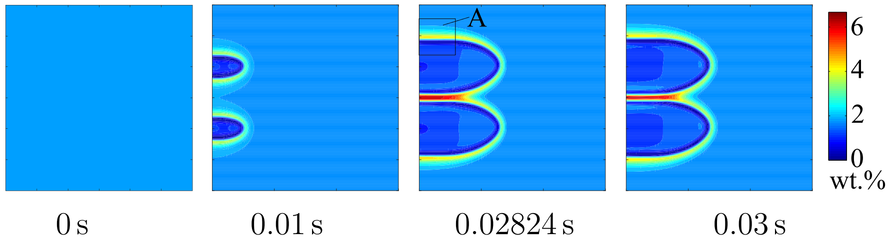

Figure 3: Upper bainitic transformation at 0 s, 0.01 s, 0.02824 s and 0.03 s.

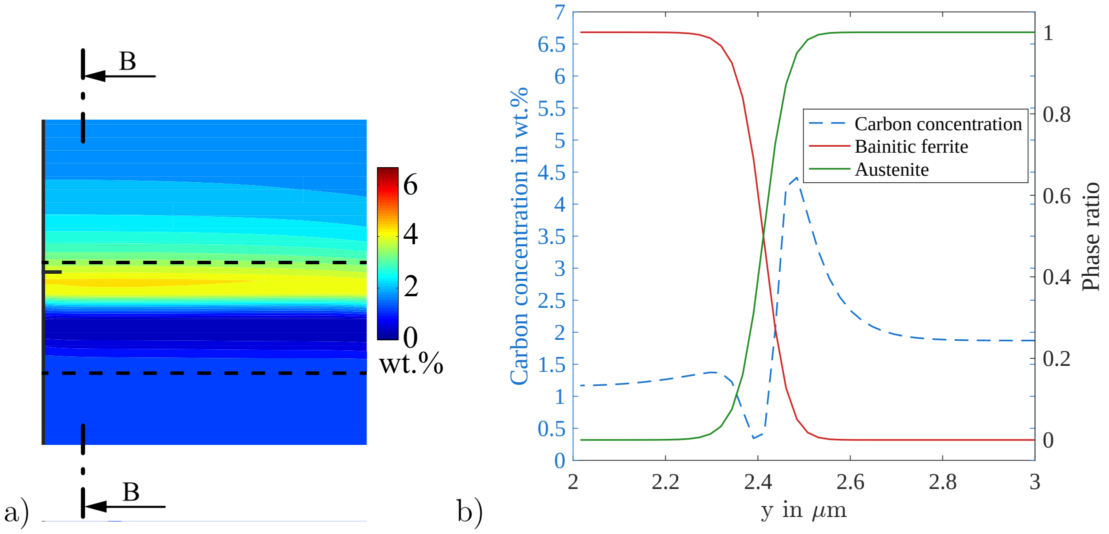

Figure 4: Carbon accumulation within the diffuse interface in upper bainite: a) Subregion A of Figure 3.d, b) intersection B-B carbon concentration and phases vs. y coordinate at $x = 0.117\,\mu\mathrm{m}$.

conditions (7), (10) and (13) are prescribed for all variables as

$$\bar{\mu} = 0, \quad \bar{c} = 0, \quad \bar{\phi}_i = 0. \tag{65}$$

The carbon concentration has an initial condition of $c(t = 0) = 1.87\,\mathrm{wt.\%}$ with small random perturbations. The carbides ϕ_3 are initially zero, but do have small random perturbations which are also uniformly distributed. The total time is $0.03\,\mathrm{s}$ and the time step is chosen as $\Delta t = 0.00001\,\mathrm{s}$. The material parameters used for the examples are summarized in Table 2. Most of the parameters are tentative and a field for further investigations. We choose the same material parameters for upper and lower bainite, in order to highlight differences in the diffusion mechanisms.

(a) Austenite

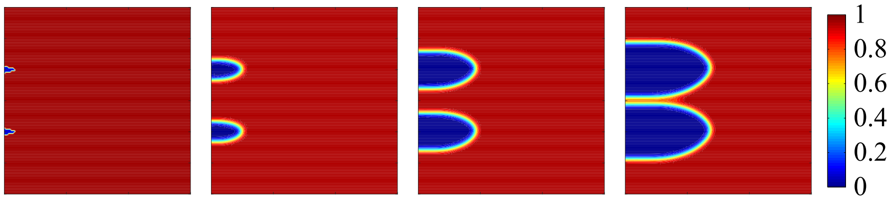

(b) Bainitic ferrite

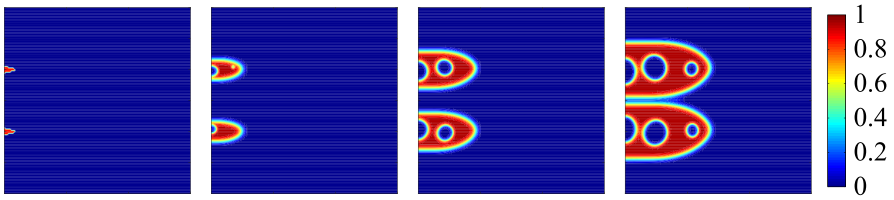

(c) Carbide

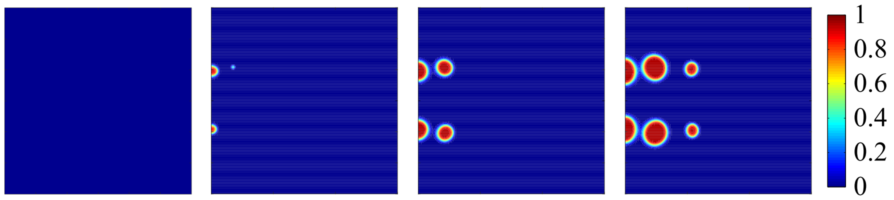

(d) Carbon concentration

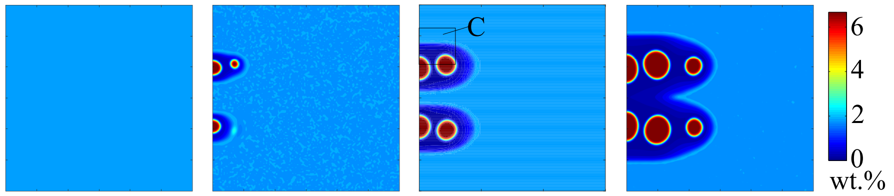

0 s 0.01 s 0.02 s 0.03 s

Figure 5: Lower bainitic transformation at 0 s, 0.01 s, 0.02 s and 0.03 s.

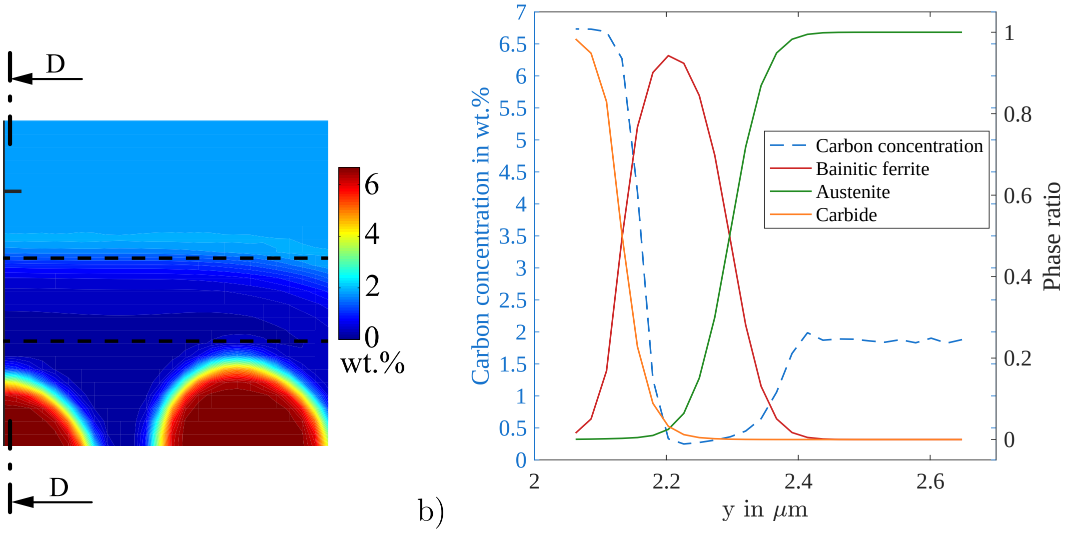

a) b)

Figure 6: Carbon accumulation within the diffuse interface in lower bainite: a) Subregion C of Figure 5.d, b) intersection D-D carbon concentration and phases vs. y coordinate at $x = 0\,\mu\text{m}$.

6.1 Upper bainite transformation

The first example illustrates an upper bainite transformation at $\theta = 700$ K. The initial conditions are visualized in the first column of Figure 3. There are two nuclei of bainitic ferrite while austenite dominates the rest of the domain. Both nuclei grow and within the bainitic ferrite the carbon concentration declines. In the second column of Figure 3, at $t = 0.01\,\text{s}$, it can be seen that carbon moves across the interface out of the supersaturated bainitic ferrite and into the austenite. This mechanism continues in the following time steps while the bainitic ferrite grows. The carbon concentration c within the austenite phase increases close to the interface with the bainitic ferrite. At places where the carbon concentration reaches its maximum of $c = 6.67\,\text{wt.\%}$ carbides ϕ_3 precipitate, as can be seen in Figure 3.c at $t = 0.02824\,\text{s}$ between both bainitic sheaves. The precipitation is a self-enhancing process, because the carbide nucleus attracts the surrounding carbon into the carbide phase which enforces the growth of the carbide. The carbides ϕ_3 limit the growth of the bainitic ferrite ϕ_1. The transformation process of this example differs fundamentally from the pearlite growth [28], even though both microstructures consist of ferrite and carbide and the final structure may look similar. In bainite the ferrite growth displacively, that is independently from the carbon movement, whereas the pearlite growth is diffusional and ferrite and carbide grow cooperatively at the same time. In this example it can be seen that the diffusion of carbon and the precipitation of carbides are subsequent processes in bainite.

Figure 4.a illustrates the subregion A of Figure 3.d at $t = 0.02824\,\mathrm{s}$ in detail. The two horizontal dashed black lines show the limits of the interface between austenite (Figure 3.a) and bainitic ferrite (Figure 3.b). Figure 4.b shows the corresponding intersection B-B of Figure 4 at $x = 0.117\,\mu\mathrm{m}$. The carbon concentration, the bainitic ferrite and the austenite phase are plotted vs. the y coordinate. The change of the carbon concentration within the interface can be seen clearly here in both figures. The minimum and maximum carbon concentrations are within the interface. This output is a result of Type II diffusion (accumulation within the interface) as described in Section 2 in Figure 1.II. Furthermore one can see the influence of Type III diffusion (balancing within in the phases). Due to this mechanism the carbon concentration within the austenite domain increases significantly.

6.2 Lower bainite transformation

The second example at $\theta = 600$ K treats the lower bainitic case. The initial state in the first column of Figure 5 is similar to upper bainitic transformation. It starts with nuclei of bainitic ferrite ϕ_1 at the left boundary while the rest of the domain is austenite. During the ensuing time steps the nuclei grow. The bainitic sheaves ϕ_1 become supersaturated, such that the carbon starts to move. Due to the lower temperature and the likewise slower diffusion speed, most of the carbon c stays within the bainitic ferrite ϕ_1. Here it starts to build accumulations. However some atoms accomplish to move across the interface into the austenite as can be seen in Figure 5.d. At accumulations of carbon, carbides ϕ_3 precipitate. As it is typical for lower bainite, this precipitation process takes place within the bainitic ferrite phase.

Comparable to Figure 4, Figure 6 illustrates the subregion C of Figure 5.d at $t = 0.02\,\mathrm{s}$ in detail. The two horizontal dashed black lines show again the limits of the interface between austenite and bainitic ferrite. Figure 6.b shows the corresponding intersection D-D of Figure 6 at $x = 0\,\mu\mathrm{m}$. The carbon concentration, bainitic ferrite, austenite and carbide phases are plotted vs. the y coordinate. In this example for lower bainite, it can be seen that the diffusion across the interface plays a minor role. Due to the accumulation within the interface (Type II diffusion Figure in 1.II) only a very little peak grows close to the austenite phase. On the left side of the diagram there is an accumulation of carbon as a result of separation within the bainitic ferrite (Type I diffusion).

7 Conclusions

This work describes a new model for the simulation of the transformation of upper and lower bainite. It is based on a thermodynamic framework of generalized forces and stresses as published before [15]. The core of this unified model for both bainitic transformations are weighted Helmholtz energy equations which lead to an extended Cahn-Hilliard diffusion equation to model the movement of the carbon. It combines the typical Cahn-Hilliard separation mechanism, which is used for the supersaturated lower bainitic ferrite, with diffusion across the phase interface, as introduced by Wheeler et al. [21] and Fick's law of diffusion within the austenite.

The examples for upper and lower bainite show the expected characteristics. While in upper bainite the carbon moves out of the supersaturated bainitic ferrite, most of the carbon remains within the bainitic ferrite in lower bainite to build accumulations. At places where the carbon concentration reaches its maximum, carbides precipitate. In lower bainite this process takes place within the bainitic ferrite whereas in upper bainite the carbides formate between bainitic sheaves within the austenite. An extension of this model with coupled deformations and an implementation using the isogeometric finite element method are planned for future work.

Appendix A

In this appendix we provide a detailed derivation of equation (37) starting from equation (36). Inserting the mobility tensor $\boldsymbol{A}$ from equation (27) into equation (36) renders

$$\begin{aligned}\dot{c} = \nabla\cdot &\left[\left(w_f^2 D_f(\phi) f_q(c) + w_s w_f D_s(\phi)\right)\nabla\mu_f\right] \\ &+ \nabla\cdot\left[\left(w_s w_f D_f(\phi) f_q(c) + w_s^2 D_s(\phi)\right)\nabla\mu_s\right]. \qquad \text{(A.1)}\end{aligned}$$

Using equation (33) for the chemical potential μ_f, while leaving μ_s we obtain

$$\begin{aligned}\dot{c} = \nabla\cdot &\left[\left(w_f^2 D_f(\phi) f_q(c) + w_s w_f D_s(\phi)\right)\nabla\left(\frac{\partial\hat{\psi}_f(c)}{\partial c} + \sum_{i=1}^{N_p}\sum_{j>i}^{N_p}\frac{s_{ij}}{4a_{ij}}\phi_i^2\phi_j^2\right)\right] \\ &+ \nabla\cdot\left[\left(w_s w_f D_f(\phi) f_q(c) + w_s^2 D_s(\phi)\right)\nabla\mu_s\right] \qquad \text{(A.2)}\end{aligned}$$

Applying the gradient operator (as introduced in equation (1.1)) on the term in brackets leads to

$$\begin{aligned}\dot{c} = \nabla\cdot \Bigg[&\big(w_f^2 D_f(\phi) f_q(c) + w_s w_f D_s(\phi)\big) \\ &\qquad \left(\frac{\partial^2 \hat{\psi}_f(c)}{\partial c^2} \nabla c + \sum_{i=1}^{N_p} \sum_{j>i}^{N_p} v_{ij} \left(2\nabla\phi_i \phi_i \phi_j^2 + 2\phi_i^2 \phi_j \nabla\phi_j\right) \right) \Bigg] \\ &\qquad\qquad + \nabla\cdot \left[\big(w_s w_f D_f(\phi) f_q(c) + w_s^2 D_s(\phi)\big) \nabla\mu_s \right].\end{aligned} \tag{A.3}$$

Applying the divergence operator in the last term and using the distributive law we obtain

$$\begin{aligned}\dot{c} = \nabla\cdot \Bigg[& w_f^2 D_f(\phi) \underbrace{f_q(c) \frac{\partial^2 \hat{\psi}_f(c)}{\partial c^2}}_{=1} \nabla c + w_s w_f D_s(\phi) \frac{\partial^2 \hat{\psi}_f(c)}{\partial c^2} \nabla c \\ & + \big(w_f^2 D_f(\phi) f_q(c) + w_s w_f D_s(\phi)\big) \sum_{i=1}^{N_p} \sum_{j>i}^{N_p} v_{ij} \left(2\nabla\phi_i \phi_i \phi_j^2 + 2\phi_i^2 \phi_j \nabla\phi_j\right) \Bigg] \\ & + \left(w_s w_f \nabla D_f(\phi) f_q(c) + w_s w_f D_f(\phi) \frac{\partial f_q(c)}{\partial c} \nabla c + w_s^2 \nabla D_s(\phi) \right) \nabla\mu_s \\ & \qquad + \big(w_s w_f D_f(\phi) f_q(c) + w_s^2 D_s(\phi)\big) \Delta\mu_s,\end{aligned} \tag{A.4}$$

where in the first term a product vanishes. The Helmholtz energy $\hat{\psi}_f(c)$ is postulated in equation (21) to fulfil the condition

$$f_q(c) \frac{\partial^2 \hat{\psi}_f(c)}{\partial c^2} = 1, \tag{A.5}$$

such that the first term in equation (A.4) reduces to $w_f^2 D_f(\phi) \nabla c$. This leads to Fick's second law which is needed for the upper and lower bainitic transformation model as documented in Table 1 and schematically illustrated as Type III in Figure 1.III. The function $f_q(c)$ defined in equation (30) is crucial for the diffusion across the interface, because it limits the movement across the interface with an upper c_{carb} and lower c_{eq} bound and is therefore a multiplier of the double well potentials (24) and its derivatives.

The first and second derivative of the Helmholtz energy (21) are

$$\frac{\partial \hat{\psi}_f(c)}{\partial c} = \frac{\ln \frac{c_{\mathrm{carb}}-c}{c_{\mathrm{eq}}-c}}{c_{\mathrm{eq}} - c_{\mathrm{carb}}}, \tag{A.6}$$

$$\frac{\partial^2 \hat{\psi}_f(c)}{\partial c^2} = \frac{1}{(c - c_{\mathrm{eq}})(c_{\mathrm{carb}} - c)} = \frac{1}{f_q(c)}, \tag{A.7}$$

such that the balancing condition (A.5) is satisfied.

Applying the divergence we end up with the evolution equation for c

$$\begin{aligned}
\dot{c} = w_f^2 \nabla D_f(\phi) \cdot \nabla c + w_f^2 D_f(\phi) \Delta c + w_s w_f \nabla D_s(\phi) \frac{\partial^2 \hat{\psi}_f(c)}{\partial c^2} \nabla c& \\
+ w_s w_f D_s(\phi) \frac{\partial^3 \hat{\psi}_f(c)}{\partial c^3} (\nabla c)^2 + w_s w_f D_s(\phi) \frac{\partial^2 \hat{\psi}_f(c)}{\partial c^2} \Delta c& \\
+ \left(w_f^2 \nabla D_f(\phi) f_q(c) + w_f^2 D_f(\phi) \frac{\partial f_q(c)}{\partial c} \nabla c + w_s w_f \nabla D_s(\phi) \right)& \\
\cdot \sum_{i=1}^{N_p} \sum_{j>i}^{N_p} v_{ij} \left(2\phi_i \phi_j^2 \nabla \phi_i + 2\phi_j \phi_i^2 \nabla \phi_j \right)& \\
+ \left(w_f^2 D_f(\phi) f_q(c) + w_s w_f D_s(\phi) \right)& \\
\sum_{i=1}^{N_p} \sum_{j>i}^{N_p} 2 v_{ij} \left(\nabla \phi_i \phi_j^2 \nabla \phi_i + \nabla \phi_j \phi_i^2 \nabla \phi_j + 4 \phi_i \phi_j \nabla \phi_i \nabla \phi_j + \phi_j \phi_i^2 \Delta \phi_j + \phi_i \phi_j^2 \Delta \phi_i \right)& \\
+ \left(w_s w_f \nabla D_f(\phi) f_q(c) + w_s w_f D_f(\phi) \frac{\partial f_q(c)}{\partial c} \nabla c + w_s^2 \nabla D_s(\phi) \right) \cdot \nabla \mu_s& \\
+ \left(w_s w_f D_f(\phi) f_q(c) + w_s^2 D_s(\phi) \right) \Delta \mu_s,&
\end{aligned} \tag{A.8}$$

where the first two terms can be identified as Fick's second law with a diffusion coefficient $D_f(\phi)$ and its gradient.

The first special case of the equation (A.8) with $w_f = 1$ and $w_s = 0$ gives an evolution equation describing only Fick's diffusion and diffusion across the interface

$$\begin{aligned}\dot{c} = \nabla D_f(\phi) \cdot \nabla c + D_f(\phi)\Delta c + &\left(\nabla D_f(\phi) f_q(c) + D_f(\phi)\frac{\partial f_q(c)}{\partial c}\nabla c\right) \\ &\cdot \sum_{i=1}^{N_p}\sum_{j>i}^{N_p} v_{ij}\left(2\phi_i\phi_j^2\nabla\phi_i + 2\phi_j\phi_i^2\nabla\phi_j\right) \\ &+ \left(D_f(\phi) f_q(c)\right) \\ \sum_{i=1}^{N_p}\sum_{j>i}^{N_p} 2v_{ij}\left(\nabla\phi_i\phi_j^2\nabla\phi_i + \nabla\phi_j\phi_i^2\nabla\phi_j + 4\phi_i\phi_j\nabla\phi_i\nabla\phi_j + \phi_j\phi_i^2\Delta\phi_j + \phi_i\phi_j^2\Delta\phi_i\right), \quad &\text{(A.9)}\end{aligned}$$

while for $w_f = 0$ and $w_s = 1$ it reduces to a purely separating equation of Cahn-Hilliard type

$$\dot{c} = \nabla D_s(\phi) \cdot \nabla\mu_s + D_s(\phi)\Delta\mu_s. \tag{A.10}$$

References

[1] G. Olson, H. Bhadeshia, M. Cohen, Coupled Diffusional / Displacive Transformations, Acta Metallurgica 37 (2) (1989) 381–389.

[2] H. K. D. H. Bhadeshia, Bainite in steels, 2nd Edition, Maney Materials Science, 2001.

[3] H. Bhadeshia, The lower bainite transformation and the significance of carbide precipitation, Acta Metallurgica 28 (8) (1980) 1103–1114.

[4] I. Steinbach, Phase-field models in materials science, Modelling Simul. Mater. Sci. Eng. 17.

[5] M. Militzer, M. Mecozzi, J. Sietsma, S. van der Zwaag, Three-dimensional phase field modelling of the austenite-to-ferrite transformation, Acta Materilia 54 (15) (2006) 3961–3972.

[6] C.-J. Huang, D. J. Browne, S. McFadden, A phase-field simulation of austenite to ferrite transformation kinetics in low carbon steels, Acta Materilia 54 (2005) 11–21.

[7] M. Mecozzi, J. Sietsma, S. van der Zwaag, M. Apel, P. Schaffnit, I. Steinbach, Analysis of the $\gamma \rightarrow \alpha$ Transformation in a C-Mn Steel by Phase-Field Modeling, Metallurgical and Materials Transactions A 36A (2005) 2327–2340.

[8] I. Steinbach, M. Apel, The influence of lattice strain on pearlite formation in fe-c, Acta Materialia 55 (14) (2007) 4817–4822.

[9] A. Yamanaka, T. Takaki, Y. Tomita, Elastoplastic phase-field simulation of self-and plastic accommodations in cubic tetragonal martensitic transformation, Materials Science and Engineering: A 491 (1) (2008) 378–384.

[10] R. Schmitt, R. Müller, C. Kuhn, H. M. Urbassek, A phase field approach for multivariant martensitic transformations of stable and metastable phases, Archive of Applied Mechanics 83 (6) (2013) 849–859.

[11] A. Yamanaka, T. Takaki, Y. Tomita, Phase-Field Simulation of Austenite to Ferrite Transformation and Widmanstätten Ferrite Formation in Fe-C Alloy, Materials Transactions 47 (11) (2006) 2725–2731.

[12] T. Arif, R. Qin, A phase-field model for bainitic transformation, Computational Materials Science 77 (2013) 230–235.

[13] W. Song, U. Prahl, W. Bleck, K. Mukherjee, Phase-field simulations of bainitic phase transformation in 100cr6, TMS 2011 140th Annual Meeting and Exhibition (2011) 417–425.

[14] M. Düsing, R. Mahnken, Simulation of lower bainitic transformation with the phase-field method considering carbide formation, Computational Materials Science 111 (2016) 91–100.

[15] M. Düsing, R. Mahnken, A thermodynamic framework for coupled multiphase ginzburg-landau/cahn-hilliard systems for simulation of lower bainitic transformation, Archive of Applied Mechanics 86 (12) (2016) 1947–1964.

[16] M. Weikamp, C. Hüter, M. Lin, U. Prahl, D. Schicchi, M. Hunkel, R. Spatschek, Scale Bridging Simulations of Large Elastic Deformations and Bainitic Transformations, Springer International Publishing, Cham, 2017, pp. 125–138.

[17] R. Mahnken, A. Schneidt, T. Antretter, U. Ehlenbröker, M. Wolff, Multi-scale modeling of bainitic phase transformation in multi-variant polycrystalline low alloy steels, International Journal of Solids and Structures 54 (2015) 156–171.

[18] M. E. Gurtin, Generalized Ginzburg-Landau and Cahn-Hilliard equations based on a microforce balance, Physica D: Nonlinear Phenomena 92 (3) (1996) 178–192.

[19] E. Fried, M. E. Gurtin, Continuum theory of thermally induced phase transitions based on an order parameter, Physica D: Nonlinear Phenomena 68 (3) (1993) 326–343.

[20] E. Fried, M. E. Gurtin, Dynamic solid-solid transitions with phase characterized by an order parameter, Physica D: Nonlinear Phenomena 72 (4) (1994) 287–308.

[21] A. A. Wheeler, W. J. Boettinger, G. B. McFadden, Phase-field model for isothermal phase transitions in binary alloys, Phys. Rev. A 45 (1992) 7424–7439.

[22] R. Kobayashi, Modeling and numerical simulations of dendritic crystal growth, Physica D 63 (1993) 410–423.

[23] I. Steinbach, F. Pezzolla, B. Nestler, M. Seeßelberg, R. Ptieler, G. Schmitz, J. Rezende, A phase field concept for multiphase systems, Physica D 94 (1996) 135–147.

[24] G. B. McFadden, A. A. Wheeler, R. J. Braun, S. R. Coriell, R. F. Sekerkat, Phase-field models for anisotropic interfaces, Physical Review E 48 (3) (1993) 2016–2024.

[25] D. Horstmann, Das Zustandsschaubild Eisen-Kohlenstoff und die Grundlagen der Wärmebehandlung der Eisenkohlenstoff-Legierungen., Stahleisen, Ddf., 1985.

[26] T. J. Hughes, J. A. Cottrell, Y. Bazilevs, Isogeometric analysis: Cad, finite elements, nurbs, exact geometry and mesh refinement, Computer methods in applied mechanics and engineering 194 (39) (2005) 4135–4195.

[27] H. Gómez, V. M. Calo, Y. Bazilevs, T. J. Hughes, Isogeometric analysis of the cahn–hilliard phase-field model, Computer methods in applied mechanics and engineering 197 (49) (2008) 4333–4352.

[28] H. Engel, C. Kestner, Metallfachkunde 1: Grundlagen, Vieweg+Teubner Verlag, 1990.

Paper D

M. Düsing and R. Mahnken

A coupled phase field/diffusional/mechanical framework for simulation of upper and lower bainitic transformation

submitted 2018

A coupled phase field/diffusional/mechanical framework for simulation of upper and lower bainitic transformation

Martin Düsing and Rolf Mahnken

Chair of Engineering Mechanics, Paderborn University,

Warburger Str. 100, 33098 Paderborn, Germany

Abstract

The microstructure bainite in steels consists of three phases, namely bainitic ferrite, austenite and carbide. Two different arrangements of these phases can be observed denoted as upper and lower bainite which develop at different temperatures. For both morphologies the growth starts with a displacive transformation from austenite to bainitic ferrite. The bainitic sheaf has a preferred direction of growth due to eigenstrains which evolve during the transformation. Subsequently a temperature dependent diffusion process starts to redistribute the carbon and carbides precipitate at accumulations of carbon. The goal of this work is to simulate the upper and lower bainite transformation considering eigenstrain effects. To this end, we extend an own previously developed model by mechanical contributions. The related coupling terms of the phase field/diffusional/mechanical model are derived within a thermodynamic framework. Two representative examples illustrate the capability of the extended framework and show the expected transformation of upper and lower bainite.

1 Introduction

Bainite is a steel microstructure with useful properties since it has a high ultimate strength combined with a higher ductility as tempered steels. The microstructure consists of three different phases, that are bainitic ferrite, austenite and carbide which arrange to two different morphologies, upper bainite and lower bainite [1]. In materials science the transformation from pure austenite to bainite is not fully understood and so far under discussion [2]. We follow those scientists who describe the transformation from austenite to bainitic ferrite as a displacive transformation independent of carbon diffusion. From this it follows that bainitic ferrite must be supersaturated of carbon directly after the phase transformation. In a subsequent process the carbon within the bainitic ferrite diffuses, which is highly dependent on the temperature. At high temperatures the carbon atoms are highly mobile. Those who are close to the interface to unsaturated austenite diffuse across the interface while atoms in the bulk phase move in the direction of the interface. At accumulations of carbon within the austenite, carbides precipitate. The resulting microstructure is called upper bainite. In contrast to upper bainite, lower bainite evolves at lower temperatures where the mobility of the carbon atoms is much lower. Therefore, only a few carbon atoms close to the interface diffuse across the interface into the austenite while most of the carbon stays within the supersaturated bainitic ferrite to separate and build accumulations. Carbides precipitate at these accumulations within the bainitic ferrite.

Phase transformations in steel and their simulations are important topics in materials science and mechanics. There are several models simulating phase transformations with the phase field model, some are summarized in a topical review by Steinbach [3]. One of the first works about dendritic growth is published by Kobayashi [4]. Other important models are presented by Militzer *et al.* [5], Huang *et al.* [6] and Mecozzi *et al.* [7] on the austenite-to-ferrite transformation. Diffusion-controlled growth is simulated by Steinbach and Apel [8] to model the austenite-to-pearlite transition whereas the martensite transformation is investigated e.g. by Yamanaka *et al.* [9] and Schmitt *et al.* [10]. Widmanstätten formation is simulated in [11]. There are a few models describing parts of the bainitic transformation with the phase field method. Song *et al.* [12] simulate the growth of upper bainite neglecting the precipitation of carbide and Arif and Qin [13] describe the autocatalysis event between two subunits. To the authors knowledge, firstly a phase field model for the lower bainitic transformation is presented in [14] and [15] showing the separation of carbon within the bainitic ferrite and the precipitation of carbides. This model is e.g. applied in [16] and extended to upper bainite in [17].

A further challenge of the multiphase field method is the modelling of the directed growth of the bainitic ferrite. This effect has been modelled in [14], [15] and [17] in a phenomenological way by manipulating the interface energy depending on the direction of the gradient of the phase order parameter. In this work the directed growth is governed by a coupling with mechanical contributions such that the manipulated interface energy is no longer required. At interfaces between phases, eigenstrains strains due to the phase transformation are induced which lead to a directed growth of a new phase. The new coupling terms have to be consistent with the multiphase field formulation of [17]. In particular the mechanical contribution to the multiphase field evolution equation has to govern on the expense of which phase j a new phase i may grow.

The model derived in this paper is based on the concept of generalized stresses as introduced by Gurtin and Fried in [18], [19] and [20] and extended e.g. in [15] and in [21]. In this paper mechanical contributions are added to the framework. For this step we found [10] and [22] inspiring.

This work is divided into the following sections: Section 2 describes the thermodynamic framework for a coupled multiphase transformation, diffusion and deformation model based on generalized forces. Section 3 is concerned with a prototype model for upper and lower bainite. Here the constitutive equations are postulated and a set of resulting partial differential equations is provided. Section 4 is concerned with the implementation of the model equations whereas the numerical examples are shown in Section 5.

Notations: Vectors $\boldsymbol{a}$ and second-order tensors $\boldsymbol{A}$ are bold and matrices $\underline{B}$ are underlined. In the three-dimensional Cartesian coordinate system, the gradient and the Laplacian, respectively, of a scalar field $\alpha(\boldsymbol{x})$ are given by

$$1.\ \ \nabla\alpha(\boldsymbol{x}) = \sum_{i=1}^{3} \frac{\partial \alpha(\boldsymbol{x})}{\partial x_i}\boldsymbol{e}_i \qquad\qquad 2.\ \ \Delta\alpha(\boldsymbol{x}) = \nabla\cdot\nabla\alpha(\boldsymbol{x}) = \sum_{i=1}^{3} \frac{\partial^2 \alpha(\boldsymbol{x})}{\partial x_i^2}. \tag{1}$$

where $\boldsymbol{e}_i, i = 1, 2, 3$ are standard unit vectors and x_i are the coordinates of $\boldsymbol{x}$. The divergence of a vector field $\boldsymbol{a}(\boldsymbol{x})$ reads

$$\nabla\cdot\boldsymbol{a}(\boldsymbol{x}) = \sum_{i=1}^{3} \frac{\partial a_i}{\partial x_i}. \tag{2}$$

2 Thermodynamic framework for generalized forces coupled to mechanics

In this section the thermodynamic framework introduced in [15] is extended for deformable continua, based on the work by Gurtin [20].

2.1 Balance laws

Firstly, we introduce N_p phase order parameters ϕ_i $(i = 1, ..., N_p)$ and the concentration of a solute c. Considering a body B with an arbitrary control volume V as a subregion of the body B and phase stresses $\boldsymbol{\xi}_i$, internal phase forces π_i, external phase forces γ_i, a diffusion stress $\boldsymbol{\lambda}$ and an internal diffusion force ω. The integrals

$$\mathcal{P}_{\phi 1}^{\text{int}} = \int_V -\boldsymbol{\xi}_i \cdot \nabla\dot{\phi}_i \, dV, \quad \mathcal{P}_{\phi 2}^{\text{int}} = \int_V \pi_i \dot{\phi}_i \, dV, \quad \mathcal{P}_{\phi}^{\text{ext}} = \int_V \gamma_i \dot{\phi}_i \, dV, \qquad i = 1, ..., N_p, \tag{3}$$

$$\mathcal{P}_{c1}^{\text{int}} = \int_V -\boldsymbol{\lambda} \cdot \nabla\dot{c} \, dV, \quad \mathcal{P}_{c2}^{\text{int}} = \int_V \omega \dot{c} \, dV, \tag{4}$$

describe powers performed on the atomic configuration of V as proposed in [15]. Furthermore, we introduce the powers

$$\mathcal{P}_{M}^{\text{int}} = \int_V -\boldsymbol{P} : \nabla_X \dot{\boldsymbol{u}} \, dV, \quad \mathcal{P}_{M}^{\text{ext}} = \int_V \boldsymbol{b} \cdot \dot{\boldsymbol{u}} \, dV, \tag{5}$$

where $\boldsymbol{P}$ is the first Piola-Kirchhoff stress tensor, ∇_X is a gradient with respect to the reference configuration, $\dot{\boldsymbol{u}}$ is the time derivative of the displacement $\boldsymbol{u}$ and $\boldsymbol{b}$ is a body force per unit reference volume. With the powers (3), (4) and (5) the microforce balance equations

$$\nabla \cdot \boldsymbol{\xi}_i + \pi_i + \gamma_i = 0 \ \text{ in } \ V \quad \text{ for } \ i = 1, ..., N_p, \tag{6}$$

$$\nabla \cdot \boldsymbol{\lambda} + \omega = 0 \ \text{ in } \ V, \tag{7}$$

$$\boldsymbol{\xi}_i \cdot \boldsymbol{n} = 0 \ \text{ on } \ \partial V \quad \text{ for } \ i = 1, ..., N_p, \tag{8}$$

$$\boldsymbol{\lambda} \cdot \boldsymbol{n} = 0 \ \text{ on } \ \partial V. \tag{9}$$

and the balance of linear momentum

$$\nabla_X \cdot \boldsymbol{P} + \boldsymbol{b} = \boldsymbol{0} \ \text{ in } \ V \tag{10}$$

for non-accelerated systems is derived. The body force $\boldsymbol{b}$ is introduced for the sake of completeness, but is not needed anymore and therefore, is set to zero $\boldsymbol{b} = \boldsymbol{0}$.

The first law of thermodynamics

$$\dot{\mathcal{E}} = \dot{\mathcal{K}} + \mathcal{P}^{\text{ext}} \tag{11}$$

is used to ensure the conservation of energy, where $\dot{\mathcal{E}}$ is the time derivative of the internal energy, $\mathcal{K}$ the kinetic energy and $\mathcal{P}^{\text{ext}}$ the external power. The kinetic energy rate $\dot{\mathcal{K}} = 0$, because only non-accelerated systems are considered and therefore, inertia effects are neglected. A local internal energy rate $\dot{e}$ can be related to the global internal energy rate $\dot{\mathcal{E}}$ as

$$\dot{\mathcal{E}} = \int_V \dot{e} \; dV. \tag{12}$$

Following [23] the external power $\mathcal{P}^{\text{ext}}$ is equal to the negative internal power $\mathcal{P}^{\text{int}}$

$$\mathcal{P}^{\text{ext}} = -\mathcal{P}^{\text{int}}. \tag{13}$$

The internal power is the sum of all powers on atoms of V with internal contribution in (3), (4) and (5)

$$\mathcal{P}^{\text{int}} = \mathcal{P}^{\text{int}}_M + \mathcal{P}^{\text{int}}_{c2} + \mathcal{P}^{\text{int}}_{c1} + \sum_{i=1}^{N_p} (\mathcal{P}^{\text{int}}_{\phi 2} + \mathcal{P}^{\text{int}}_{\phi 1}) \tag{14}$$

$$= \int_V \left(-\boldsymbol{P} : \dot{\boldsymbol{F}} + \omega \dot{c} - \boldsymbol{\lambda} \cdot \nabla \dot{c} + \sum_{i=1}^{N_p} (\pi_i \dot{\phi}_i - \boldsymbol{\xi}_i \cdot \nabla \dot{\phi}_i) \right) \; dV \tag{15}$$

where $\boldsymbol{F} = \mathbf{1} + \nabla_X \boldsymbol{u}$ is the deformation gradient. The internal power $\mathcal{P}^{\text{int}}$ in equation (15) and the global internal energy rate of equation (12) are inserted into the first law (11) to obtain a local form

$$\dot{e} = \boldsymbol{P} : \dot{\boldsymbol{F}} + \boldsymbol{\lambda} \cdot \nabla \dot{c} - \omega \dot{c} + \sum_{i=1}^{N_p} \left(\boldsymbol{\xi}_i \cdot \nabla \dot{\phi}_i - \dot{\phi}_i \pi_i \right). \tag{16}$$

2.2 Dissipation inequality/entropy principle

The second law of thermodynamics is used to obtain the Clausius-Duhem inequality (see e.g. [24, 25, 26]) in global form as follows

$$\int_V \dot{s} \; dV \geq - \int_{\partial V} \boldsymbol{\Phi} \; \cdot \boldsymbol{n} \; dA, \tag{17}$$

where the local entropy density is denoted as s and $\boldsymbol{\Phi}$ is the vector entropy flux, defined as, [23, 27]

$$\boldsymbol{\Phi} = -\mu \frac{\boldsymbol{J}}{T}. \tag{18}$$

This entropy flux introduces three additional quantities, the scalar chemical potential μ, the chemical flux $\boldsymbol{J}$ and the absolute temperature T. A local form of inequality (17) is obtained by applying Gauss's theorem and inserting equation (18)

$$T\dot{s} - \nabla \cdot (\mu \boldsymbol{J}) \geq 0. \tag{19}$$

In the next step we utilise the Helmholtz energy ψ, which is a thermodynamic function of state like the internal energy e, the temperature T and the entropy s. They depend only on the current state of the system and not on the path by which they arrived at their present state. The Helmholtz energy ψ is defined as

$$\psi = e - Ts. \tag{20}$$

The time derivative of the Helmholtz energy ψ for the isothermal case reads

$$\dot{\psi} = \dot{e} - T\dot{s}. \tag{21}$$

Inserting equation (21) into the inequality (19) leads to

$$-\dot{\psi} + \dot{e} - \nabla \cdot (\mu \boldsymbol{J}) \geq 0. \tag{22}$$

In the next step mass conservation of the concentration of a solute c is applied. The conservative quantity c has to fulfil the mass conservation equation

$$\dot{c} = -\nabla \cdot \boldsymbol{J}. \tag{23}$$

Applying equation (23) and inserting equation (16) into inequality (22) the *local dissipation inequality* reads

$$-\dot{\psi} + \boldsymbol{P} : \dot{\boldsymbol{F}} + \boldsymbol{\lambda} \cdot \nabla \dot{c} - \omega \dot{c} + \mu \dot{c} - \boldsymbol{J} \cdot \nabla \mu + \sum_{i=1}^{N_p} \left(\boldsymbol{\xi}_i \cdot \nabla \dot{\phi}_i - \pi_i \dot{\phi}_i \right) \geq 0. \tag{24}$$

2.3 Restrictions to constitutive equations imposed by the second law of thermodynamics

In this subsection restrictions to constitutive equations are formulated which are imposed by the local dissipation inequality (24). This subsection is an extension of subsection 2.3

in [15]. For convenience we define the *constitutive variables*

$$\boldsymbol{z} = [\boldsymbol{F},\ c,\ \nabla c,\ \dot{c},\ \mu,\ \nabla\mu,\ \{\phi_i,\ \nabla\phi_i,\ \dot{\phi}_i\}_{i=1}^{N_p}]. \tag{25}$$

and the *constitutive functions*

$$\boldsymbol{Z}(\boldsymbol{z}) = [\hat{\boldsymbol{P}}(\boldsymbol{z}),\ \hat{\psi}(\boldsymbol{z}),\ \hat{\boldsymbol{J}}(\boldsymbol{z}),\ \hat{\omega}(\boldsymbol{z}),\ \hat{\boldsymbol{\lambda}}(\boldsymbol{z}),\ \{\hat{\pi}_i(\boldsymbol{z}),\ \hat{\boldsymbol{\xi}}_i(\boldsymbol{z})\}_{i=1}^{N_p}], \tag{26}$$

which, at this point, may depend on the constitutive variables $\boldsymbol{z}$.

Then the total time derivative of the Helmholtz energy becomes

$$\begin{aligned}\dot{\psi} = \frac{\partial\hat{\psi}(\boldsymbol{z})}{\partial\boldsymbol{F}}\frac{\partial\boldsymbol{F}}{\partial t} + \frac{\partial\hat{\psi}(\boldsymbol{z})}{\partial c}\frac{\partial c}{\partial t} + \frac{\partial\hat{\psi}(\boldsymbol{z})}{\partial\nabla c}\frac{\partial\nabla c}{\partial t} + \frac{\partial\hat{\psi}(\boldsymbol{z})}{\partial\dot{c}}\frac{\partial\dot{c}}{\partial t} + \frac{\partial\hat{\psi}(\boldsymbol{z})}{\partial\mu}\frac{\partial\mu}{\partial t} + \frac{\partial\hat{\psi}(\boldsymbol{z})}{\partial\nabla\mu}\frac{\partial\nabla\mu}{\partial t}\\ + \sum_{i=1}^{N_p}\left(\frac{\partial\hat{\psi}(\boldsymbol{z})}{\partial\phi_i}\frac{\partial\phi_i}{\partial t} + \frac{\partial\hat{\psi}(\boldsymbol{z})}{\partial\nabla\phi_i}\frac{\partial\nabla\phi_i}{\partial t} + \frac{\partial\hat{\psi}(\boldsymbol{z})}{\partial\dot{\phi}_i}\frac{\partial\dot{\phi}_i}{\partial t}\right).\end{aligned} \tag{27}$$

Inserting equation (27) into the local dissipation inequality (24) gives

$$\begin{aligned}&\underbrace{\left(\hat{\boldsymbol{P}}(\boldsymbol{z}) - \frac{\partial\hat{\psi}(\boldsymbol{z})}{\partial\boldsymbol{F}}\right) : \dot{\boldsymbol{F}}}_{2.} +\\ &\quad\underbrace{\left(\mu - \hat{\omega}(\boldsymbol{z}) - \frac{\partial\hat{\psi}(\boldsymbol{z})}{\partial c}\right)\dot{c}}_{3.} + \underbrace{\left(\hat{\boldsymbol{\lambda}}(\boldsymbol{z}) - \frac{\partial\hat{\psi}(\boldsymbol{z})}{\partial\nabla c}\right)\nabla\dot{c}}_{2.} \underbrace{-\frac{\partial\hat{\psi}(\boldsymbol{z})}{\partial\dot{c}}\ddot{c}}_{1.} \underbrace{-\frac{\partial\hat{\psi}(\boldsymbol{z})}{\partial\mu}\dot{\mu}}_{1.} \underbrace{-\frac{\partial\hat{\psi}(\boldsymbol{z})}{\partial\nabla\mu}\nabla\dot{\mu}}_{1.}\\ &\quad\underbrace{-\nabla\mu\cdot\hat{\boldsymbol{J}}(\boldsymbol{z})}_{3.} + \sum_{i=1}^{N_p}\left[\underbrace{\left(\hat{\boldsymbol{\xi}}_i(\boldsymbol{z}) - \frac{\partial\hat{\psi}(\boldsymbol{z})}{\partial\nabla\phi_i}\right)\nabla\dot{\phi}_i}_{2.} \underbrace{-\left(\hat{\pi}_i(\boldsymbol{z}) + \frac{\partial\hat{\psi}(\boldsymbol{z})}{\partial\phi_i}\right)\dot{\phi}_i}_{3.} \underbrace{-\frac{\partial\hat{\psi}(\boldsymbol{z})}{\partial\dot{\phi}_i}\ddot{\phi}_i}_{1.}\right] \geq 0.\end{aligned} \tag{28}$$

Next, the aim is to formulate restrictions to the constitutive equations (26) to fulfil inequality (28) for arbitrary values of $\boldsymbol{z}$ and the higher order derivatives $\nabla\dot{c}, \ddot{c}, \dot{\mu}, \nabla\dot{\mu}, \ddot{\phi}_i, \nabla\dot{\phi}_i$ at any time and any material point. Analogously to [15] and [20] all terms are analysed by use of three different groups as indicated in equation (28):

1. The first group contains all terms with the higher derivatives $\ddot{c}, \dot{\mu}, \nabla\dot{\mu}$ and $\ddot{\phi}_i$ in inequality (28). The characteristic property of these quantities is that they appear linearly in (28) which is straightforward because they are not constitutive variables

of the vector $\boldsymbol{z}$ in equation (25). One could easily find values for $\boldsymbol{z}$ and the higher order derivatives of group one which would violate (28) such that the relations

$$\frac{\partial \hat{\psi}(\boldsymbol{z})}{\partial \dot{c}} = 0, \quad \frac{\partial \hat{\psi}(\boldsymbol{z})}{\partial \mu} = 0, \quad \frac{\partial \hat{\psi}(\boldsymbol{z})}{\partial \nabla \mu} = 0, \quad \frac{\partial \hat{\psi}(\boldsymbol{z})}{\partial \dot{\phi}_i} = 0, \qquad \text{for} \;\; i = 1, ..., N_p, \tag{29}$$

are necessary conditions to fulfil inequality (28), see [20] and [15]. From equations (29) it can be concluded that the Helmholtz energy $\hat{\psi}(\boldsymbol{z})$ cannot be a function of $\dot{c}$, μ, $\nabla\mu$ and $\dot{\phi}_i$ as initially proposed in equation (26) but only of the variables $\tilde{\boldsymbol{z}}$, resulting into

$$\hat{\psi}(\tilde{\boldsymbol{z}}), \quad \text{where} \quad \tilde{\boldsymbol{z}} = [\boldsymbol{F}, c, \nabla c, \{\phi_i, \nabla\phi_i\}_{i=1}^{N_p}]. \tag{30}$$

2. The second group consists of the three terms containing $\dot{\boldsymbol{F}}$, $\nabla\dot{\phi}_i$ and $\nabla\dot{c}$ in inequality (28). The argumentation for these terms goes along the same lines as for the first group. As for group one, the related higher order derivatives are not constitutive variables of the vector $\boldsymbol{z}$ in equation (25) and thus they appear linearly in (28). In contrast to the first group, the corresponding factors are composed of additive terms in inequality (28). Here $\dot{\boldsymbol{F}}$, $\nabla\dot{\phi}_i$ and $\nabla\dot{c}$ could be chosen to violate inequality (28). Thus it can be stated without loss of generality that the factors have to be zero as necessary conditions, leading to

$$\hat{\boldsymbol{P}}(\boldsymbol{z}) = \frac{\partial \hat{\psi}(\boldsymbol{z})}{\partial \boldsymbol{F}}, \quad \hat{\boldsymbol{\lambda}}(\boldsymbol{z}) = \frac{\partial \hat{\psi}(\tilde{\boldsymbol{z}})}{\partial \nabla c}, \quad \hat{\boldsymbol{\xi}}_i(\boldsymbol{z}) = \frac{\partial \hat{\psi}(\tilde{\boldsymbol{z}})}{\partial \nabla \phi_i} \qquad \text{for} \;\; i = 1, ..., N_p. \tag{31}$$

While for both groups the argumentation goes along the same lines, the results differ. As a result of the first group the number of constitutive variables for the Helmholtz energy is reduced, see equation (30). Here the number of the constitutive equations reduces to $3 + N_p$, because $\hat{\boldsymbol{P}}(\boldsymbol{z})$, $\boldsymbol{\xi}_i$ and $\boldsymbol{\lambda}$ are no longer independent but directly dependent on the choice of $\hat{\psi}(\tilde{\boldsymbol{z}})$.

With the results of equations (30) and (31) the dissipation inequality (28) renders a reduced dissipation as

$$\mathcal{D} = -\nabla\mu \cdot \hat{\boldsymbol{J}}(\boldsymbol{z}) - \left(\hat{\omega}(\boldsymbol{z}) + \frac{\partial \hat{\psi}(\tilde{\boldsymbol{z}})}{\partial c} - \mu \right) \dot{c} - \sum_{i=1}^{N_p} \left(\hat{\pi}_i(\boldsymbol{z}) + \frac{\partial \hat{\psi}(\tilde{\boldsymbol{z}})}{\partial \phi_i} \right) \dot{\phi}_i \geq 0. \tag{32}$$

Due to our choice for $\boldsymbol{z}$ in equation (25) where the deformation gradient $\boldsymbol{F}$ is a constitutive variable but not its time derivative $\dot{\boldsymbol{F}}$, the inequality (32) does not contain a strain measurement anymore. Therefore, the following analysis does not differ from [15] but is continued here for the sake of completeness.

3. Group three consists of the remaining terms in inequality (32). Their characteristic property is that $\nabla\mu, \dot{c}$ and $\dot{\phi}_i$ are constitutive variables of the vector $\boldsymbol{z}$ and therefore, may appear linearly or non-linearly in inequality (32). Since it is not known whether these terms violate the inequality (32), they cannot be set to zero as a necessary condition [15]. One could of course choose the additive terms as zero again, however, this would not be a necessary but only a sufficient condition and would lead to a non-dissipative system. Instead inequality (32) is written as

$$\mathcal{D} = -\nabla\mu \cdot \hat{\boldsymbol{J}}(\boldsymbol{z}) - \omega^{dis}\dot{c} - \sum_{i=1}^{N_p} \pi_i^{dis}\dot{\phi}_i \geq 0 \tag{33}$$

with additional quantities

$$\omega^{dis} = \hat{\omega}(\boldsymbol{z}) + \frac{\partial\hat{\psi}(\tilde{\boldsymbol{z}})}{\partial c} - \mu, \tag{34}$$

$$\pi_i^{dis} = \hat{\pi}_i(\boldsymbol{z}) + \frac{\partial\hat{\psi}(\tilde{\boldsymbol{z}})}{\partial\phi_i}, \quad i = 1, ..., N_p \ . \tag{35}$$

In the next step, we choose

$$\omega^{dis} = -\tau(\boldsymbol{z})\dot{c}, \tag{36}$$

$$\pi_i^{dis} = -\beta_i(\boldsymbol{z})\dot{\phi}_i, \quad i = 1, ..., N_p, \tag{37}$$

where $\tau(\boldsymbol{z})$ and $\beta_i(\boldsymbol{z})$ are *constitutive moduli.* The chemical flux is chosen as

$$\hat{\boldsymbol{J}}(\boldsymbol{z}) = -\boldsymbol{A}(\boldsymbol{z})\nabla\mu, \tag{38}$$

where $\boldsymbol{A}(\boldsymbol{z})$ is the second order *mobility tensor* [20]. Inserting the three definitions (34)-(38) into the dissipation inequality (33) renders

$$\mathcal{D} = \nabla\mu \cdot \boldsymbol{A}(\boldsymbol{z})\nabla\mu + \tau(\boldsymbol{z})\dot{c}^2 + \sum_{i=1}^{N_p} \beta_i(\boldsymbol{z})\dot{\phi}_i^{\,2} \geq 0. \tag{39}$$

The inequality (39) holds for any choice of $\nabla\mu, \dot{c}$ and $\dot{\phi}_i$ if and only if

$$\tau(\boldsymbol{z}) \geq 0, \quad \beta_i(\boldsymbol{z}) \geq 0, \quad \boldsymbol{s} \cdot \boldsymbol{A}(\boldsymbol{z})\boldsymbol{s} \geq 0 \;\; \forall \boldsymbol{s}. \tag{40}$$

The restrictions imposed by the second law of thermodynamics leads to $3 + N_p$ constitutive equations. These are the Helmholtz energy $\psi(\tilde{\boldsymbol{z}})$, the constitutive moduli $\beta_i(\boldsymbol{z})$, $\tau(\boldsymbol{z})$ and the mobility tensor $\boldsymbol{A}(\boldsymbol{z})$, which have to fulfil the criteria of (30) and (40). Every set of functions that satisfies these restrictions is in accordance with the microforce balance equations (6) and (7), mass conservation (23), the first (11) and the second law of thermodynamics (17) [15].

2.4 General partial differential equations

In order to simulate physical processes with the framework derived of the previous subsections, evolution equations for the quantities c and ϕ_i are derived. To this end, an equation for the chemical potential μ which is needed for the concentration c. Inserting equation (34) into equation (36) eliminates ω^{dis} and gives

$$\mu = \frac{\partial \hat{\psi}(\tilde{\boldsymbol{z}})}{\partial c} + \hat{\omega}(\boldsymbol{z}) + \tau(\boldsymbol{z})\dot{c}. \tag{41}$$

Using the force balance (7) the constitutive relation $\hat{\omega}(\boldsymbol{z})$ in equation (41) can be replaced by $-\nabla \cdot \boldsymbol{\lambda}$ and further transformed using restriction (31.2) into

$$\mu = \frac{\partial \hat{\psi}(\tilde{\boldsymbol{z}})}{\partial c} - \nabla \cdot \frac{\partial \hat{\psi}(\tilde{\boldsymbol{z}})}{\partial \nabla c} + \tau(\boldsymbol{z})\dot{c}. \tag{42}$$

The evolution equation for the concentration can be transformed in a straightforward manner from the mass conservation law (23) using the chemical flux proposed in equation (38)

$$\dot{c} = \nabla \cdot (\boldsymbol{A}(\boldsymbol{z})\nabla\mu). \tag{43}$$

Inserting equation (42) into equation (43) leads to the evolution equation of the concentration, the viscous Cahn-Hilliard equation [28]

$$\dot{c} = \nabla \cdot \left(\boldsymbol{A}(\boldsymbol{z})\nabla \left(\frac{\partial \hat{\psi}(\tilde{\boldsymbol{z}})}{\partial c} - \nabla \cdot \frac{\partial \hat{\psi}(\tilde{\boldsymbol{z}})}{\partial \nabla c} + \tau(\boldsymbol{z})\dot{c} \right) \right). \tag{44}$$

Inserting equation (37) into equation (35) and using equations (6) and (31) leads to the partial differential equations for the phase order parameters

$$\dot{\phi}_i = \frac{1}{\beta_i(\boldsymbol{z})} \left(\nabla \cdot \frac{\partial \hat{\psi}(\tilde{\boldsymbol{z}})}{\partial \nabla \phi_i} - \frac{\partial \hat{\psi}(\tilde{\boldsymbol{z}})}{\partial \phi_i} + \gamma_i \right), \quad i = 1, ..., N_p \text{ on } V. \tag{45}$$

Please recall, that equation (44) constitutes a conservative fourth order Cahn-Hilliard differential equation, whereas equation (45) governing multiphase transformations is a non-conservative second-order Ginzburg-Landau equation.

Inserting equation (31) into the balance of linear momentum (10) leads to

$$\nabla_X \cdot \frac{\partial \hat{\psi}(\boldsymbol{z})}{\partial \boldsymbol{F}} = \boldsymbol{0}. \tag{46}$$

3 A prototype model for upper and lower bainite

This section specifies the governing equations of the thermodynamic framework in section 2. Thereby, to account for upper and lower bainite we provide an extension of the constitutive equations in [15] and [17]. The prototype model developed in this paper describes the growth of $N_p = 3$ phases

1. bainitic ferrite (ϕ_1),
2. austenite (ϕ_2) and
3. carbide (ϕ_3)

to simulate upper and lower bainite formation. Moreover, c represents the carbon concentration and $\boldsymbol{u}$ is the displacement vector.

3.1 Diffusion mechanisms in upper and lower bainite

A main challenge describing the growth of upper and lower bainite is the carbon diffusion which takes place subsequently to the phase transformation of austenite to bainitic ferrite. As already stated in the Introduction there are two diffusional phenomena working during the transition. As a model assumption we introduce three diffusion mechanisms which are combined to describe the two phenomena *separation within the bainitic ferrite* in lower bainite and *diffusion across the interface* for both morphologies. Our model ideas can be found in detail in [17]. For the sake of completeness we provide a short summary here.

The three diffusion mechanisms are shown in Figure 1 and are henceforth denoted as Type I, Type II and Type III, respectively. For the bainitic transformation, red colour is used for bainitic ferrite and yellow represents austenite. The interface regions are illustrated by black dashed lines.

I. *Separation within a phase*: Within the supersaturated lower bainitic ferrite the carbon builds accumulations surrounded by an area of low concentration.

II. *Accumulation within an interface*: Carbon atoms within the diffuse interface between bainitic ferrite and austenite are moved from the supersaturated bainitic ferrite side to the unsaturated austenite region. This mechanism is very strong in upper bainite and rather weak in lower bainite.

III. *Balancing within the phases*: Here carbon atoms are distributed equally throughout the phase. This mechanism governs a redistribution of carbon within the austenite which is enriched only near the interface with the bainitic ferrite. Furthermore, in upper bainitic ferrite, this mechanism, provides the transport of carbon atoms towards the interface which is depleted of carbon due to Type II diffusion.

Accumulation within an interface (Type II) and balancing within the phases (Type III) together are denoted as *diffusion across the interface*.

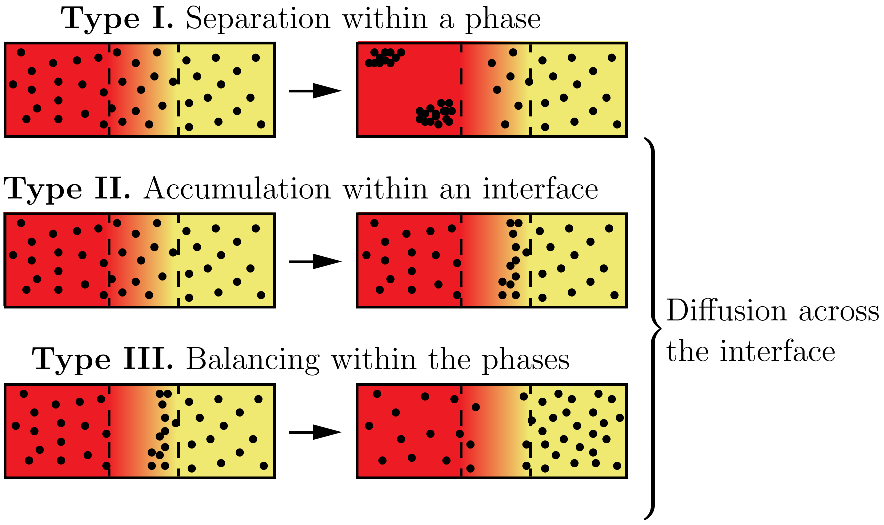

Figure 1: Schematics of three diffusion mechanisms [17]

3.2 Weighted Helmholtz energy

In subsection 2.3 which is concerned with restrictions to constitutive equations and subsection 2.4 which summarizes the temporarily results, it becomes clear that the Helmholtz energy function is the most important constitutive equation of the model presented in this paper. Amongst other equations the Helmholtz energy function is the key ingredient to model the different diffusion types described in subsection 3.1.

The Helmholtz energy is postulated as a specification of equation (26) as

$$\hat{\psi}(\tilde{\boldsymbol{z}}) = \hat{\psi}_c(c, \nabla c) + \hat{\psi}_\phi(c, \phi_k, \nabla\phi_k) + \psi_{el}(\phi_k, \boldsymbol{F}), \tag{47}$$

where $\hat{\psi}_c(c, \nabla c)$ is a part which governs diffusion of Type I and Type III and does not contain any coupling terms, whereas $\hat{\psi}_\phi(c, \phi_k, \nabla\phi_k)$ contains the phase field energies and governs the diffusion Type II. The energy $\psi_{el}(\phi_k, \boldsymbol{\varepsilon})$ includes the mechanical terms and the coupling between deformations and phase fields. The diffusive part is a sum of two energies

$$\hat{\psi}_c(c, \nabla c) = w_f(T)\hat{\psi}_f(c) + w_s(T)\hat{\psi}_s(c, \nabla c), \tag{48}$$

where both summands are weighted by functions $w_f(T)$ and $w_s(T)$, respectively, which depend on the temperature T. The term $\hat{\psi}_f(c)$ is important for Type III diffusion and multiplied with w_f which governs the diffusion across the interface whereas $\hat{\psi}_s(c, \nabla c)$ is relevant for Type I diffusion and multiplied with the corresponding weighting function w_s for the separation which is only relevant for lower bainite. The weighting functions are defined as

$$w_f(T) = \begin{cases} 0 & \text{for } T < T_D - \varepsilon_T \\ 1 & \text{for } T > T_D + \varepsilon_T \\ \dfrac{1}{2} + \dfrac{L_D}{2} + \left(\dfrac{1}{2} - \dfrac{L_D}{2}\right) \sin\left(\pi\left(\dfrac{T - T_D}{2\varepsilon_T} + 2\right)\right) & \text{otherwise} \end{cases} \tag{49}$$

and

$$w_s(T) = \begin{cases} 1 & \text{for } T < T_D - \varepsilon_T \\ 0 & \text{for } T > T_D + \varepsilon_T \\ \dfrac{1}{2} - \dfrac{L_D}{2} + \left(\dfrac{1}{2} - \dfrac{L_D}{2}\right) \sin\left(\pi\left(\dfrac{T - T_D}{2\varepsilon_T} + 1\right)\right) & \text{otherwise.} \end{cases} \tag{50}$$

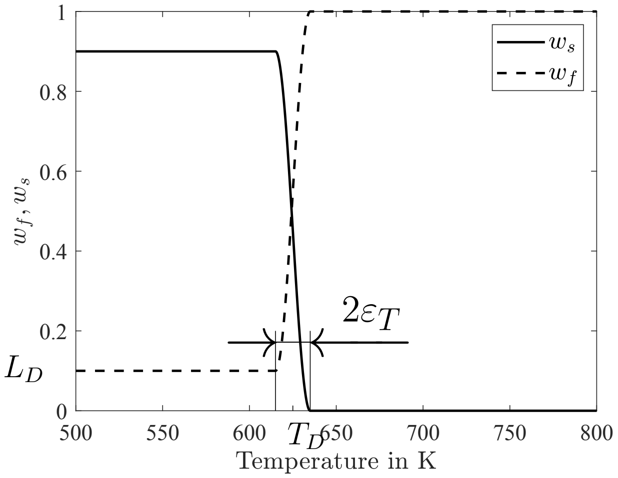

Figure 2: Weighting functions for different diffusion processes

Here T is the temperature of the isothermal transformation, T_D is the transition temperature marking the boundary between upper and lower bainite, ε_T is a factor to soften the sharp boundary for better numerical characteristics and L_D ensures the interaction of both diffusion mechanisms.

Both weighting functions are illustrated in Figure 2 versus the temperature T. Note, that w_f and w_s satisfy the completeness condition

$$w_f(T) + w_s(T) = 1. \tag{51}$$

For further details on the weighting functions see [17].

For Type I diffusion (separation) a Cahn-Hilliard equation is used. To receive such an equation a suitable Helmholtz energy is

$$\hat{\psi}_s(c, \nabla c) = f(c) + \frac{1}{2}\rho|\nabla c|^2, \tag{52}$$

$$f(c) = d(c_{\text{eq}} - c)^2(c_{\text{carb}} - c)^2. \tag{53}$$

where $\sqrt{\rho}$ is a measure of the interface thickness and $f(c)$ is a double well energy function limiting the separation process. The limits of the separation are defined by c_{eq} which is the equilibrium carbon concentration in bainitic ferrite and c_{carb} which is the carbon concentration of carbides.

For Type III diffusion we postulate

$$\hat{\psi}_f(c) = \frac{c_{\mathrm{eq}} \ln(c_{\mathrm{eq}} - c) - c_{\mathrm{carb}} \ln(c_{\mathrm{carb}} - c) + c \ln(\frac{c_{\mathrm{carb}} - c}{c_{\mathrm{eq}} - c})}{c_{\mathrm{eq}} - c_{\mathrm{carb}}}. \tag{54}$$

Details on this formulation can be found in [17].

For the multiphase field equation (47) a Helmholtz energy with a double sum formulation is used

$$\hat{\psi}_\phi(\phi_k, \nabla\phi_k) = \sum_{i=1}^{N_p} \sum_{j>i}^{N_p} \frac{1}{q_{ij}} \left[h_{ij}(\phi_i, \phi_j, \nabla\phi_i, \nabla\phi_j) + (1 + c\ s_{ij}\ w_f)\ g_{ij}(\phi_i, \phi_j)\right] \tag{55}$$

where $h_{ij}(\phi_i, \phi_j, \nabla\phi_i, \nabla\phi_j)$ is an interfacial energy density and $g_{ij}(\phi_i, \phi_j)$ is a potential energy containing a double well potential between phases i and j which is additionally used to model Type II diffusion and therefore, multiplied by c and an interface diffusion factor s_{ij}. The potential reads

$$g_{ij}(\phi_i, \phi_j) = \frac{1}{4a_{ij}} \phi_i^2 \phi_j^2, \tag{56}$$

where a_{ij} are potential constants. Furthermore, we chose an interfacial energy density, following [29]

$$h_{ij}(\phi_i, \phi_j, \nabla\phi_i, \nabla\phi_j) = \frac{1}{2} \alpha_{ij} (\phi_j \nabla\phi_i - \phi_i \nabla\phi_j)^2 \tag{57}$$

where α_{ij} is a phase gradient energy coefficient.

For the bainitic transformation model only infinitesimal strains are considered. Therefore, the engineering strain tensor is

$$\boldsymbol{\varepsilon} = \mathrm{sym}(\boldsymbol{F} - \mathbf{1}) = \frac{1}{2}(\nabla\boldsymbol{u} + \nabla\boldsymbol{u}^T) \tag{58}$$

and the symmetric engineering stress tensor is

$$\boldsymbol{\sigma} = \boldsymbol{\sigma}^T. \tag{59}$$

The Helmholtz energy ψ_{el} in equation (47) can now be written as a function of $\boldsymbol{\varepsilon}$

instead of $\boldsymbol{F}$ and is proposed as

$$\psi_{el}(\phi_k, \boldsymbol{\varepsilon}) = \sum_{i=1}^{N_p} \sum_{j>i}^{N_p} \frac{p_{ij}}{2} (\boldsymbol{\varepsilon} - \boldsymbol{\varepsilon}_{ij}^0 \phi_i \phi_j) : \mathbb{C}_{ij} (\boldsymbol{\varepsilon} - \boldsymbol{\varepsilon}_{ij}^0 \phi_i \phi_j), \tag{60}$$

where $\boldsymbol{\varepsilon}_{ij}^0$ are eigenstrain tensors due to a phase transformation from phase i to j, p_{ij} is a coupling parameter and $\mathbb{C}_{ij}$ are symmetric fourth order material tensors.

3.3 Coupled partial differential equations

In this section we formulate the model partial differential equations using the results of subsections 2.4 and 3.2. For the diffusion equation (44) the mobility tensor $\boldsymbol{A}$ and the constitutive moduli τ must be chosen. In this case τ is a constant

$$\tau(\boldsymbol{z}) = \tau w_s = \text{const.}, \tag{61}$$

while the mobility tensor is weighted like the Helmholtz energy (48) and reads

$$\boldsymbol{A}(\boldsymbol{z}) = (w_f D_f(\phi) f_q(c) + w_s D_s(\phi))\, \mathbf{1}, \tag{62}$$

where the diffusion coefficients $D_f(\phi)$ and D_s are proposed as

$$1.\;\; D_f(\phi) = \sum_{i=1}^{N_p} \phi_i D_{fi}, \qquad 2.\;\; D_s(\phi) = \sum_{i=1}^{N_p} \phi_i D_{si}, \qquad 3.\;\; f_q(c) = (c - c_{\text{eq}})(c_{\text{carb}} - c), \tag{63}$$

where f_q is chosen to limit the otherwise unbounded Type II diffusion between c_{eq} and c_{carb}.

Inserting equation (61) and (47) with equations (48) and (55) into equation (42) leads to

$$\mu = w_f \frac{\partial \hat{\psi}_f(c)}{\partial c} + w_f \sum_{i=1}^{N_p} \sum_{j>i}^{N_p} \frac{1}{q_{ij}} s_{ij} \;\; g_{ij}(\phi_i, \phi_j) + w_s \frac{\partial \hat{\psi}_s(c, \nabla c)}{\partial c} - w_s \nabla \cdot \frac{\partial \hat{\psi}_s(c, \nabla c)}{\partial \nabla c} + w_s \tau \dot{c}. \tag{64}$$

which we split up into

$$\mu = w_f(T) \mu_f + w_s(T) \mu_s, \tag{65}$$

where using equations (56) and (52)

$$1.\ \ \mu_s = \frac{\partial f}{\partial c} - \rho\Delta c + \tau\dot{c}, \qquad 2.\ \ \mu_f \quad = \frac{\partial\hat{\psi}_f(c)}{\partial c} + \sum_{i=1}^{N_p}\sum_{j>i}^{N_p} v_{ij}\phi_i^2\phi_j^2, \qquad 3.\ \ v_{ij} = \frac{s_{ij}}{4a_{ij}q_{ij}}. \tag{66}$$

Here μ_f and μ_s are chemical potentials for diffusion across the interface (Type II + Type III) and separation (Type I), respectively.

Inserting equation (65) into the evolution equation (43) leads to

$$\dot{c} = \nabla\cdot(w_f\boldsymbol{A}(\boldsymbol{z})\nabla\mu_f) + \nabla\cdot(w_s\boldsymbol{A}(\boldsymbol{z})\nabla\mu_s). \tag{67}$$

In the next step we only insert the chemical potential for diffusion across the interface μ_f (66.2) into the evolution equation (67), which leads to simplifications that can be found in the appendix of [17]. The chemical potential for the separation μ_s (66.1) is calculated as a single degree of freedom to avoid fourth order derivatives. The partial differential equation (67) of the concentration field c reads

$$\begin{aligned}
\dot{c} = {} & w_f^2\nabla D_f(\phi)\cdot\nabla c + w_f^2 D_f(\phi)\Delta c + w_s w_f\nabla D_s(\phi)\frac{\partial^2\hat{\psi}_f(c)}{\partial c^2}\nabla c \\
& + w_s w_f D_s(\phi)\frac{\partial^3\hat{\psi}_f(c)}{\partial c^3}(\nabla c)^2 + w_s w_f D_s(\phi)\frac{\partial^2\hat{\psi}_f(c)}{\partial c^2}\Delta c \\
& + \left(w_f^2\nabla D_f(\phi) f_q(c) + w_f^2 D_f(\phi)\frac{\partial f_q(c)}{\partial c}\nabla c + w_s w_f\nabla D_s(\phi)\right) \\
& \cdot\sum_{i=1}^{N_p}\sum_{j>i}^{N_p} v_{ij}\left(2\phi_i\phi_j^2\nabla\phi_i + 2\phi_j\phi_i^2\nabla\phi_j\right) \\
& + \left(w_f^2 D_f(\phi) f_q(c) + w_s w_f D_s(\phi)\right) \\
& \sum_{i=1}^{N_p}\sum_{j>i}^{N_p} 2v_{ij}\left(\nabla\phi_i\phi_j^2\nabla\phi_i + \nabla\phi_j\phi_i^2\nabla\phi_j + 4\phi_i\phi_j\nabla\phi_i\nabla\phi_j + \phi_j\phi_i^2\Delta\phi_j + \phi_i\phi_j^2\Delta\phi_i\right) \\
& + \left(w_s w_f\nabla D_f(\phi) f_q(c) + w_s w_f D_f(\phi)\frac{\partial f_q(c)}{\partial c}\nabla c + w_s^2\nabla D_s(\phi)\right)\cdot\nabla\mu_s \\
& + \left(w_s w_f D_f(\phi) f_q(c) + w_s^2 D_s(\phi)\right)\Delta\mu_s.
\end{aligned} \tag{68}$$

For the partial differential equations governing the phase order parameters (45) an equation for the constitutive moduli $\beta_i(\boldsymbol{z})$ is needed. We postulate

$$\beta_i(\boldsymbol{z}) = \beta_i = \text{const.} \tag{69}$$

such that equation (45) using equation (55) reads

$$\begin{aligned}\dot{\phi}_i = \sum_{j=1,j\neq i}^{N_p} \frac{1}{\beta_i q_{ij}} \left(\alpha_{ij} \left(\phi_j \Delta\phi_i - \phi_i \Delta\phi_j \right) - \frac{\phi_i \phi_j \cdot (1 + c\ s_{ij}\ w_f)}{2a_{ij}} (\phi_j - \phi_i) \right) + \frac{\gamma_i}{\beta_i} \\ - \frac{1}{\beta_i} \sum_{j=1,j\neq i}^{N_p} p_{ij}(\phi_i - \phi_j) \boldsymbol{\varepsilon}^0_{ij} : \mathbb{C}_{ij}(\boldsymbol{\varepsilon} - \boldsymbol{\varepsilon}^0_{ij}\phi_i\phi_j), \\ \text{for} \quad i = 1, ..., N_p \ .\end{aligned} \tag{70}$$

The external phase forces γ_i, introduced in (3) and appearing in equation (70), are crucial for the phase field method since they are the thermodynamic driving forces governing the phase growth. Due to the fact that the model presented here is a multiphase model, where each phase may grow at the expense of any other remaining phase, we need to postulate the external phase forces as connected functions between two phases i and j

$$\gamma_i = \sum_{j=1,j\neq i}^{N_p} \gamma_{ij} = - \sum_{j=1,j\neq i}^{N_p} \frac{6\Delta G_{ij}(\boldsymbol{z})}{q_{ij}}\ \phi_i\ \phi_j \tag{71}$$

and introduce the new quantity ΔG_{ij} which is a Gibbs energy between two phases i and j. The arbitrary factor 6 is introduced to be consistent with the evolution equations of [14] and [7].

For a better physical interpretation we change the material constants of equation (70) according to [7]. The dissipative moduli β_i, the phase gradient energy coefficients α_{ij}, the potential constants a_{ij} and the phase energy coefficients q_{ij} are replaced by the interface mobilities ζ_{ij}, interface energies σ_{ij} and interface thicknesses η_{ij}

$$\beta_i q_{ij} = \frac{\eta_{ij}}{\zeta_{ij}}, \qquad a_{ij} = \frac{\eta_{ij}}{72\sigma_{ij}}, \qquad \alpha_{ij} = \sigma_{ij}\eta_{ij}, \qquad \frac{p_{ij}}{\beta_i} = r_{ij}\zeta_{ij}. \tag{72}$$

The parameter change (72) is done using the Gibbs-Thomson equation ([7]) as is presented in detail in the appendix of [14]. Note, that $\zeta_{ij} = \zeta_{ji}$, $\sigma_{ij} = \sigma_{ji}$ and $\eta_{ij} = \eta_{ji}$ but $\Delta G_{ij} = -\Delta G_{ji}$.

With the new parameters (72) the final partial differential equations (70) governing the phase order parameters read

$$\begin{aligned}\dot{\phi}_i = \sum_{j=1,j\neq i}^{N_p} \zeta_{ij}\Bigg[&\sigma_{ij}\left((\phi_j\Delta\phi_i - \phi_i\Delta\phi_j) - \frac{36}{\eta_{ij}^2}(1+c\ s_{ij}\ w_f)\phi_i\phi_j(\phi_j-\phi_i)\right) - \frac{6\Delta G_{ij}(\boldsymbol{z})}{\eta_{ij}}\phi_i\phi_j \\ &- r_{ij}(\phi_i-\phi_j)\boldsymbol{\varepsilon}^0_{ij} : \mathbb{C}_{ij}(\boldsymbol{\varepsilon} - \boldsymbol{\varepsilon}^0_{ij}\phi_i\phi_j)\Bigg] \quad \text{for} \quad i=1,...,N_p. \end{aligned} \tag{73}$$

The coupling terms with the mechanical contribution in equation (73) are additional thermodynamic driving forces which govern the growth of the phases.

As explained for the external phases forces γ_i, the coupling terms with the mechanical contribution are connected functions between two phases i and j, too. Thereby any phase i can grow on the expense of any phase j.

Remarks

1. The elastic energy in equation (60) is inspired by Schmitt *et al.* [10] and [22] who simulate the growth of martensite variants from austenite but changed in a significant way. To motivate the changes, the multiphase field formulation (73) is compared with the multiphase field of [22] which reads

$$\dot{\phi}_i = -M\left[\frac{\partial W}{\partial \phi_i} + G\left(\frac{1}{L}\frac{\partial f}{\partial \phi_i} - L\Delta\phi_i\right)\right], \tag{74}$$

where ϕ_i is a phase order parameter for phase i, M is a mobility factor, W the elastic energy, G and L are material parameters. The function f yields a Landau polynomial

$$f(\phi_i) = 1 + \frac{A}{2}\left(\sum_i \phi_i^2\right) + \frac{B}{3}\left(\sum_i \phi_i^2\right) + \frac{C}{4}\left(\sum_i \phi_i^2\right)^2, \tag{75}$$

where A, B and C are temperature-dependent coefficients [22]. The elastic energy W reads

$$W(\boldsymbol{\varepsilon}, \phi_i) = \frac{1}{2}[\boldsymbol{\varepsilon} - \boldsymbol{\varepsilon}^0(\phi_i)] : \mathbb{C}(\phi_i)[\boldsymbol{\varepsilon} - \boldsymbol{\varepsilon}^0(\phi_i)], \qquad \text{with} \tag{76}$$

$$\boldsymbol{\varepsilon}^0(\phi_i) = \sum_i \phi_i \boldsymbol{\varepsilon}^0_i, \qquad \mathbb{C}(\phi_i) = \mathbb{C}_0 + \sum_i \phi_i(\mathbb{C}_i - \mathbb{C}_0), \tag{77}$$

where $\boldsymbol{\varepsilon}$ is the strain, $\boldsymbol{\varepsilon}^0_i$ is the eigenstrain, $\mathbb{C}$ is a material tensor of a parent phase and $\mathbb{C}_i$ is a material tensor of phase i [22].

2. The differences between the multiphase field models in equations (73) and (74) are obvious. In equation (73) all phase parameters occur in pairs of ϕ_i and ϕ_j whereas in equations (74) - (77) ϕ_i occurs only on its own. Furthermore, the Laplace operator is used in equation (73) on ϕ_i and ϕ_j.

3. The elastic energies ψ_{el} in (60) and W in (76) differ in the way that ψ_{el} uses double sums while W uses only one sum. All material parameters in equation (73) have two indices, describing the phase transformation between any phases i and j while in equation (76) only single indices occur. These differences lead to different multiphase field methods as illustrated exemplarily in Figure 3. The phase field model in Figure 3.a) allows only the growth of the phases $2, 3, 4$ at the expense of phase 1, while the model presented in Figure 3.b) allows the transformation from any phase into any other phase.

4. The multiphase field formulation of equations (74) - (77) provides a model with a parent phase ϕ_1 as illustrated in Figure 3.a). The parent phase ϕ_1 is present as an initial condition and all other $i = 2, ..., n$ phases can grow out of this parent phase. The parent phase itself is not computed or described by an equation, such that the completeness condition $\sum \phi_i = 1$ is trivially satisfied. This is useful in their model since all martensite variants grow out of the parent austenite. However, it is not possible that any phase ϕ_i may grow directly out of phase ϕ_j if $j \neq 1$. Such a model is not able to describe the bainitic transformation, because here bainitic ferrite grows at the expense of austenite while carbide grows at the expense of bainitic ferrite or austenite.

5. In the phase field model presented in this paper every phase can evolve at the expense of all other phases as illustrated in Figure 3.b). This generality requires a formulation which states clearly at whose expense a phase should grow, such that the completeness condition $\sum \phi_i = 1$ is fulfilled. The model described in equation (73) is able to simulate the growth of any phase k out of any other phase l, because every term $\zeta_{kl}[...]$ of an evolution equation for ϕ_k can be found, with negative sign in the evolution equation for ϕ_l. This requirement is obviously not fulfilled by equations (74) - (77).

The Gibbs energy is used to model the precipitation of carbides. In case the carbon concentration reaches the concentration of carbides (6.67 wt.%), carbides precipitate.

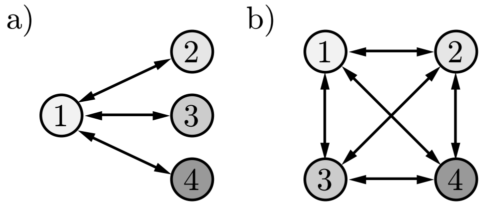

Figure 3: Multiphase field models where a) transformations between all phases are possible and b) transformations can only evolve from the parent phase 1.

Therefore, we postulate as described in [15]:

$$\Delta G_{ij}(\boldsymbol{z}) = \Delta G_{ij}^0 \; v(\phi_i, \phi_j, c) \tag{78}$$

with

$$v(\phi_i, \phi_j, c) = \begin{cases} \dfrac{w(c)}{\phi_3^2 + \varepsilon_\phi} & \text{for } i = 3 \vee j = 3 \\ 1 & \text{otherwise.} \end{cases} \tag{79}$$

The variables ΔG_{ij}^0 in equations (78) are constant Gibbs energies between phases i and j and w is a smooth step function proposed as

$$w(c) = \begin{cases} 0 & \text{for } c < c_{\text{carb}} - \varepsilon \\ 1 & \text{for } c > c_{\text{carb}} \\ \frac{1}{2} + \frac{1}{2}\sin(\frac{\pi}{\varepsilon}c + \frac{\pi}{2} - \frac{\pi}{\varepsilon}c_{\text{carb}}) & \text{otherwise,} \end{cases} \tag{80}$$

where the width of the smooth step is defined by the parameter ε.

The equations (78)-(80) are chosen such that, carbides will grow only if the carbon concentration reaches $c_{\text{carb}} = 6.67\,\text{wt.\%}$ [30]. The divisor ϕ_3^2 in equation (79) guarantees that the phase ϕ_3 can grow even if the current value of ϕ_3 is close to zero and the very small constant numerical perturbation $\varepsilon_\phi > 0$ prevents the equation from dividing by zero in case $\phi_3 = 0$.

Redefining equation (46) for infinitesimal strain and inserting equation (60) renders a partial differential equation for the mechanical problem

$$\nabla \cdot \frac{\partial \hat{\psi}(\boldsymbol{z})}{\partial \boldsymbol{\varepsilon}} = \nabla \cdot \left(\sum_{i=1}^{N_p} \sum_{j>i}^{N_p} p_{ij} \mathbb{C}_{ij} (\boldsymbol{\varepsilon} - \boldsymbol{\varepsilon}_{ij}^0 \phi_i \phi_j) \right) = \mathbf{0}. \tag{81}$$

4 Numerical implementation

This section provides the information about the implementation. The resulting system of partial differential equations (66.1), (68), (73) and (81) is solved numerically with the finite element method in a two dimensional space. Furthermore, the backward Euler method is used for the time discretization. For the finite element formulation quadrilateral elements with linear shape functions are implemented. To solve the algebraic system of equation Newton's method is applied.

At every node the following seven unknowns are computed: $c, \mu_s, \phi_1, \phi_2, \phi_3, u_x, u_y$. The chemical potential μ_s for the lower bainitic transformation is computed separately to avoid fourth order derivates in equation (68). It would be sufficient to calculate only two of the three phases. However, we calculate all of them to check that the sum is zero at every time and position.

The lower chemical potential (66.1) reads in weak formulation

$$\int_V \nu_\mu \tau \dot{c} + \rho \nabla \nu_\mu \nabla c + \nu_\mu \frac{\partial f(c)}{\partial c} - \nu_\mu \mu_s \; dV = 0, \tag{82}$$

where ν_μ denotes the test function for the lower chemical potential. For the diffusion equation (68) the weak formulation reads

$$\begin{aligned}
\int_V \nu_c \dot{c} \; dV = \int_V \nu_c w_f^2 \nabla D_f(\phi) \nabla c \; dV + \int_V \nu_c w_f^2 D_f(\phi) \Delta c \; dV \\
+ \int_V \nu_c w_s w_f \nabla D_s(\phi) \frac{\partial^2 \hat{\psi}_f(c)}{\partial c^2} \nabla c \; dV + \int_V \nu_c w_s w_f D_s(\phi) \frac{\partial^3 \hat{\psi}_f(c)}{\partial c^3} (\nabla c)^2 \; dV \\
+ \int_V \nu_c w_s w_f D_s(\phi) \frac{\partial^2 \hat{\psi}_f(c)}{\partial c^2} \Delta c \; dV \\
+ \int_V \nu_c \left(w_f^2 \nabla D_f(\phi) f_q(c) + w_f^2 D_f(\phi) \nabla f_q(c) + w_s w_f \nabla D_s(\phi) \right) \\
\cdot \sum_{i=1}^{N_p} \sum_{j>i}^{N_p} 2 v_{ij} (\nabla \phi_i \phi_i \phi_j^2 + \phi_i^2 \phi_j \nabla \phi_j) \; dV + \int_V \nu_c \left(w_f^2 D_f(\phi) f_q(c) + w_s w_f D_s(\phi) \right) \\
\sum_{i=1}^{N_p} \sum_{j>i}^{N_p} 2 v_{ij} (\Delta \phi_i \phi_i \phi_j^2 + (\nabla \phi_i)^2 \phi_j^2 + 4 \nabla \phi_i \phi_i \phi_j \nabla \phi_j + \Delta \phi_j \phi_i^2 \phi_j + (\nabla \phi_j)^2 \phi^2) \; dV \\
+ \int_V \nu_c (w_f w_s \nabla D_f(\phi) f_q(c) + w_f w_s D_f(\phi) \nabla f_q(c) + w_s^2 \nabla D_s(\phi)) \cdot \nabla \mu_s \; dV \\
+ \int_V \nu_c (w_f w_s D_f(\phi) f_q(c) + w_s^2 D_s(\phi)) \Delta \mu_s \; dV,
\end{aligned} \tag{83}$$

where ν_c is the test function for the concentration c needed for the finite element formulation.

The test functions for the phase order parameters are denoted as ν_ϕ, such that the weak formulation of the phase field evolution equations (73) with applied Gauss theorem and homogeneous Neumann boundary conditions read

$$\int_V \nu_\phi \dot{\phi}_i \; dV = \int_V \sum_{j=1, j\neq i}^{N_p} \zeta_{ij} \Bigg[\sigma_{ij} \bigg(\nabla\nu_\phi (\nabla\phi_j \phi_i - \nabla\phi_i \phi_j) - \frac{36}{\eta_{ij}^2} \nu_\phi \phi_i \phi_j (1 + c \; s_{ij} \; w_f)(\phi_j - \phi_i) \bigg) \\ - \frac{6\Delta G_{ij}(\boldsymbol{z})}{\eta_{ij}} \nu_\phi \phi_i \phi_j - \nu_\phi r_{ij} (\phi_i - \phi_j) \boldsymbol{\varepsilon}_{ij}^0 : \mathbb{C}_{ij} (\boldsymbol{\varepsilon} - \boldsymbol{\varepsilon}_{ij}^0 \phi_i \phi_j) \Bigg] \; dV. \tag{84}$$

With homogeneous Neumann boundary conditions the weak formulation of equation (81) is derived as

$$0 = \int_V \nabla\nu_u \cdot \left(\sum_{i=1}^{N_p} \sum_{j>i}^{N_p} p_{ij} \mathbb{C}_{ij} (\boldsymbol{\varepsilon} - \boldsymbol{\varepsilon}_{ij}^0 \phi_i \phi_j) \right) \; dV. \tag{85}$$

In the next step a matrix formulation is used where degrees of freedom at every node are denoted with the superimposed hat $\hat{(\cdot)}$. Furthermore, we introduce a row vector $\underline{N}$ containing the shape function values, such that the degrees of freedom may be written as

$$c = \underline{N}\underline{\hat{c}} \; , \qquad \mu_s = \underline{N}\underline{\hat{\mu}_s} \; , \qquad \phi_i = \underline{N}\underline{\hat{\phi}_i} \; , \quad i = 1, 2, 3 \tag{86}$$

while gradient terms are described by

$$\nabla c = \underline{B}\underline{\hat{c}} \; , \qquad \nabla\mu_s = \underline{B}\underline{\hat{\mu}_s} \; , \qquad \nabla\phi_i = \underline{B}\underline{\hat{\phi}_i} \; , \quad i = 1, 2, 3. \tag{87}$$

where $\underline{B}$ is defined as

$$\underline{B} = \begin{bmatrix} \underline{N}_{,x} \\ \underline{N}_{,y} \end{bmatrix} , \qquad \text{with} \qquad \underline{N}_{,x} = \frac{\partial \underline{N}}{\partial x}. \tag{88}$$

The displacement $\underline{\hat{u}}$ and the total strain $\underline{\boldsymbol{\varepsilon}}$ in Voigt notation read

$$\underline{\hat{u}} = \begin{bmatrix} \underline{\hat{u}}_x \\ \underline{\hat{u}}_y \end{bmatrix} , \qquad \underline{\boldsymbol{\varepsilon}} = \underline{B}_f \underline{\hat{u}} = \begin{bmatrix} \varepsilon_x \\ \varepsilon_y \\ \gamma \end{bmatrix} , \quad \text{where} \quad \underline{B}_f = \begin{bmatrix} \underline{N}_{,x} & 0 \\ 0 & \underline{N}_{,y} \\ \underline{N}_{,y} & \underline{N}_{,x} \end{bmatrix} \tag{89}$$

The relations in equations (86) - (89) are used in the same manner for the test functions

ν_ϕ, ν_c, ν_μ and ν_u respectively. The element residual terms are derived from the weak formulations (82) - (85) and read

$$
\begin{aligned}
\underline{R}^c = \int\limits_{\Omega_e} \underline{N}^T \underline{N} \frac{\hat{\underline{c}}^n - \hat{\underline{c}}^{n-1}}{\Delta t} + \underline{B}^T \underline{B} \hat{\underline{c}} \left(w_f^2 D_f(\phi) + w_f w_s D_s(\phi) \frac{\partial^2 \hat{\psi}_f(c)}{\partial c^2} \right) \\
+ \underline{B}^T (w_f^2 D_f(\phi) f_q(\hat{\underline{c}}) + w_s w_f D_s(\phi)) \\
\sum_{i=1}^{N_p} \sum_{j>i}^{N_p} 2 v_{ij} \left((\underline{N} \hat{\underline{\phi}}_i)(\underline{N} \hat{\underline{\phi}}_j)^2 \underline{B} \hat{\underline{\phi}}_i + \underline{N} \hat{\underline{\phi}}_j (\underline{N} \hat{\underline{\phi}}_i)^2 \underline{B} \hat{\underline{\phi}}_j) \right) \\
+ \underline{B}^T \underline{B} \underline{\hat{\mu}_s} \left(w_f w_s D_f(\phi) f_q(\hat{\underline{c}}) + w_s^2 D_s(\phi) \right) \, d\Omega,
\end{aligned}
\tag{90}
$$

$$
\underline{R}^{\mu_s} = \int\limits_{\Omega_e} \tau (\underline{N}^T \underline{N}) \frac{\hat{\underline{c}}^n - \hat{\underline{c}}^{n-1}}{\Delta t} + \underline{N}^T \frac{\partial f(\underline{N} \hat{\underline{c}})}{\partial c} + \rho (\underline{B}^T \underline{B}) \hat{\underline{c}} - (\underline{N}^T \underline{N}) \underline{\hat{\mu}_s} \, d\Omega,
\tag{91}
$$

$$
\begin{aligned}
\underline{R}^{\phi_i} = \int\limits_{\Omega_e} \underline{N}^T \underline{N} \, \frac{\hat{\underline{\phi}}_i^n - \hat{\underline{\phi}}_i^{n-1}}{\Delta t} + \sum_{j=1, j \neq i}^{N_p} \zeta_{ij} \, \Bigg[\sigma_{ij} \Bigg(- (\underline{B}^T \underline{B}) \hat{\underline{\phi}}_j (\underline{N} \hat{\underline{\phi}}_i) + (\underline{B}^T \underline{B}) \hat{\underline{\phi}}_i (\underline{N} \hat{\underline{\phi}}_j) \\
- \frac{36}{\eta_{ij}^2} \underline{N}^T (1 + s_{ij} w_f (\underline{N} \hat{\underline{c}})) \underline{N} (\hat{\underline{\phi}}_i - \hat{\underline{\phi}}_j) \left((\underline{N} \hat{\underline{\phi}}_i)(\underline{N} \hat{\underline{\phi}}_j) \right) \Bigg) + \frac{6}{\eta_{ij}} \Delta G_{ij}(\boldsymbol{z}) \underline{N}^T (\underline{N} \hat{\underline{\phi}}_i)(\underline{N} \hat{\underline{\phi}}_j) \\
- r_{ij} \underline{N} (\hat{\underline{\phi}}_i - \hat{\underline{\phi}}_j) \underline{\varepsilon}_{ij}^0 : \underline{\mathbb{C}}_{ij} (\underline{B}_f \underline{\hat{\boldsymbol{u}}} - \underline{\varepsilon}_{ij}^0 \underline{N} \hat{\underline{\phi}}_i \underline{N} \hat{\underline{\phi}}_j) \Bigg] \, d\Omega.
\end{aligned}
\tag{92}
$$

$$
\underline{R}^u = \int\limits_{\Omega_e} \sum_{i=1}^{N_p} \sum_{j>i}^{N_p} p_{ij} \underline{B}_f^T \mathbb{C}_{ij} (\underline{B}_f \underline{\hat{\boldsymbol{u}}} - \underline{\varepsilon}_{ij}^0 \underline{N} \hat{\underline{\phi}}_i \underline{N} \hat{\underline{\phi}}_j) \, d\Omega.
\tag{93}
$$

The superimposed n is used in equations (90)-(92) to denote the actual time step in the backward Euler terms. It is omitted for brevity in other parts. To evaluate the integrals a Gauss-Legendre rule is applied.

The non-linear algebraic system of equations

$$
\underline{R}(\hat{\underline{d}}) = \underline{0} \quad \text{where} \quad \underline{R} = [\underline{R}^c \;\; \underline{R}^{\mu_s} \;\; \underline{R}^{\phi_i} \;\; \underline{R}^u]^T, \quad \hat{\underline{d}} = [\hat{\underline{c}} \;\; \hat{\underline{\mu}} \;\; \hat{\underline{\phi}_i} \;\; \hat{\underline{u}}]^T
\tag{94}
$$

is solved with Newton's method. For that purpose the derivatives of the residual function

(94) are needed

$$\underline{K} = \frac{\partial \underline{R}}{\partial \hat{\underline{d}}} = \begin{bmatrix} \underline{K}^{cc} & \underline{K}^{c\mu_s} & \underline{K}^{c\phi_o} & \underline{K}^{c\phi_p} & \underline{0} \\ \underline{K}^{\mu_s c} & \underline{K}^{\mu_s\mu_s} & \underline{0} & \underline{0} & \underline{0} \\ \underline{K}^{\phi_o c} & \underline{0} & \underline{K}^{\phi_o\phi_o} & \underline{K}^{\phi_o\phi_p} & \underline{K}^{\phi_o u} \\ \underline{K}^{\phi_p c} & \underline{0} & \underline{K}^{\phi_p\phi_o} & \underline{K}^{\phi_p\phi_p} & \underline{K}^{\phi_p u} \\ \underline{0} & \underline{0} & \underline{K}^{u\phi_o} & \underline{K}^{u\phi_p} & \underline{K}^{uu} \end{bmatrix}, \tag{95}$$

with the submatrices

$$\begin{aligned} \underline{K}^{\phi_i\phi_i} = \frac{\partial \underline{R}^{\phi_i}}{\partial \underline{\hat{\phi}}_i} = \int\limits_{\Omega_e} & \underline{N}^T \underline{N} \frac{1}{\Delta t} + \sum_{j=1, j\neq i}^{N_p} \zeta_{ij} \Bigg[\sigma_{ij} \Bigg((\underline{B}^T \underline{B})(\underline{N}\underline{\hat{\phi}}_j) - (\underline{B}^T \underline{B}) \underline{\hat{\phi}}_j \underline{N} \\ & - \frac{36}{\eta_{ij}^2} \underline{N}^T \underline{N} (1 + s_{ij} w_f(\underline{N}\underline{\hat{c}}))(\underline{N}\underline{\hat{\phi}}_j) \underline{N} (2\underline{\hat{\phi}}_i - \underline{\hat{\phi}}_j) \Bigg) \\ & + \frac{6}{\eta_{ij}} \Bigg(\Delta G_{ij}(\boldsymbol{z}) \underline{N}^T \underline{N} (\underline{N}\underline{\hat{\phi}}_j) + \frac{\partial \Delta G_{ij}(\boldsymbol{z})}{\partial \underline{\hat{\phi}}_i} \underline{N}^T (\underline{N}\underline{\hat{\phi}}_i)(\underline{N}\underline{\hat{\phi}}_j) \Bigg) \\ - r_{ij} \underline{N}^T \underline{N} & \left[\underline{\varepsilon}_{ij}^0 : \mathbb{C}_{ij} (\underline{B}_f \hat{\boldsymbol{u}} - \underline{\varepsilon}_{ij}^0 \underline{N}\underline{\hat{\phi}}_i \underline{N}\underline{\hat{\phi}}_j) + (\underline{N}\underline{\hat{\phi}}_i - \underline{N}\underline{\hat{\phi}}_j) \underline{\varepsilon}_{ij}^0 : \mathbb{C}_{ij} (-\underline{\varepsilon}_{ij}^0 \underline{N}\underline{\hat{\phi}}_j) \right] \Bigg] \, d\Omega, \end{aligned} \tag{96}$$

$$\begin{aligned} \underline{K}^{\phi_i\phi_j} = \frac{\partial \underline{R}^{\phi_i}}{\partial \underline{\hat{\phi}}_j} = \int\limits_{\Omega_e} & \zeta_{ij} \Bigg[\sigma_{ij} \Bigg(-(\underline{B}^T \underline{B})(\underline{N}\underline{\hat{\phi}}_i) + (\underline{B}^T \underline{B}) \underline{\hat{\phi}}_i \underline{N} \\ & - \frac{36}{\eta_{ij}^2} \underline{N}^T \underline{N} (1 + s_{ij} w_f(\underline{N}\underline{\hat{c}}))(\underline{N}\underline{\hat{\phi}}_i) \underline{N} (\underline{\hat{\phi}}_i - 2\underline{\hat{\phi}}_j) \Bigg) \\ & + \frac{6}{\eta_{ij}} \Bigg(\Delta G_{ij}(\boldsymbol{z}) \underline{N}^T \underline{N} (\underline{N}\underline{\hat{\phi}}_i) + \frac{\partial \Delta G_{ij}(\boldsymbol{z})}{\partial \underline{\hat{\phi}}_j} \underline{N}^T (\underline{N}\underline{\hat{\phi}}_i)(\underline{N}\underline{\hat{\phi}}_j) \Bigg) \\ - r_{ij} \underline{N}^T \underline{N} & \left[-\underline{\varepsilon}_{ij}^0 : \mathbb{C}_{ij} (\underline{B}_f \hat{\boldsymbol{u}} - \underline{\varepsilon}_{ij}^0 \underline{N}\underline{\hat{\phi}}_i \underline{N}\underline{\hat{\phi}}_j) + (\underline{N}\underline{\hat{\phi}}_i - \underline{N}\underline{\hat{\phi}}_j) \underline{\varepsilon}_{ij}^0 : \mathbb{C}_{ij} (-\underline{\varepsilon}_{ij}^0 \underline{N}\underline{\hat{\phi}}_i) \right] \Bigg] \, d\Omega, \end{aligned} \tag{97}$$

$$\begin{aligned} \underline{K}^{\phi_i c} = \frac{\partial \underline{R}^{\phi_i}}{\partial \underline{\hat{c}}} = \int\limits_{\Omega_e} \sum_{j=1, j\neq i}^{N_p} \zeta_{ij} \Bigg[& - \frac{36\sigma_{ij}}{\eta_{ij}^2} \underline{N}^T \underline{N} s_{ij} w_f \underline{N} (\underline{\hat{\phi}}_i - \underline{\hat{\phi}}_j) \Big((\underline{N}\underline{\hat{\phi}}_i)(\underline{N}\underline{\hat{\phi}}_j) \Big) \\ & + \frac{6}{\eta_{ij}} \frac{\partial \Delta G_{ij}(\boldsymbol{z})}{\partial \underline{\hat{c}}} \underline{N}^T (\underline{N}\underline{\hat{\phi}}_i)(\underline{N}\underline{\hat{\phi}}_j) \Bigg] \, d\Omega, \end{aligned} \tag{98}$$

$$\underline{K}^{\phi_i u} = \frac{\partial \underline{R}^{\phi_i}}{\partial \underline{\hat{\boldsymbol{u}}}} = \int\limits_{\Omega_e} \sum_{j=1, j\neq i}^{N_p} \zeta_{ij} r_{ij} \underline{N}^T \left((\underline{N}\underline{\hat{\phi}}_i - \underline{N}\underline{\hat{\phi}}_j) \underline{\varepsilon}_{ij}^0 \underline{\mathbb{C}}(\phi_l) \underline{B}_f \right) \, d\Omega, \tag{99}$$

$$\begin{aligned} \underline{K}^{cc} = \frac{\partial \underline{R}^c}{\partial \underline{\hat{c}}} = \int\limits_{\Omega_e} & \frac{1}{\Delta t} \underline{N}^T \underline{N} + \underline{B}^T \underline{B} \left(w_f^2 D_f(\phi) + w_f w_s D_s(\phi) \frac{\partial^2 \hat{\psi}_u(\underline{N\hat{c}})}{\partial c^2} \underline{N} \right) \\ & + \underline{B}^T w_f^2 D_f(\phi) \frac{\partial f_q(\underline{\hat{N}c})}{\partial c} \underline{N} \sum_{i=1}^{N_p} \sum_{j>i}^{N_p} 2 v_{ij} \left((\underline{N}\underline{\hat{\phi}}_i)(\underline{N}\underline{\hat{\phi}}_j)^2 \underline{B}\underline{\hat{\phi}}_i + \underline{N}\underline{\hat{\phi}}_j (\underline{N}\underline{\hat{\phi}}_i)^2 \underline{B}\underline{\hat{\phi}}_j) \right) \\ & + (\underline{B}^T \underline{B}) \underline{\hat{c}} w_f w_s D_s(\phi) \frac{\partial^3 \hat{\psi}_u(\underline{N\hat{c}})}{\partial c^3} + (\underline{B}^T \underline{B}) \underline{\hat{\mu}_s} w_f w_s D_f(\phi) \frac{\partial f_q(\underline{\hat{N}c})}{\partial c} \underline{N} \, d\Omega, \end{aligned} \tag{100}$$

$$\underline{K}^{\mu_s \mu_s} = \frac{\partial \underline{R}^{\mu_s}}{\partial \underline{\hat{\mu}_s}} = \int\limits_{\Omega_e} -\underline{N}^T \underline{N} \, d\Omega, \tag{101}$$

$$\underline{K}^{c \mu_s} = \frac{\partial \underline{R}^{c}}{\partial \underline{\hat{\mu}_s}} = \int\limits_{\Omega_e} \underline{B}^T \underline{B} (w_f w_s D_f(\phi) f_q(\underline{N\hat{c}}) + w_s^2 D_s(\phi)) \, d\Omega, \tag{102}$$

$$\underline{K}^{\mu_s c} = \frac{\partial \underline{R}^{\mu_s}}{\partial \underline{\hat{c}}} = \int\limits_{\Omega_e} \frac{\tau}{\Delta t} \underline{N}^T \underline{N} + \rho \underline{B}^T \underline{B} + \underline{N}^T \frac{\partial^2 f(c)}{\partial c^2} \underline{N} \, d\Omega, \tag{103}$$

$$\begin{aligned} \underline{K}^{c\phi_i} = \frac{\partial \underline{R}^c}{\partial \underline{\hat{\phi}_i}} = \int\limits_{\Omega_e} & \underline{B}^T \underline{B\hat{c}} \left(w_f^2 \frac{\partial D_f(\phi)}{\partial \underline{\hat{\phi}}_i} \underline{N} + w_f w_s \frac{\partial D_s(\phi)}{\partial \underline{\hat{\phi}}_i} \underline{N} \frac{\partial^2 \hat{\psi}_u(\underline{N\hat{c}})}{\partial c^2} \right) \\ & + \underline{B}^T (w_f^2 D_f(\phi) f_q(\underline{\hat{c}}) + w_s w_f D_s(\phi)) \\ & \sum_{j=1, j\neq i}^{N_p} 2 v_{ij} \left(\underline{B} (\underline{N}\underline{\hat{\phi}}_i)(\underline{N}\underline{\hat{\phi}}_j)^2 + (\underline{B}\underline{\hat{\phi}}_i) \underline{N} (\underline{N}\underline{\hat{\phi}}_j)^2 + 2 (\underline{B}\underline{\hat{\phi}}_j)(\underline{N}\underline{\hat{\phi}}_j)(\underline{N}\underline{\hat{\phi}}_i \underline{N}) \right) \\ & + \underline{B}^T \left(w_f^2 \frac{\partial D_f(\phi)}{\partial \underline{\hat{\phi}}_i} f_q(\underline{\hat{c}}) + w_s w_f \frac{\partial D_s(\phi)}{\partial \underline{\hat{\phi}}_i} \right) \\ & \sum_{k=1}^{N_p} \sum_{j>k}^{N_p} 2 v_{kj} \left((\underline{N}\underline{\hat{\phi}}_k)(\underline{N}\underline{\hat{\phi}}_j)^2 \underline{B}\underline{\hat{\phi}}_k + \underline{N}\underline{\hat{\phi}}_j (\underline{N}\underline{\hat{\phi}}_k)^2 \underline{B}\underline{\hat{\phi}}_j) \right) \\ & + \underline{B}^T \underline{B} \underline{\hat{\mu}_s} \left(w_f w_s \frac{\partial D_f(\phi)}{\partial \underline{\hat{\phi}}_i} f_q(\underline{\hat{c}}) \underline{N} + w_s^2 \frac{\partial D_s(\phi)}{\partial \underline{\hat{\phi}}_i} \underline{N} \right) \, d\Omega. \end{aligned} \tag{104}$$

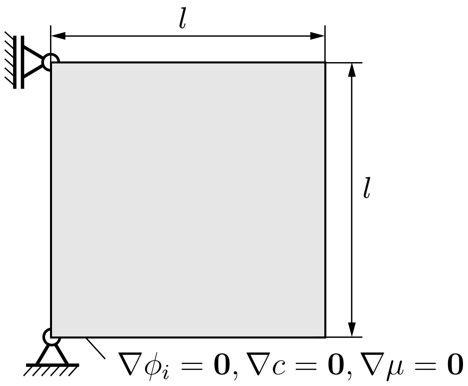

Figure 4: Quadratic domain: Geometry and boundary conditions

$$\underline{K}^{uu} = \int\limits_{\Omega_e} \underline{B}_f^T \mathbb{C}(\phi_l) \underline{B}_f \; d\Omega \tag{105}$$

$$\underline{K}^{u\phi_i} = \frac{\partial \underline{R}^u}{\partial \underline{\hat{\phi}_i}} = \int\limits_{\Omega_e} \sum_{j=1, j\neq i}^{N_p} p_{ij} \underline{B}_f^T \underline{\mathbb{C}}_{ij} \left(-\underline{\varepsilon}_{ij}^0 \underline{N} (\underline{N} \underline{\hat{\phi}}_j) \right) \; d\Omega, \tag{106}$$

5 Representative examples

Two representative examples are presented in this section. They are chosen to demonstrate the capability of the framework described in Section 2 and the prototype model in Section 3. The finite element method explained in Section 4 is used to solve the system of coupled partial differential equations. Both examples are solved on a domain of $l = 180$ nm × $l = 180$ nm discretized into 16384 quadrilateral elements. We prescribe homogeneous Neumann boundary conditions for the chemical potentials μ, the carbon concentration c and all phase order parameters ϕ_i. As shown in Figure 4 the mechanical problem is statically determined supported by Dirichlet boundary conditions such that the boundaries are stress free. In that way, the formation of individual nuclei can be studied [10]. The eigenstrain $\underline{\varepsilon}_{12}^0$ reads in Voigt notation

$$\underline{\varepsilon}_{12}^0 = \begin{bmatrix} 0.1 \\ -0.3 \\ 0 \end{bmatrix} \tag{107}$$

Parameter	**Symbol**	**Value/Unit**
Maximum carbon concentration in ferrite	c_{eq}	0.0704 wt.% [12]
Maximum carbon concentration in steel	c_{carb}	6.67 wt.% [30]
Cahn-Hilliard viscosity factor	τ	$2 \cdot 10^{-11}\mathrm{s}$
Cahn-Hilliard balance factor	ρ	$0.576\ \mathrm{nm}^2$
Cahn-Hilliard potential factor	d	$0.014\ \frac{1}{(\mathrm{wt.\%})^2}$
Bainitic ferrite/austenite interface energy	σ_{12}	$9600\ \frac{\mathrm{J}}{\mathrm{nm}^2}$
Bainitic ferrite/carbide interface energy	σ_{13}	$9600\ \frac{\mathrm{J}}{\mathrm{nm}^2}$
Austenite/carbide interface energy	σ_{23}	$9600\ \frac{\mathrm{J}}{\mathrm{nm}^2}$
Bainitic ferrite/austenite interface mobility	ζ_{12}	$9.6 \cdot 10^6\ \frac{\mathrm{nm}^4}{\mathrm{Js}}$
Bainitic ferrite/carbide interface mobility	ζ_{13}	$9.6 \cdot 10^6\ \frac{\mathrm{nm}^4}{\mathrm{Js}}$
Austenite/carbide interface mobility	ζ_{23}	$9.6 \cdot 10^6\ \frac{\mathrm{nm}^4}{\mathrm{Js}}$
Gibbs energy between bainitic ferrite and austenite	ΔG^0_{12}	$-2494.153\ \frac{\mathrm{J}}{\mathrm{nm}^3}$
Gibbs energy between bainitic ferrite and carbide	ΔG^0_{13}	$554.256\ \frac{\mathrm{J}}{\mathrm{nm}^3}$
Gibbs energy between austenite and carbide	ΔG^0_{23}	$554.256\ \frac{\mathrm{J}}{\mathrm{nm}^3}$
Interfacial thickness	η	17.3205nm
Step function width	ε	0.1
Transition temperature	T_D	625K
Temperature step function width	ε_T	1 K
Interface diffusion coefficient bainitic ferrite → austenite	s_{12}	$0.0068\frac{1}{\mathrm{wt.\%}}$
Interface diffusion coefficient bainitic ferrite → carbide	s_{13}	$0.0098\frac{1}{\mathrm{wt.\%}}$
Interface diffusion coefficient austenite → carbide	s_{23}	$0\frac{1}{\mathrm{wt.\%}}$
Cahn-Hilliard diffusion coefficient within bainitic ferrite	D_{s1}	$2 \cdot 10^7\frac{\mathrm{nm}^2}{\mathrm{s}}$
Cahn-Hilliard diffusion coefficient within austenite	D_{s2}	$0\frac{\mathrm{nm}^2}{\mathrm{s}}$
Cahn-Hilliard diffusion coefficient within carbide	D_{s3}	$0\frac{\mathrm{nm}^2}{\mathrm{s}}$
Fick's diffusion coefficient within bainitic ferrite	D_{f1}	$4 \cdot 10^{10}\frac{\mathrm{nm}^2}{\mathrm{s}}$
Fick's diffusion coefficient within austenite	D_{f2}	$8 \cdot 10^{10}\frac{\mathrm{nm}^2}{\mathrm{s}}$
Fick's diffusion coefficient within carbide	D_{f3}	$0\frac{\mathrm{nm}^2}{\mathrm{s}}$
Bainitic ferrite/austenite mechanical coupling parameter	p_{12}	1
Austenite/carbide mechanical coupling parameter	p_{23}	0
Bainitic ferrite/carbide mechanical coupling parameter	p_{13}	0
Bainitic ferrite/austenite phase field coupling parameter	r_{12}	$1\frac{1}{\mathrm{nm}}$
Austenite/carbide phase field coupling parameter	r_{23}	$0\frac{1}{\mathrm{nm}}$
Bainitic ferrite/carbide phase field coupling parameter	r_{13}	$0\frac{1}{\mathrm{nm}}$
Lower diffusion-across-the-interface parameter	L_D	0.5
Young's modulus	E	$77000\frac{\mathrm{N}}{\mathrm{mm}^2}$
Possion's ratio	ν	0.375

Table 1: Material parameters

(a) **Austenite**

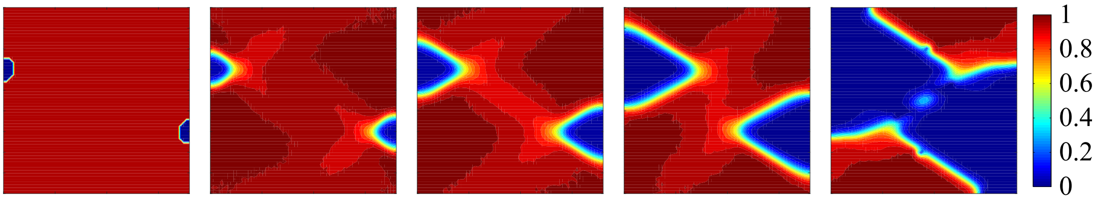

(b) **Bainitic ferrite**

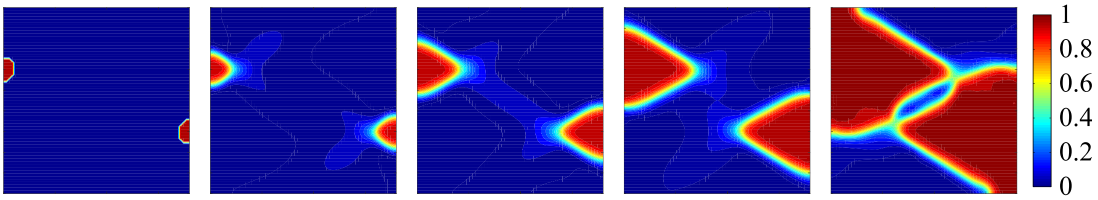

(c) ε_x

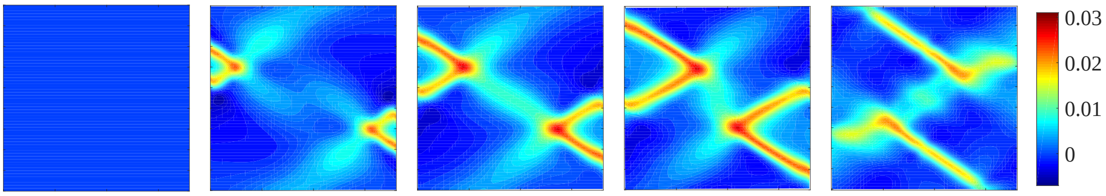

(d) ε_y

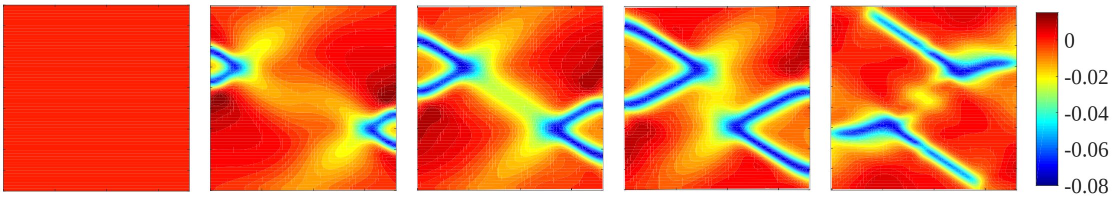

(e) **Carbide**

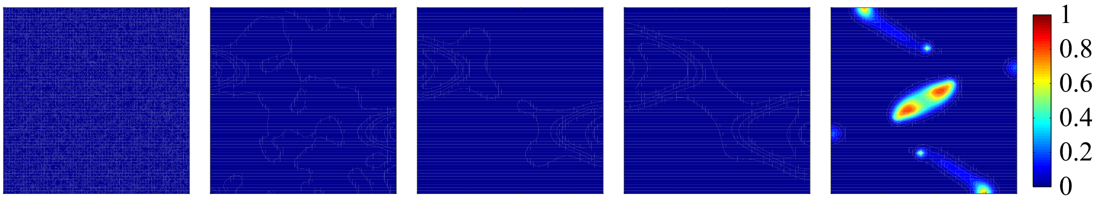

(f) **Carbon concentration**

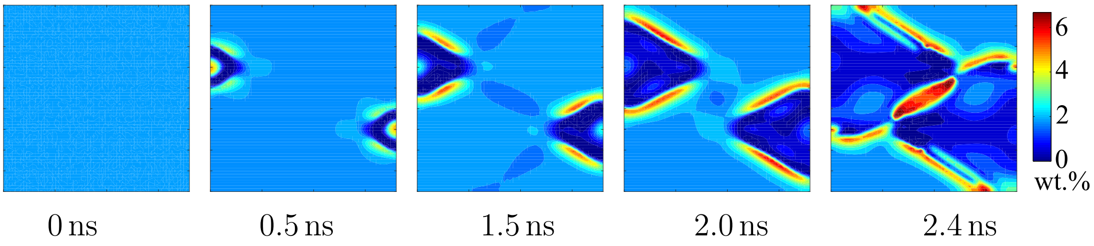

Figure 5: Upper bainitic transformation at 0 ns, 0.5 ns, 1.5 ns, 2.0 ns and 2.4 ns.

(a) Austenite

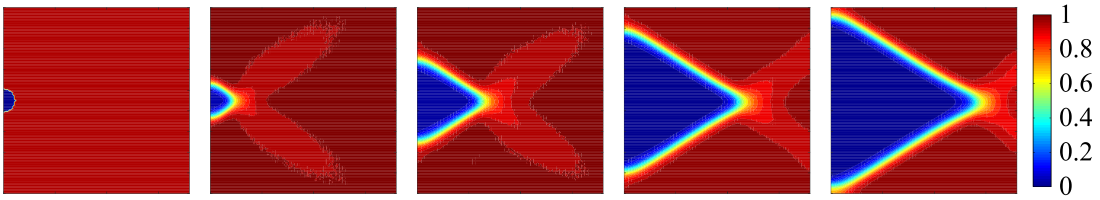

(b) Bainitic ferrite

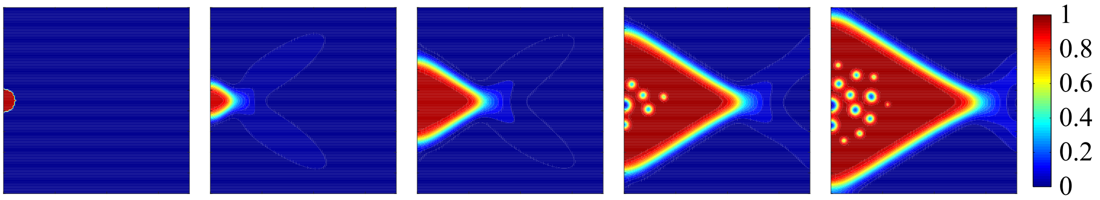

(c) ε_x

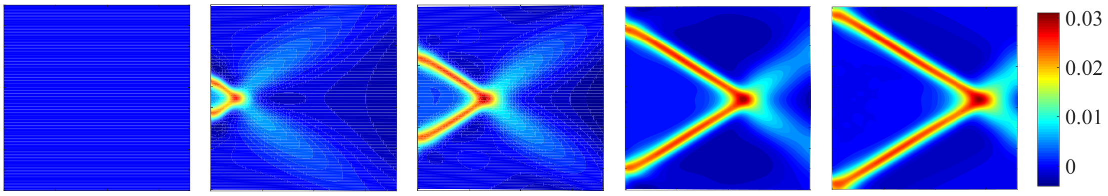

(d) ε_y

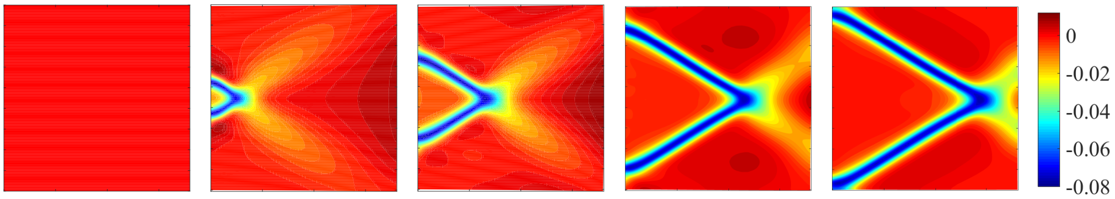

(e) Carbide

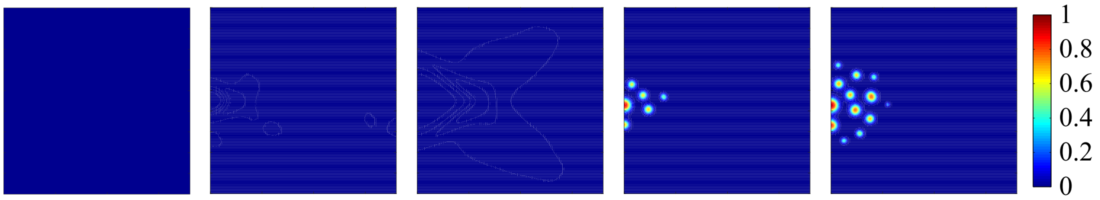

(f) Carbon concentration

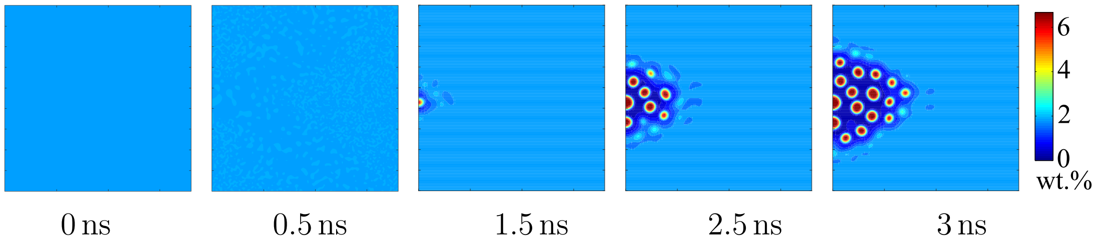

Figure 6: Lower bainitic transformation at 0 ns, 0.5 ns, 1.5 ns, 2.5 ns and 3 ns.

and the corresponding material tensor $\underline{\mathbb{C}}_{12}$ reads in Voigt notation

$$\underline{\mathbb{C}}_{12} = \frac{E(1-\nu)}{(1+\nu)\cdot(1-2\nu)} \cdot \begin{bmatrix} 1 & \nu/(1-\nu) & 0 \\ \nu/(1-\nu) & 1 & 0 \\ 0 & 0 & (1-2\nu)/(2(1-\nu)) \end{bmatrix} \tag{108}$$

where E is Young's modulus and ν is Poisson's ratio. Only $\underline{\varepsilon}^0_{12}$ and $\underline{\mathbb{C}}_{12}$ are considered, because a mechanical contribution is only taken into account for the displacive transformation from austenite (ϕ_1) to bainitic ferrite (ϕ_2) and not for the precipitation of carbides.

The initial conditions are illustrated in the first columns of Figures 5 and 6. However, the initial carbon concentration of $c(t=0) = 1.87\,\text{wt.\%}$ has very small random perturbations which cannot be observed with the scale in Figure 6. These perturbations are needed to start the separation of carbon. The same goes for the carbide phase ϕ_3 which is zero initially but has very small random perturbations. The size of each time step is $\Delta t = 10^{-10}\,\text{s}$. The material parameters are summarized in Table 1. Most of the parameters are tentative and a field for further investigations.

5.1 Upper bainite transformation

The first example in Figure 5 illustrates an upper bainite transformation at $T = 700$ K. As the initial condition two nuclei of bainitic ferrite ϕ_1 are proposed on the left and right boundary. The strains ε_x and ε_y in Figure 5.c and 5.d, respectively are zero initially. After 0.5 ns the nuclei grow in a directed way. Furthermore, strains can be observed in the interface region. While there is no change in the carbide phase ϕ_3 a carbon movement is observed. Carbon atoms leave the supersaturated bainitic ferrite to move across the interface into the austenite subsequently to the phase transformation from austenite to bainitic ferrite as described in subsection 3.1. During the next time steps this process goes on, such that the bainitic ferrite grows in a pointed shape, due to the coupling with the strains. Within the bainitic ferrite, the carbon starts to diffuse and move out of the supersaturated phase into the austenite. At around 2.3 ns the carbon concentration in Figure 5 reaches it maximum. As a consequence carbides precipitate in between the two sheaves of bainitic ferrite as described in the Introduction.

5.2 Lower bainite transformation

The second example at $T = 600$ K shows a lower bainite transformation. The initial conditions can be seen in the first column of Figure 6. There is a single circular nucleus of bainitic ferrite ϕ_1 on the left boundary while the rest of the domain is austenitic ϕ_2. We refrain from a second nucleus, because the interesting part of the transformation in lower bainite takes place within the bainitic ferrite and not between two bainitic sheaves. The third phase ϕ_3 is naturally zero. At the beginning there are no strains and the carbon is uniformly distributed over the domain. During the next time steps the bainitic ferrite grows in a directed way with a tip at its front like in the upper bainite example, see Figure 5.b. The subsequent carbon diffusion is different here. Only a small amount of carbon atoms reaches the interface of austenite and bainitic ferrite and succeed in leaving the supersaturated phase while most of the carbon stays within the bainitic ferrite to build accumulations. At these accumulations carbides precipitate.

6 Conclusions and outlook

In this work we present a framework for coupled multiphase, diffusion and mechanics models based on generalized forces and stresses which is an extension of our previously published work in [15]. Furthermore, we combine the framework with the diffusion mechanisms introduced in [17]. To couple the multiphase field method with mechanics, a new energy potential in equation (60) is introduced and implemented. The resulting model comes close to the physical reality considering the displacive growth from austenite to bainitic ferrite including the transformation strains which lead to directed growth of the bainitic phase.

The numerical examples show the described transformation followed by carbon movement. In upper bainite the carbon diffuses across the interface from the supersaturated bainitic ferrite into the austenite while in lower bainite most of the carbon starts to separate using a classical Cahn-Hilliard approach and stays within the bainitic ferrite. At accumulations of carbon carbides precipitate subsequently. An implementation using the isogemetric finite element method and an extension for non isothermal systems are planned for future work.

References

[1] H. K. D. H. Bhadeshia, Bainite in steels, 2nd Edition, Maney Materials Science, 2001.

[2] L. Fielding, The bainite controversy, Materials Science and Technology 29 (4) (2013) 383–399.

[3] I. Steinbach, Phase-field models in materials science, Modelling Simul. Mater. Sci. Eng. 17.

[4] R. Kobayashi, Modeling and numerical simulations of dendritic crystal growth, Physica D 63 (1993) 410–423.

[5] M. Militzer, M. Mecozzi, J. Sietsma, S. van der Zwaag, Three-dimensional phase field modelling of the austenite-to-ferrite transformation, Acta Materilia 54 (15) (2006) 3961–3972.

[6] C.-J. Huang, D. J. Browne, S. McFadden, A phase-field simulation of austenite to ferrite transformation kinetics in low carbon steels, Acta Materilia 54 (2005) 11–21.

[7] M. Mecozzi, J. Sietsma, S. van der Zwaag, M. Apel, P. Schaffnit, I. Steinbach, Analysis of the $\gamma \rightarrow \alpha$ Transformation in a C-Mn Steel by Phase-Field Modeling, Metallurgical and Materials Transactions A 36A (2005) 2327–2340.

[8] I. Steinbach, M. Apel, The influence of lattice strain on pearlite formation in fe-c, Acta Materialia 55 (14) (2007) 4817–4822.

[9] A. Yamanaka, T. Takaki, Y. Tomita, Elastoplastic phase-field simulation of self-and plastic accommodations in cubic tetragonal martensitic transformation, Materials Science and Engineering: A 491 (1) (2008) 378–384.

[10] R. Schmitt, R. Müller, C. Kuhn, H. M. Urbassek, A phase field approach for multivariant martensitic transformations of stable and metastable phases, Archive of Applied Mechanics 83 (6) (2013) 849–859.

[11] A. Yamanaka, T. Takaki, Y. Tomita, Phase-Field Simulation of Austenite to Ferrite Transformation and Widmanstätten Ferrite Formation in Fe-C Alloy, Materials Transactions 47 (11) (2006) 2725–2731.

[12] W. Song, U. Prahl, W. Bleck, K. Mukherjee, Phase-field simulations of bainitic phase transformation in 100cr6, TMS 2011 140th Annual Meeting and Exhibition (2011) 417–425.

[13] T. Arif, R. Qin, A phase-field model for bainitic transformation, Computational Materials Science 77 (2013) 230–235.

[14] M. Düsing, R. Mahnken, Simulation of lower bainitic transformation with the phase-field method considering carbide formation, Computational Materials Science 111 (2016) 91–100.

[15] M. Düsing, R. Mahnken, A thermodynamic framework for coupled multiphase ginzburg-landau/cahn-hilliard systems for simulation of lower bainitic transformation, Archive of Applied Mechanics 86 (12) (2016) 1947–1964.

[16] M. Weikamp, C. Hüter, M. Lin, U. Prahl, D. Schicchi, M. Hunkel, R. Spatschek, Scale bridging simulations of large elastic deformations and bainitic transformations, High-Performance Scientific Computing: First JARA-HPC Symposium, JHPCS 2016, Aachen, Germany, October 4–5, 2016, Revised Selected Papers (2017) 125–138.

[17] M. Düsing, R. Mahnken, A coupled phase field/diffusion model for upper and lower bainitic transformation, International Journal of Solids and Structures 135 (2018) 172–183.

[18] E. Fried, M. E. Gurtin, Continuum theory of thermally induced phase transitions based on an order parameter, Physica D: Nonlinear Phenomena 68 (3) (1993) 326–343.

[19] E. Fried, M. E. Gurtin, Dynamic solid-solid transitions with phase characterized by an order parameter, Physica D: Nonlinear Phenomena 72 (4) (1994) 287–308.

[20] M. E. Gurtin, Generalized Ginzburg-Landau and Cahn-Hilliard equations based on a microforce balance, Physica D: Nonlinear Phenomena 92 (3) (1996) 178–192.

[21] R. Mahnken, C. Cheng, M. Düsing, U. Ehlenbröker, T. Leismann, The concept of generalized stresses for computational manufacturing and beyond, GAMM-Mitteilungen 39 (2) (2016) 229–265.

[22] R. Schmitt, B. Wang, H. Urbassek, R. Müller, Modeling of martensitic transformations in pure iron by a phase field approach using information from atomistic simulation, Technische Mechanik 33 (2013) 119–130.

[23] K. Ammar, Modelling and Simulation of Phase Transformation-Mechanics coupling Using a Phase Field Method, Ph.D. thesis, l'École nationale supérieure des mines de Paris (2010).

[24] H. Altenbach, Kontinuumsmechanik: Einführung in die materialunabhängigen und materialabhängigen Gleichungen, Springer Berlin Heidelberg, 2012.

[25] I. Müller, W. Weiss, Entropy and Energy: A Universal Competition, Interaction of Mechanics and Mathematics, Springer Berlin Heidelberg, 2006.

[26] M. Silhavy, The Mechanics and Thermodynamics of Continuous Media, Theoretical and Mathematical Physics, Springer Berlin Heidelberg, 2013.

[27] A. Villani, E. P. Busso, K. Ammar, S. Forest, M. Geers, A fully coupled diffusional-mechanical formulation: numerical implementation, analytical validation, and effects of plasticity on equilibrium, Archive of Applied Mechanics 84 (9-11) (2014) 1647–1664.

[28] W. Dreyer, C. Guhlke, Sharp limit of the viscous Cahn-Hilliard equation and thermodynamic consistency, Continuum Mechanics and Thermodynamics (2015) 1–22.

[29] I. Steinbach, F. Pezzolla, B. Nestler, M. Seeßelberg, R. Ptieler, G. Schmitz, J. Rezende, A phase field concept for multiphase systems, Physica D 94 (1996) 135–147.

[30] D. Horstmann, Das Zustandsschaubild Eisen-Kohlenstoff und die Grundlagen der Wärmebehandlung der Eisenkohlenstoff-Legierungen., Stahleisen, Ddf., 1985.

5 Summary of the papers

Paper A proposes a multiphase field model coupled to Cahn-Hilliard diffusion to simulate the lower bainitic transformation. To the author's knowledge, this is the first work concerning a phase field model for the lower bainitic transformation considering the subsequent carbon diffusion and precipitation of carbides. The main idea is to activate the carbon diffusion within the bainitic ferrite phase, which grows displacively. The diffusion equation used to simulate the supposed accumulation of carbon is the viscous Cahn-Hilliard equation. At accumulations of carbon carbides precipitate due to a high concentration. The precipitation of carbides is modelled using the phase field model. The finite element method is applied to solve the system of coupled partial differential equations. The results confirm the described transformation.

Paper B is concerned with a thermodynamic framework for a multiphase field model coupled with Cahn-Hilliard diffusion. The focus of this paper is the derivation of the evolution equations for phase order parameters and the carbon concentration. The described framework is based on the concept of generalized stresses as introduced by Gurtin [10]. A microforce balance for N_p phases and the concentration of a solute is derived and used in conjunction with the first and second law of thermodynamics to formulate restrictions to constitutive equations. A prototype model with constitutive equations for the lower bainitic transformation is proposed. The resulting system of partial differential equations is solved using the finite element method. The numerical examples are compared with micrographs and show similar microstructures.

Paper C focusses on the diffusion of carbon in bainite. While the previous papers only consider the separation of carbon within the bainitic ferrite, here the diffusion of carbon across the interface between bainitic ferrite and austenite is taken into account. This extension enables the model to simulate the upper bainitic transformation and improves the simulation of lower bainitic transformation. A new unified model is created which can describe upper and lower bainite depending only on the constant temperature. A weighted Helmholtz energy is introduced to distinguish between the diffusion mechanics.

On the one hand, upper bainite grows at high temperatures where the carbon can diffuse across the interface from the supersaturated bainitic ferrite into the austenite. On the other hand, at low temperatures lower bainite grows where most of the carbon starts to build accumulations within the bainitic ferrite while only a small amount of carbon moves across the interface. To the author's knowledge the model described in this paper is the first one considering these two diffusion phenomena in one model and it is the first model capable of describing upper and lower bainitic transformation. Numerical results achieved with the finite element method show the subsequent diffusion of carbon. In the example of upper bainite, the movement of carbon from the supersaturated bainitic ferrite into the austenite can be seen. In addition the precipitation of carbides from the austenite phase at accumulations of carbon is simulated. The lower bainite example shows that only a few carbon atoms succeed in leaving the bainitic ferrite.

Paper D deals with the extension of the already published model to mechanics. The thermodynamic framework introduced by Gurtin [10] and extended in Paper B is improved in this work. The balance equations of linear momentum and angular momentum are added to the framework and the first and second law of thermodynamics take deformations into account, such that the number of restrictions imposed on the constitutive equations grows. The key idea is to simulate the directed growth of the displacive transformation from bainitic ferrite to austenite by coupling mechanics with the multiphase field equations. Due to eigenstrains during the displacive transformation some growth directions are favoured, such that the phase grows faster in these directions. This extension to the previous model replaces a mechanism which manipulates the interface mobility dependent on the local phase gradient and a specified growth angle. Numerical examples are calculated with the phase field method considering seven unknowns per node. The results show the directed growth of the bainitic ferrite for upper and lower bainite taking into account the corresponding diffusion mechanisms and the precipitation of carbides.

6 Summary

In this work, composed of four papers, a model to simulate the upper and lower bainitic transformation is presented. Bainite is a steel microstructure with desirable macroscopic qualities, like the combination of high toughness and high hardness. Thus, bainitic steels have gained increased popularity for example in the aerospace and car industry. The microstructure of bainite consists of bainitic ferrite, carbide and retained austenite. The bainitic transformation is one of the most complex in steel. It starts with a displacive transformation from austenite to bainitic ferrite. The carbon concentration and its diffusion have no influence on the transformation, such that the bainitic ferrite is supersaturated with carbon right after the phase transformation. In a subsequent process depending on the temperature the carbon starts to diffuse due to the supersaturation. At high temperatures the carbon atoms move across the interface into the austenite whereas at lower temperatures most of the carbon stays within the bainitic ferrite and builds accumulations. At places where the carbon concentration reaches its maximum carbides precipitate. In upper bainite, at higher temperatures, the precipitation of carbides takes place within the austenite phase whereas in lower bainite, at lower temperatures, the precipitation of carbides takes place within the bainitic ferrite phase.

To simulate the described transformation a multiphase field method coupled to diffusion and mechanics is developed. The coupled model is based on the concept of generalized stresses and the microforce balance as described in Papers B and D. A thermodynamic framework including the multiphase field, the carbon concentration and mechanics is presented in this work to guarantee the strict separation between universal physical laws, such as the balance equations, the first and the second law of thermodynamics, and constitutive equations which differ depending on the material. In addition restrictions to constitutive equations due to the second law of thermodynamics are derived and applied to propose a prototype model for the bainitic transformation. The key ideas of the model can be summarized in the following steps. The first step is the phase transformation from austenite to bainitic ferrite coupled to mechanics to simulate the directed growth as presented in Paper D. The second step is the diffusion of carbon. To model the diffusion of carbon in lower bainite a Cahn-Hilliard equation is implemented as published in Paper A. The complex combined diffusion phenomena including diffusion across the interface is considered for upper bainite and lower bainite in Paper C. In the third and last step carbides precipitate at places where the carbon concentration reaches its maximum.

The system of partial differential equations is solved using the finite element method. The numerical results of the four papers confirm the expected and described transformations of upper and lower bainite.

7 Outlook

A main part of the future work is the parameter identification for the models presented in this work. Due to the small size and the high speed of the transformations difficulties occur within this identification. One way to obtain parameters is to compare numerical results with micrographs from transmission electron microscopy as done for example in Paper B. To prove the timing of the transformation, which is a key part of the simulation, in-situ experiments are needed. Another way to parameterise the model is to use results of other simulations, such as atomistic simulations [28].

The models presented in this work are two dimensional representations of a three dimensional problem. A next step could be the extension to three dimensions. However, this would increase the already high computational costs and the development time.

Another step in future research could be the implementation of plastitcity. During the displacive transformation from austenite to bainitic ferrite transformation plasticity occurs which is not considered yet.

The models presented in this work consider isothermal transformations, as this is the most common way to produce bainite. However, for future work an extension to a thermo-multiphase-diffusion-mechanics model is reasonable. A simulation could start with arbitrary initial conditions for the phases. In a first step the workpiece is heated until it consists purely of austenite. In a next step a quenching process with holding at a certain temperature or continuous cooling could be simulated. Depending on the temperature and the temperature rate different phases, such as ferrite, pearlite, upper and lower bainite or martensite may occur in such a simulation. This modelling idea could lead to a simulation which describes diffusional and displacive transformations in one model depending on the temperature. The thermodynamic framework, derived in Paper B and extended in Paper D, has to be changed significantly to consider heat and temperature changes. The result would be a model which can predict the ratio of the different phases depending on the temperature profile.

Bibliography

[1] L. D. Landau and V. Ginzburg. On the theory of superconductivity. *Zh. Eksp. Teor. Fiz.* 20 (1950), 1064.

[2] J. W. Cahn and J. E. Hilliard. Free energy of a nonuniform system. I. Interfacial free energy. *The Journal of chemical physics* 28.2 (1958), 258–267.

[3] J. Rowlinson. Translation of JD van der Waals': The thermodynamik theory of capillarity under the hypothesis of a continuous variation of density. *Journal of Statistical Physics* 20.2 (1979), 197–200.

[4] J.-C. Tolédano and P. Tolédano. *The Landau theory of phase transitions.* World Scientific, 1987.

[5] A. A. Wheeler, W. J. Boettinger, and G. B. McFadden. Phase-field model for isothermal phase transitions in binary alloys. *Phys. Rev. A* 45 (10 May 1992), 7424–7439.

[6] E. Fried and M. E. Gurtin. Continuum theory of thermally induced phase transitions based on an order parameter. *Physica D: Nonlinear Phenomena* 68.3 (1993), 326–343.

[7] R. Kobayashi. Modeling and numerical simulations of dendritic crystal growth. *Physica D* 63 (1993), 410–423.

[8] A. A. Wheeler, W. J. Boettinger, and G. B. McFadden. Phase-field model of solute trapping during solidification. *Physical Review E* 47.3 (1993), 1893.

[9] E. Fried and M. E. Gurtin. Dynamic solid-solid transitions with phase characterized by an order parameter. *Physica D: Nonlinear Phenomena* 72.4 (1994), 287–308.

[10] M. E. Gurtin. Generalized Ginzburg-Landau and Cahn-Hilliard equations based on a microforce balance. *Physica D: Nonlinear Phenomena* 92.3 (1996), 178–192.

[11] N. Ahmad, A. Wheeler, W. Boettinger, and G. McFadden. Solute trapping and solute drag in a phase-field model of rapid solidification. *Physical Review E* 58.3 (1998), 3436.

[12] H. K. D. H. Bhadeshia. *Bainite in steels.* 2nd. Maney Materials Science, Mar. 2001.

[13] C.-J. Huang, D. J. Browne, and S. McFadden. A phase-field simulation of austenite to ferrite transformation kinetics in low carbon steels. *Acta Materilia* 54 (2005), 11–21.

[14] M. Militzer, M. Mecozzi, J. Sietsma, and S. van der Zwaag. Three-dimensional phase field modelling of the austenite-to-ferrite transformation. *Acta Materilia* 54.15 (2006), 3961–3972.

[15] A. Yamanaka, T. Takaki, and Y. Tomita. Phase-Field Simulation of Austenite to Ferrite Transformation and Widmanstätten Ferrite Formation in Fe-C Alloy. *Materials Transactions* 47.11 (2006), 2725–2731.

[16] I. Steinbach and M. Apel. The influence of lattice strain on pearlite formation in Fe-C. *Acta Materialia* 55.14 (2007), 4817–4822.

[17] N. Moelans, B. Blanpain, and P. Wollants. An introduction to phase-field modeling of microstructure evolution. *Calphad* 32.2 (2008), 268–294.

[18] A. Yamanaka, T. Takaki, and Y. Tomita. Elastoplastic phase-field simulation of self-and plastic accommodations in cubic tetragonal martensitic transformation. *Materials Science and Engineering: A* 491.1 (2008), 378–384.

[19] I. Steinbach. Phase-field models in materials science. *Modelling Simul. Mater. Sci. Eng.* 17 (2009).

[20] C. Miehe, F. Welschinger, and M. Hofacker. Thermodynamically consistent phase-field models of fracture: Variational principles and multi-field FE implementations. *International Journal for Numerical Methods in Engineering* 83.10 (2010), 1273–1311.

[21] R. Mahnken, A. Schneidt, S. Tschumak, and H. Maier. On the simulation of austenite to bainite phase transformation. *Computational Materials Science* 50.6 (2011), 1823–1829.

[22] W. Song, U. Prahl, W. Bleck, and K. Mukherjee. Phase-field simulations of bainitic phase transformation in 100Cr6. *TMS 2011 140th Annual Meeting and Exhibition* (2011), 417–425.

[23] M. J. Borden, C. V. Verhoosel, M. A. Scott, T. J. Hughes, and C. M. Landis. A phase-field description of dynamic brittle fracture. *Computer Methods in Applied Mechanics and Engineering* 217 (2012), 77–95.

[24] *DB Mobility Networks Logistics*. Deutsche Bahn. 2012. URL: `https://archive.is/20130121093033/http://www.deutschebahn.com/de/konzern/im_blickpunkt/2733814/spezialstahl_bainit.html` (visited on June 6, 2018).

[25] R. Mahnken, M. Wolff, A. Schneidt, and M. Böhm. Multi-phase transformations at large strains – Thermodynamic framework and simulation. *International Journal of Plasticity* 39 (2012), 1–26.

[26] T. Arif and R. Qin. A phase-field model for bainitic transformation. *Computational Materials Science* 77 (2013), 230–235.

[27] L. Fielding. The bainite controversy. *Materials Science and Technology* 29.4 (2013), 383–399.

[28] R. Schmitt, B. Wang, H. Urbassek, and R. Müller. Modeling of martensitic transformations in pure iron by a phase field approach using information from atomistic simulation. *Technische Mechanik* 33 (2013), 119–130.

[29] R. Schmitt, R. Müller, C. Kuhn, and H. M. Urbassek. A phase field approach for multivariant martensitic transformations of stable and metastable phases. *Archive of Applied Mechanics* 83.6 (2013), 849–859.

[30] E. A. B. F. Lima, J. T. Oden, and R. C. Almeida. A hybrid ten-species phase-field model of tumor growth. *Mathematical Models and Methods in Applied Sciences* 24.13 (2014), 2569–2599.

[31] R. Mahnken, A. Schneidt, T. Antretter, U. Ehlenbröker, and M. Wolff. Multi-scale modeling of bainitic phase transformation in multi-variant polycrystalline low alloy steels. *International Journal of Solids and Structures* 54 (2015), 156–171.

[32] T. Nguyen, J. Yvonnet, Q.-Z. Zhu, M. Bornert, and C. Chateau. A phase field method to simulate crack nucleation and propagation in strongly heterogeneous materials from direct imaging of their microstructure. *Engineering Fracture Mechanics* 139 (2015), 18–39.

[33] M. Düsing and R. Mahnken. A thermodynamic framework for coupled multiphase Ginzburg-Landau/Cahn-Hilliard systems for simulation of lower bainitic transformation. *Archive of Applied Mechanics* 86.12 (2016), 1947–1964.

[34] M. Düsing and R. Mahnken. Simulation of lower bainitic transformation with the phase-field method considering carbide formation. *Computational Materials Science* 111 (2016), 91–100.

[35] T. Hofmann, R. Müller, H. Andrä, and J. Zausch. Numerical simulation of phase separation in cathode materials of lithium ion batteries. *International Journal of Solids and Structures* 100 (2016), 456–469.

[36] *Time-Temperature-Transformation diagram.* Wikipedia, Robo Blazek, modified. 2017. URL: `https://commons.wikimedia.org/wiki/File:IRA_ADI.svg` (visited on May 24, 2018).

[37] M. Weikamp, C. Hüter, M. Lin, U. Prahl, D. Schicchi, M. Hunkel, and R. Spatschek. "Scale Bridging Simulations of Large Elastic Deformations and Bainitic Transformations". In: *High-Performance Scientific Computing: First JARA-HPC Symposium, JHPCS 2016, Aachen, Germany, October 4–5, 2016, Revised Selected Papers.* Ed. by E. Di Napoli, M.-A. Hermanns, H. Iliev, A. Lintermann, and A. Peyser. Cham: Springer International Publishing, 2017, 125–138.

[38] M. Düsing and R. Mahnken. A coupled phase field/diffusion model for upper and lower bainitic transformation. *International Journal of Solids and Structures* 135 (2018), 172–183.

[39] M. Düsing and R. Mahnken. A coupled phase field/diffusional/mechanical framework for simulation of upper and lower bainitic transformation. *submitted* (2018).

[40] C. Kahle and K. F. Lam. Parameter Identification via Optimal Control for a Cahn–Hilliard-Chemotaxis System with a Variable Mobility. *Applied Mathematics & Optimization* (Mar. 2018).

Schriftenreihe des Lehrstuhls für Technische Mechanik

Bisher in dieser Reihe erschienen:

1. Gockel, Franz-Barthold: Projektierung einer Arbeitsplattform zur Schädigungsanalyse und Validierung von Simulationsmodellen unter Thermoschockbedingungen; P-2008-1; Dissertation 2008; ISBN 978-3-8322-7465-8
2. Hentrich, Manuel: Geklebte Strukturen unter Crashbeanspruchung; P-2010-2; Dissertation 2010; ISBN 978-3-8322-8964-5
3. Wilmanns, Stefan: Phänomenologische und mikroskopische Modellierung von Formgedächtnislegierungen; P-2010-3; Dissertation 2010; ISBN 978-3-8322-9485-4
4. Caylak, Ismail: Stabilized Mixed Triangular and Tetrahedral Finite Elements with Volume and Area Bubble Functions; P-2011-4; Dissertation 2011; ISBN 978-3-8440-0084-9
5. Shaban, Ahmed: Experiments and Modelling of Elasto-Viscoplasticity for Thermoplastics with Asymmetric Effects; P-2010-5; Dissertation 2010; ISBN 978-3-8440-0351-2
6. Sauerland, Kim-Henning: Phenomenological Process Simulation and Multiscale Tool Simulation directed to a Hybrid Forming Process; P-2013-6; Dissertation 2013; ISBN 978-38440-1918-6
7. Schneidt, Andreas: Mehrphasige phänomenologische sowie mehrskalige mikroskopische Modellierung von Phasenumwandlungen in einem Hybridumformprozess; P-2017-1; Dissertation 2016; ISBN 978-38440-5671-6